Russian Original Vol. 30, No. 1, January, 1971

Translation published August, 1971

SOVIET ATOMIC ENERGY

АТОМНАЯ ЭНЕРГИЯ
(ATOMNAYA ÉNERGIYA)

TRANSLATED FROM RUSSIAN

CONSULTANTS BUREAU, NEW YORK

SOVIET ATOMIC ENERGY

Soviet Atomic Energy is a cover-to-cover translation of *Atomnaya Énergiya*, a publication of the Academy of Sciences of the USSR.

An arrangement with Mezhdunarodnaya Kniga, the Soviet book export agency, makes available both advance copies of the Russian journal and original glossy photographs and artwork. This serves to decrease the necessary time lag between publication of the original and publication of the translation and helps to improve the quality of the latter. The translation began with the first issue of the Russian journal.

Consultants Bureau journals appear about six months after the publication of the original Russian issue. For bibliographic accuracy, the English issue published by Consultants Bureau carries the same number and date as the original Russian from which it was translated. For example, a Russian issue published in December will appear in a Consultants Bureau English translation about the following June, but the translation issue will carry the December date. When ordering any volume or particular issue of a Consultants Bureau journal, please specify the date and, where applicable, the volume and issue numbers of the original Russian. The material you will receive will be a translation of that Russian volume or issue.

Subscription
$67.50 per volume (6 Issues)
2 volumes per year
(Add $5 for orders outside the United States and Canada.)

Single Issue: $30
Single Article: $15

CONSULTANTS BUREAU, NEW YORK AND LONDON

227 West 17th Street
New York, New York 10011

Davis House
8 Scrubs Lane
Harlesden, NW10 6SE
England

Second-class postage paid at Jamaica, New York 11431.

SOVIET ATOMIC ENERGY

A translation of *Atomnaya Énergiya*
Translation published August, 1971

Volume 30, Number 1 January, 1971

CONTENTS

CONTENTS

(continued)

The Russian press date (podpisano k pechati) of this issue was 12/28/1970. Publication therefore did not occur prior to this date, but must be assumed to have taken place reasonably soon thereafter.

INVESTIGATION OF URANIUM MONOCARBIDE FUEL ELEMENTS IN THE FUEL BUNDLES OF THE BR-5 REACTOR

Sh. Sh. Ibragimov, T. S. Men'shikova,
A. Ya. Ladygin, Yu. I. Aleksandrov,
Yu. I. Likhachev, V. T. Galkov,
A. N. Vorob'ev, and L. I. Moseev

UDC 621.039.548

The use of uranium monocarbide as nuclear fuel for power reactors holds great promise [1-3]. However, the available information (see, for example, [4-7]) concerning the behavior of uranium monocarbide under irradiation and concerning its compatibility under reactor conditions with the material of the cladding is still insufficient, and therefore research on uranium monocarbide fuel elements is a field of great interest.

We investigated three fuel bundles – K-7, K-13, and K-12 – which had been in the active zone of the BR-5 reactor for 1 year, 3 years, and 4 years, respectively (Table 1). The average linear power for each bundle was 230 W/cm. The maximum temperature of the fuel element cladding was 570°C, and the value at the center of the cores was approximately 1000°C.

Design of the Bundles and Fuel Elements

Each bundle contained seven fuel elements [8], enclosed in hexagonal stainless steel cans, with a wall thickness of 0.3 mm and measuring 26 mm across flats. The coolant (sodium) circulation was upward.

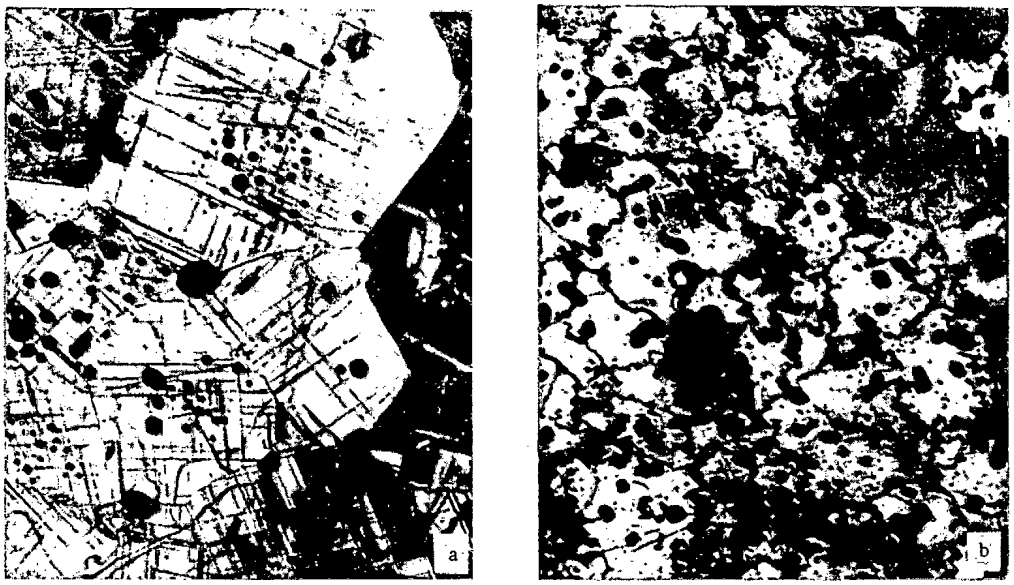

Fig. 1. Microstructure of uranium monocarbide (at center of pellet), in the middle section of the fuel element (×500): a) 0.8% burnup; b) 3% burnup.

Translated from Atomnaya Énergiya, Vol. 30, No. 1, pp. 3-7, January, 1971. Original article submitted January 4, 1970; revision submitted June 4, 1970.

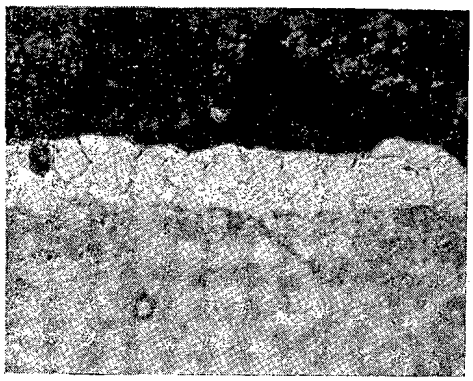

Fig. 2

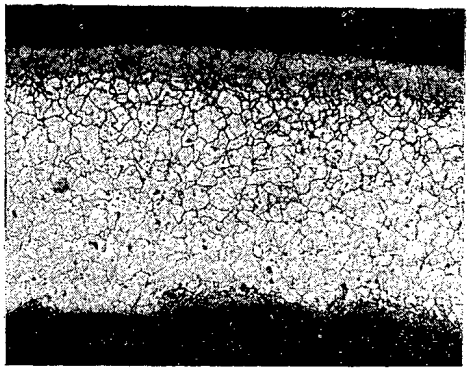

Fig. 3

Fig. 2. Zone of interaction between the jacket and a pellet (fuel element from bundle K-12, middle section) (× 1100).

Fig. 3. Zone of interaction between the jacket and the sodium (fuel element from bundle K-12, middle section) (× 175).

Each fuel element of a bundle is a tube made of 0Kh18N9T steel, with an outer diameter of 8.7 mm and a wall thickness of 0.4 mm. The tube contains uranium carbide pellets obtained by high-temperature sintering. The pellets have a diameter of 7.65 mm, a density not less than 88% of the theoretical density, and a carbon content of 5.3-5.4% by weight. The pellets are piled to a height of 380 mm. The space between the jacket and the core (up to 0.45 mm) is filled with helium.

In the upper part of the fuel element a cavity approximately 60 mm high, containing no pellets, is left in order to compensate for the thermal expansion and to accommodate the gaseous fission products.

Investigation of the Fuel Elements

External Inspection. Fuel Density and Distribution of Fission Products. Inspection of the bundles revealed no external damage. All the fuel elements (21) were free from breaks and defects. An increase in fuel element diameter (up to 0.5% on the average) was found only in bundle K-13 (2.1% burnup). In some fuel elements we observed a bend in the middle section (2-4 mm), probably due to the circular nonuniformity of the temperature field of the fuel elements near the wall.

Density measurements made by the hydrostatic weighing method showed that the pellets swell at a rate of 1.9 ± 0.4% for each 1% of burnup.

The airtight seal of the fuel elements was broken, and the gases removed, by puncturing the jacket in a vacuum at $2 \cdot 10^{-2}$ mm Hg. The amount of gas inside the jacket was determined from readings on a U-shaped manometer with an error of 0.2 cm^3 at normal conditions. For bundle K-13 this value was 2% of the total amount of gas. The ratio between the krypton and the xenon generated in the fuel element was roughly the same as the ratio of the amounts of these gases produced during fission (approximately 1 : 6). The distribution of Kr^{85} and solid fission products agrees with the distribution of the amount of burnup along the length of the fuel elements.

The Effect of Irradiation on Changes in Fuel Composition. The metallographic examination of the uranium carbide was carried out on specimens taken from the top, bottom, and middle sections of the fuel element. The following findings were made (Fig. 1):

1. All the pellets investigated showed a number of large and small cracks running in various directions.

2. As the burnup proceeds, there is a decrease in the amount of the dicarbide component in the uranium carbide pellets. This is also confirmed by data from X-ray and chemical analysis.

3. Pore formation takes place in the uranium carbide pellets; the size and distribution of the pores depend on the operating temperature of the fuel. The highest porosity was observed in pellets from the middle section of the fuel elements. At the center of the pellets the pores are larger (up to 15 μ) and are arranged partly along the grain boundaries; on the periphery the pore diameter usually does not exceed 4 μ.

TABLE 1. Characteristics of the Bundles

Bundle	Operating time, months	Heavy-atom burnup, %	Accumulation of fission fragments, g/cm³	Cumulative dose, 10^{22} neutrons/cm²
K-7	12	0,8	0,082	0,5
K-13	32	2,1	0,212	1,5
K-12	47	3,0	0,304	2,1

Interaction of the Jacket with the Uranium Carbide and the Coolant. The 0Kh18N9T steel was subjected to radiation aging under irradiation conditions, and its microhardness was found to have increased from 240 to 270-300 kg/mm².

On the inner surface of the jackets we found interaction zones and individual blisters.

The interaction zones are observed along the whole length of the fuel elements, including the region not filled with pellets. Their shape and thickness is approximately the same everywhere. The zones are light-colored diffusion layers up to 10 μ thick, with a clearly marked boundary and a base (Fig. 2).

The maximum diameter of the blisters on the inner surface of the fuel element jackets is 120 μ, the depth 50 μ. The grains of the base around the blisters are fine-structured, and the boundaries between the grains are corroded. The microhardness of the material around the blisters is approximately equal to the microhardness of the base.

The outer surface of the steel (on the coolant side) interacted with the sodium and its impurities,* which led to the formation of interaction zones. The characteristic microstructure of such a zone (Fig. 3) indicates that the interaction took place by intragranular diffusion and diffusion along the grain boundaries. The width of the interaction zones is 50-75 μ. The microhardness of the surface layer of the jacket, with a thickness of about 100 μ, is very high, and it reaches its maximum values (400-500 kg/mm²) in these zones.

Mechanical Properties of the Jacket Material. The mechanical properties of the fuel element jacket material were determined on annular specimens 4 mm high. The tests were conducted on the UMD-5 rupture testing machine at a rate of travel of 4 mm/min. Before being pulled apart the specimens were kept at a prescribed temperature for 10 minutes. The test results (Table 2) show that after the fuel elements had been operated in the reactor for some time, the plasticity of the jackets was considerably reduced, especially in the middle section of the elements.

Evaluation of Results

A comparison of the diameters of the irradiated fuel elements from bundles K-7 and K-12 with the diameters of the unirradiated fuel elements shows that for 3% or less heavy-atom burnup there is no increase in fuel element diameter caused by fuel swelling.

The increase in the diameter of the fuel elements in bundle K-13 (2.1% burnup), as was mentioned earlier, averaged 0.5%. Up to the present time we have measured the diameters of 28 other fuel elements with burnup values of up to 4.2%, and no increase in diameter has been found in any of them. We must therefore assume that in bundle K-13 the initial diametral gap was close to zero.

The fatigue life of the jackets was evaluated for the cases in which the space between the fuel and the jacket was maintained throughout the entire period of operation of the fuel element (including all the bundles investigated except K-13). The jackets underwent gradually increasing pressure caused by the gaseous fission fragments emitted by the fuel, and temperature stresses caused by the heat flux and by the circular nonuniformity of the heat field.

It is shown by simulation of heat removal conditions in the heat-generating assemblies, and also by calculations, that the maximum nonuniformity of the circumferential temperature in the fuel elements near the wall may reach 70°C. This corresponds to the appearance of axial stresses of up to 10 kg/mm² in straight fuel elements. The greatest heat-flux stresses are approximately 5 kg/mm², and the circumferential stresses caused by the pressure of the gaseous fission fragments do not go above 1 kg/mm². The intensity of the total stresses does not exceed the yield point of the jacket material; consequently, thermal cycling produces only elastic deformation, so that the damage caused by thermal cycling is slight, and the

* According to chemical analysis data, the sodium contained up to $1.7 \cdot 10^{-2}$% carbon, $1 \cdot 10^{-2}$% oxygen, and $3 \cdot 10^{-3}$% nitrogen.

TABLE 2. Results of Tests Performed on Annular Specimens of Fuel Element Jackets from Bundle K-13 (0Kh18N9T Steel)

Testing temperature °C	Unirradiated specimens		After irradiation					
			top of fuel element		middle of fuel element		bottom of fuel element	
	σ_v, kg/mm²	δ, %	σ_v, kg/mm²	δ, %	σ_v, kg/mm²	δ, %	σ_v, kg/mm²	δ, %
25	73,5	47,0	67,0	0,2	85,0	1,3	81,0	5,0
300	49,0	12,0	62,0	1,5	38,0	0,5	40,0	0,5
550	41,5	10,0	32,0	2,0	33,0	1,0	50,0	2,5

process of relaxation of the temperature stresses may be regarded as continuous. On evaluating the operating capacity by totalling the damage caused by the relaxation temperature stresses (from the circular nonuniformity of the temperature and the heat flux), we found that there was an adequate reserve of operating capacity in the fuel element jackets, as judged by the criterion of long-term strength. As a result of the relaxation of the temperature stresses, there are residual stresses which produce a curvature in the fuel elements after removal of the hexagonal can during disassembly.

For small initial gaps (bundle K-13) the operating capacity of the jacket is determined from the deformation accumulated as a result of creep in an element charged with a solid fuel which swells isotropically (at the rate of 1.9 ± 0.4% for each 1% of heavy-atom burnup). When the diameter of the jacket increased by 0.5%, the total deformation was approximately 1% (with the axial deformation equal to the circular deformation). In an earlier charging of the BR-5 reactor, fuel elements of a similar type had gone out of order after the jacket diameter had changed by 2.5-3%; consequently, the deformation of the fuel element jackets in bundle K-13 is not a source of danger.

From the metallographic analysis data it can be seen that the material of the jackets (0Kh18N9T) steel) interacts with the coolant (sodium) and the fuel (uranium monocarbide in higher than stoichiometric proportions).

The zones of interaction on the inner surface of the jackets are observed everywhere, including the compensation volume, where we know that there are no fuel pellets, i.e., the formation of the interaction zones originates from the gaseous phase and passes through the helium. This conclusion contradicts some data [3, 8, 9], according to which at temperatures up to 800-900°C there is no appreciable interaction between stainless steel and uranium monocarbide. However, it has been found [10] that carburization of the jacket through the helium can take place at a temperature of 650°C or higher. The carburization of stainless steel from the gaseous phase at a temperature lower than 900°C is attributed [11] to the action of methane during the hydrolysis of the uranium carbide by the moisture adsorbed on it. This process is accompanied by the formation of light-colored zones similar in shape and width to those found in the fuel elements under investigation.

Data obtained by layer-by-layer chemical analysis indicate that the zones on the inner surface of the jackets contain approximately 0.7% carbon, uranium, and fission fragments (10^{-4}-10^{-5}%).

In the burnup range under investigation (0.8-3 atomic percent) the interaction between the steel and the uranium carbide takes place in a narrow surface zone (approximately 10 μ wide) and probably cannot cause any appreciable change in the mechanical properties of the jacket.

Stainless steel in contact with liquid sodium in the temperature range under consideration (up to 570°C) may undergo various types of interaction, the intensity of which depends on the operating conditions, the composition of the steel, the percentage of impurities (especially oxygen, carbon, and nitrogen) in the sodium, and other factors. The greatest effect may be produced by the carburization and nitrogenization of the jackets, since the sodium contains appreciable quantities of carbon and nitrogen. Both processes begin at temperatures above 400°C and may lead to the formation of characteristic interaction zones on the surface of the steel. The layers on the external surface of the fuel elements investigated are comparable in microstructure, shape of boundaries with the base, and microhardness with carburization zones described earlier [12, 13].

On the basis of the foregoing, we may draw the following conclusions:

1. All the fuel elements (21) maintained their airtight seal up to 3% heavy-atom burnup.

2. The change in fuel element diameter depends on the degree of burnup and the amount of space between the core and the jacket.

The volumetric swelling of the fuel, determined by the method of hydrostatic weighing, is 1.9 ± 0.4% for each 1% of heavy-atom burnup.

3. The total amount of gases under the fuel element jacket is approximately 2% of the total amount of fission gases.

4. No migration of Kr^{85} and solid fission products along the vertical length of the fuel elements was found at burnup values of 3% or less.

5. As the burnup proceeds, we observe a decrease in the dicarbide component of the uranium carbide and an increase in the amount of unbound carbon.

6. On the outer and inner surfaces of the fuel element jackets, we find interaction layers which differ from one another in external appearance and conditions of formation.

7. The material of the jackets becomes embrittled. In the range of operating temperatures the plasticity of 0Kh18N9T steel, investigated on annular specimens (fuel element from bundle K-13) is 0.5-2.5%.

I. G. Sheinker, V. S. Kadantsev, L. I. Mamaev, and G. V. Titov participated in the work.

The authors are grateful to I. S. Golovnin, L. I. Sytov, V. M. Rodin, S. N. Bashlykov, and V. K. Lesnichii for evaluating the results, and they are especially grateful to Academician A. I. Leipunskii for his constant interest in the study and his valuable comments on it.

LITERATURE CITED

1. V. S. Chirkin, Thermophysical Properties of Nuclear Engineering Materials [in Russian], Atomizdat, Moscow (1968).
2. F. S. Patton et al., Nuclear Fuel Using Enriched Uranium [Russian translation], Atomizdat, Moscow (1968).
3. B. Frost, J. Nucl. Mater., 10, 265 (1963).
4. D. Sinizer et al., Proc. Venice Conf., Vol. 3, Vienna, IAEA (1963), p. 287.
5. J. Crane and E. Gordon, Report 63/5206 on Symp. Carbides in Nucl. Energy, Harwell (1963).
6. B. Bradbury et al., ibid., Report R 4323.
7. L. Neimark et al., ibid., Report 63/6023.
8. I. S. Golovnin et al., Report 4/1, presented by the USSR at the International Conference on the Irradiation of Materials in Fast Reactors, Thurso, Gt. Britain (1969).
9. G. Pearlman and R. Dickerson, Report 234, presented by the United States of America at the Third International Conference on the Peaceful Uses of Atomic Energy, Geneva (1964).
10. G. Bishop et al., Report 4B/1, presented by Great Britain at the International Conference on Fast Reactors, London (1966).
11. D. Hodkin et al., AERE-R5173, Harwell (1966).
12. Yu. F. Balandin and V. G. Markov, Structural Materials for Installations Using Liquid-Metal Coolants [in Russian], Sudpromgiz, Moscow (1968).
13. B. A. Nevzorov, Corrosion of Structural Materials in Sodium [in Russian], Atomizdat, Moscow (1968).

THE CZECH ŠR-1 RESEARCH REACTOR

J. Kott, A. Zbytovský,
J. Flaišhans, and M. Jílek

UDC 621.039.519

The ŠR-1 research reactor (see Fig. 1) developed for the "Škoda Works" by the Chemoprojekt design agency (Prague) is a pool type reactor intended for research and testing of fissionable and nonfissionable materials at a core thermal power of 10-20 MW. A system of pools is accommodated in the hall where basic physics experiments are carried out; this system is provided with neutron beams and a thermal column. An extension of this hall takes the form of a multistory annex in which the remaining laboratories, workrooms, and accessory technological and radiation safety rooms are concentrated. The main hall and the annex are so designed to facilitate future expansions of the building.

The reactor project is based on long-term experience gained with the IRT-M Soviet reactor. Modern fuel assemblies with four IRT type tubular fuel elements containing 171 g uranium are used to load the core in the ŠR-1 project. The use of these fuel assemblies and fuel elements in combination with the pool renders the use of the reactor for in-core irradiation of specimens in a flux of 10^{14} neutrons/cm^2 · sec more convenient, and is also helpful in organizing small loops on the core periphery.

In its design and functions, the ŠR-1 reactor is not a duplicate of any of the reactors now in operation or being planned in the COMECON countries. On the contrary, it supplements the reactors used in basic nuclear physics research and later redesigned for engineering purposes (the VVR-S, VVR-M, and IRT reactors), as well as the high-output reactors with large irradiation capacities (the MR and MIR reactors).

The ŠR-1 research reactor can be used both for routine irradiation of materials and assemblies of limited volume and for research on the physics of the atomic nucleus, solid state physics, radiochemistry, and also for production of radioactive isotopes. The ŠR-1 reactor is useful in a wide range of research efforts related to the development of nuclear power in Czechoslovakia and in other socialist commonwealth countries.

Basic Characteristics of the ŠR-1 Reactor

Type	Research and engineering pool type, enriched uranium fuel (80% U^{235}) with ordinary water coolant and moderator
Output	Rating 10 MW, maximum 20 MW
Functions	Research on reactor technology, studies of materials and biological shielding, testing of reactor control instrumentation and equipment, production of radioactive isotopes
Siting	Experimental base of the Škoda Works, nuclear power plant in Bolevec
Operated by	Bolovec nuclear plant, "Škoda Works"
Peak neutron flux (at 10 MW)	Thermal 10^{14} neutrons/cm^2 · sec, fast flux $5 \cdot 10^{13}$ neutrons /cm^2 · sec
Reactivity margin	$\Delta K/K = 9\%$
Core shape, size	Made up of IRT-M type fuel assemblies and fuel elements, core configuration subjected to modification to match specific experiment. Load-carrying slab designed to support 100 fuel assemblies
First loading (10 MW)	5440 g U^{235} (32 assemblies)

Czechoslovakia. Translated from Atomnaya Énergiya, Vol. 30, No. 1, pp. 7-10, January, 1971. Original article submitted March 3, 1970.

Average specific power of fuel at 10 MW	1.84 kW/kg U^{235}
Irradiation level	7.4 kW/liter
Campaign	Over 50 MW days
Refueling	Remote control, manual, under shielding layer of water
Fuel storage	In storage pool for 450 assemblies
Fuel assemblies	IRT-M type, with tubular fuel elements of square cross section
Moderator, reflector	Ordinary demineralized water
Cooling	Ordinary water with forced circulation from top to bottom; secondary loop cooled with aid of cooling towers
Control and adjustment	Four shim rods and three safety rods of boral, and one stainless steel fine-control rod
Biological shielding	Lateral 5.2 m water and 2.5 m concrete; top shield 9 m water
Water treatment	Ion exchange column with upstream ceramic filter; hydraulic replacement of ion-exchange resin cartridges

Experimental Capabilities of the Reactor

Most of the space for testing is provided directly within the reactor core, between the fuel elements. In addition, the reactor is provided with vertical "wet" and "dry" channels which accommodate material irradiation experiments. Capsules can be suspended from the lateral construction members of the pool. The dimensions of capsules and specimens range from 16 to 71 mm in diameter and up to 650 mm in length.

The arrangement of the core and auxiliary reactor rooms allows for irradiation of small subloops around the core periphery, with an output of 50 to 100 kW. It is assumed that not more than two subloop channels will be undergoing irradiation simultaneously. Subloop channels not exceeding the pitch of the fuel assembly lattice in their diameters can also be irradiated within the core.

A neutron trap is placed at the center of the reactor core for capsule experiments at high flux, and small capsules and specimens are readily accommodated there. The reactor is provided with two radial and one tangential channels (each 200 mm in diameter), closed off by rotary gates, to facilitate beam extraction to the experimental room.

The thermal column, dimensioned 1500 × 1500 × 2300 mm, is made of graphite and covered with movable shielding consisting of layers of paraffin and iron. The column serves three functions: removal of thermal neutrons, installation of a neutron fission converter to aid in shielding studies, and removal of neutrons when large parts are irradiated, etc. By displacing the core from its basic position at the center of the pool and bringing the core right up against the thermal column, higher neutron fluxes can be obtained on emergence from the column, and this is particularly important in shielding experiments.

Large-size structures in reactor technological equipment can be irradiated in the pool in the direct vicinity of the core.

Basic Process Loop

Heat removal from the core is handled by the primary and secondary loops. The primary loop is formed by the reactor pool, water from which passes through the core to a box to allow measurement of the total reactor power in terms of nitrogen activity, and to a box where the integrity of the fuel elements is checked. The water is then directed on into the holding storage pool and to three heat exchanger units, thus forming three subloops. Each of the units includes a heat exchanger and a pump; one single subloop is sufficient at a power level of 10 MW. Cold water is returned through diffusor tubes to the bottom of the pool. The secondary-loop water is circulated under force between the pond serving the cooling towers and the primary-loop heat exchangers.

The water treatment system results in the following characteristics for the reactor pool water:

Dry residue	< 2 mg/liter
Salt content	< 1 mg/liter
pH	5.5 to 6
Electrical resistivity	0.3 to 0.5 MΩ/cm
Chloride content	< 0.02 mg/liter

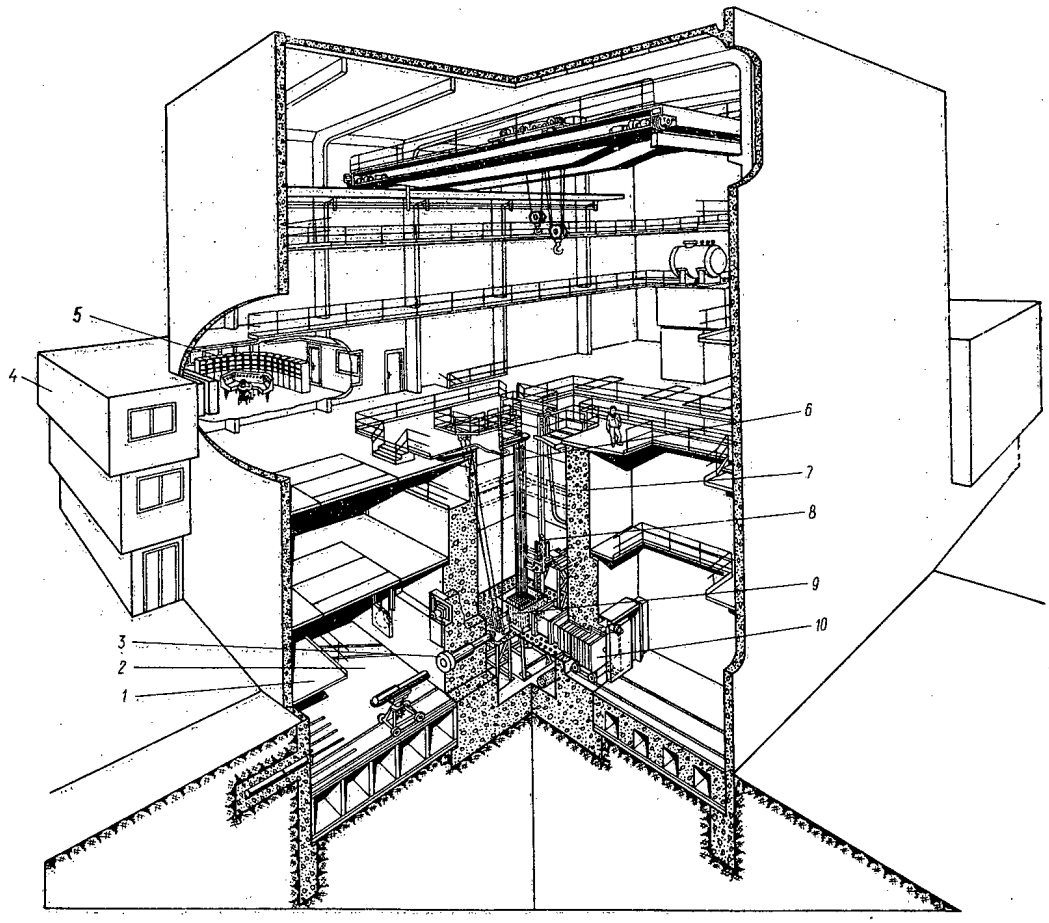

Fig. 1. Layout of the ŠR-1 reactor: 1) auxiliary process equipment floor; 2) basic physics experiments area; 3) horizontal channel; 4) laboratories annex; 5) reactor control panel; 6) control rods; 7) reactor pool concrete shield; 8) experimental subloop; 9) core; 10) thermal column.

Handling of Irradiated Materials

All handling of radioactive materials (except for materials irradiated in the experimental channels) is taken care of in the pools. Large-size equipment is transported under a layer of water through the storage pool. Activated equipment is dismantled by remote control under a layer of water. The pools are separated by removable aluminum gates with rubber seals. A crane or special fixtures handle manipulations inside the pools.

Irradiated materials to be transported out of the water are loaded in a shipping container directly in the reactor hall. These operations will be carried out rather infrequently, so that no special equipment other than remote controls for the crane has been provided for the purpose.

The technology for shipping radioactive isotopes and unpacking them is being worked out separately.

LAWS FOR THE DEPOSITION OF MATERIALS ON HEAT-TRANSMITTING SURFACES UNDER THE ACTION OF THERMOELECTRIC EFFECTS

V. P. Brusakov

UDC 536.7

It is known from the thermodynamics of irreversible processes [1-3], that an emf (a thermal emf) arises in a system containing charge carriers, in the presence of a heat flux, under the influence of a temperature gradient between sections with different temperatures.

In thermal power equipment, the existence of an electric field between a heat-transmitting surface and a moving stream of heat-transfer agent at a certain distance from the wall must generate processes associated with the interaction between the electric field and the charged particles.

The main temperature drop ($\Delta T = T_1 - T_2$) is localized in the viscous layer and intermediate layer of the heat-transfer agent, immediately adjacent to the heat-transmitting surface [4].

The maximum thickness of the thermal boundary layer, where heat-transfer takes place due to heat conduction, is determined from the equation

$$\delta_T = \frac{\lambda}{\alpha}, \tag{1}$$

where λ is the thermal conductivity; and α is the heat transfer coefficient. The thermal emf is included in the emf ΔE between sections of the electrical conducting system, if there is a temperature difference ΔT between them:

$$\Delta E = \varepsilon \Delta T, \tag{2}$$

where ε is the thermal emf coefficient, V/deg.

A theoretical analysis of the components of the thermal emf and the general expression for it are given in [1-3].

With a steady heat flux, and with no convection, the value of the steady thermal emf ε_∞, referred to a temperature difference of 1°C, is given by the expressions [5, 6]:

$$\varepsilon_\infty = \varepsilon^0_\infty + \frac{R}{zF} \ln [a_k^{+z}]; \tag{3}$$

$$\varepsilon^0_\infty = \frac{\Delta s^0}{zF}; \tag{4}$$

$$\Delta s^0 = s^0_{k+z} + s_{\bar{e}} - S_k; \tag{5}$$

$$s_k = S^0_k - R \ln a_k, \tag{5a}$$

where a_k^{+z} is the activity of the potential-forming ion k in solution; s^0_{k+z} is the entropy of the moving ion; $s_{\bar{e}}$ is the entropy of the moving electron in the metal; S_k and a_k are the entropy of element k on the electrode surface, and its activity, respectively.

It follows from Eqs. (3) and (4) that only the potential-forming ions take part in creating the steady thermal emf. This thesis was first expressed by M. I. Temkin and A. V. Khoroshin [5], and has been confirmed by Yu. A. Zyazev, both for solutions with one electrolyte [5, 6], and for a mixture of electrolytes in solutions of very complex compositions (biological extracts) [7].

The potential-forming ion is that whose electrode potential is the most positive in the given condition:

Translated from Atomnaya Énergiya, Vol. 30, No. 1, pp. 10-14, January, 1971. Original article submitted July 8, 1969; revision submitted July 28, 1970.

TABLE 1. Comparison of Theoretical and Empirical Rates of Deposition of Corrosion Products

Equipment	q, kcal /m^2·h	Q, kcal /h	c, mg/l	empirical value		theoretical value	
				A, g/m^2·h	ΣA, g/h	A, g/m^2·h	ΣA, g/h
1	2	3	4	5	6	7	8
Loop of NRU reactor under pressure [5]	$3\cdot10^5$		Fe 0,001	$1\cdot10^{-4}$		$0{,}6\cdot10^{-4}$	
Loop of the NRX (boiler) reactor [15]	$6{,}1\cdot10^5$ $8{,}65\cdot10^5$		Fe 0,006 Fe 0,035	$9{,}6\cdot10^{-4}$ $5{,}2\cdot10^{-3}$		$7{,}3\cdot10^{-4}$ $6\cdot10^{-3}$	
Atomic power plant in Garil'yano [16].		$2{,}5\cdot10^8$	Fe 1,3 Cu 0,52 Ni 0,8		52 58 0,06		65 30 40
Atomic power plant with VK-50 reactor [17]	—	$1{,}25\cdot10^8$	Fe 0,06 Cu 0,01 Zn 0,013		6,0 0,3 0,3		1,5—2 0,3 0,4
The OP-60 12/300 boiler (supercritical parameters) [18]	$1\cdot10^5$		Fe 0,16	$3{,}3\cdot10^{-3}$		$3{,}8\cdot10^{-3}$	
Experimental rig without volumetric boiling [14]	$1{,}3\cdot10^6$		Fe 0,4	0,1—0,15		0,1	
60 atm boiler [19]		$2{,}26\cdot10^7$	Fe 2,8 Cü 0,10 Al 0,43		8,4—20,5 0—0,75 1,0—3,5		12,8 1,2 1,8
100 atm PK-14-27 boiler [20]		$7\cdot10^7$	Fe 0,28		2,5—3,5		3,9
40 atm GNM-75 boiler [21]	$5\cdot10^5$	$2{,}1\cdot10^7$	Fe 2 Cü 0,160	0,13 $5{,}1\cdot10^{-2}$	10—15 2	0,20 $4{,}3\cdot10^{-2}$	9 1,9
4-36 atm (boiling) experimental rig [22]	$7{,}8\cdot10^4$		Ca 400 Mg 1300 (sulfates of Ca, Mg)	10—50		26,5	

$$E = E^0 + \frac{RT}{zF} \ln \frac{a_k^{+z}}{a_k}, \qquad (6)$$

where E^0 is the standard electrode potential: a_k^{+z} is the activity of the ion; and a_k is the activity of the reduced shape.

According to [3], in an electrical circuit consisting of conductors of the first and second kind (in the system considered: heater surface – metal of tubes – surface with lower temperature – boundary layer; turbulent region of heat transfer agent flow – boundary layer of heat transfer agent – heating surface), for constant temperature difference between two points, and with appropriate conditions for transfer of electricity via the Peltier effect, a continuous current arises. The Peltier heat Π is related to the thermal emf by the expression

$$\Pi = \varepsilon T.$$

Calculation using Eq. (6) indicates that in water with pH 7, containing different cations at concentrations limited by ion production, the potential-forming ions can only be hydrogen ions, and possibly copper.

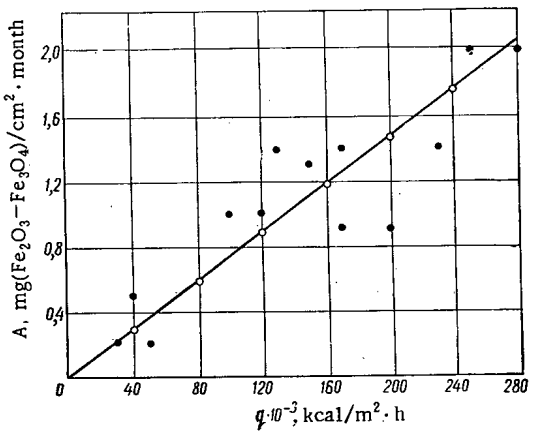

Fig. 1. Rate of deposition of corrosion products as a function of heat flux [12]: ●) empirical points, taken from [12]; ○) points calculated from Eq. (11) with $\varepsilon u = 1 \cdot 10^{-7}$ V/deg $\cdot m^2/V \cdot h$. c = 0.3-0.6 mg/liter.

The uncertainty regarding copper is due to the large scatter (eight orders of magnitude) in the value of the ion production of its hydroxide.

Reference [7] used the results of a series of experiments with solutions of complex composition (biological extracts) to calculate a value ε_∞ in a system with a hydrogen potential-forming ion at pH 7, of $(0.3\text{-}1) \cdot 10^{-3}$ V/deg. The hot part of the system was charged negatively, and the cold part positively. No explicit dependence of ε_∞ on temperature was observed. The material of the electrodes (platinum or copper) had no effect on ε_∞.

The value of ε_∞ obtained falls in the range of the absolute values $(0.2\text{-}1.5) \cdot 10^3$ V/deg, obtained by many investigators with various potential-forming ions.

Under the action of the electric field created by the thermal emf in the boundary layer, positively charged particles of corrosion products will deposit on the heated surface. The flux of particles A, expressed in $g/m^2 \cdot h$, is given by the equation

$$A = Huc, \tag{7}$$

where H is the electric field strength, V/m; u is the electrophoretic mobility of the particles, $m^2/V \cdot h$; and c is the concentration of suspended corrosion products, expressed in g/m^3, at a distance δ_T from the hot wall, from which the flux begins. According to [8], in water at a temperature 100-350°C the diffusion layer $\delta_d < \delta T$ and therefore the particle concentrations at distance δT can be assumed to be their concentration in the turbulent region of the same section.

The field strength in the thermal layer is

$$H = \frac{\Delta E}{\delta_T}. \tag{8}$$

Substituting the value $\Delta E = \varepsilon_\infty \Delta T$ and H from Eq. (8) into Eq. (7), we obtain

$$A = \frac{\varepsilon_\infty \Delta T u c}{\delta_T}. \tag{9}$$

Substituting δT from Eq. (1) and $\alpha \Delta T = q$, where q is the heat flux, expressed in kW/m^2 or $kcal/m^2 \cdot h$, into Eqs. (8) and (9), we obtain

$$H = \frac{\varepsilon_\infty q}{\lambda}; \tag{10}$$

$$A = \frac{\varepsilon_\infty u c q}{\lambda}. \tag{11}$$

With q = 500,000 $kcal/m^2 \cdot h$, the field strength is 10 V/cm. This kind of field strength is ordinarily used with electrophoretic precipitation of colloid particles.

The mobility of colloid particles of different sizes, charges, and kinds [9], including actual corrosion products [10], varies in the narrow limits $(3\text{-}9) \cdot 10^{-5}$ $m^2/V \cdot h$. With increase of temperature [11], the mobility varies in inverse proportion to the viscosity of the medium (approximately by a factor of 10 at T = 573°K, or 300°C). Taking into account also the variation in the dielectric constant of water (approximately a factor of 5), we obtain $u = (0.6\text{-}1.8) \cdot 10^{-4}$ $m^2/V \cdot h$.

Reference [12] gave data of industrial investigations of deposition of corrosion products in high-pressure boilers.

The points calculated from Eq. (11) with values of $\varepsilon_\infty = 1 \cdot 10^{-3}$ V/deg, $u = 1 \cdot 10^{-4}$ $m^2/V \cdot h$ for different heat fluxes lie in the middle of the empirical data region. Here we considered only points from the work cited for which simultaneous values of deposition rate and heat flux were given (see Fig. 1).

If the thermal emf ΔE is greater than the dissociation value ΔE_D [11] of some substance at the specific conditions, the ion will be deposited in its elementary state on the heat-transmitting surface, which is the

cathode, and transition of the element into the ion (anodic solution) or discharge of oppositely-charged ions will be observed in the part of the system with the other temperature.

With cathode control the rate of deposition is

$$A = \frac{(\Delta E - \Delta E_p)\, uc}{\delta_T}. \qquad (12)$$

When $|\Delta E| > |\Delta E_p| > 0$ there must be a certain heat load above which discharge of a specific ion will begin.

According to [13, 14], there does exist a critical value of the heat flux ($q = 200{,}000$ kcal/m$^2 \cdot$h for a specific salt composition), above which there is continuous deposition of metallic copper.

If the material of the electrodes corresponds to the potential-forming ion or their potential is determined by this ion, then $E_p = 0$ [11], and the rate of deposition of the ion is given by Eqs. (9) and (11). In this case the mobility and the concentration of the ions (u and c) differ from the values for suspended particles (for copper $u = 2.7 \cdot 10^{-4}$ m^2/V$\cdot$h).

If the corrosion products of copper under specific conditions are in the form of suspended particles, they will be deposited for any heat flux, and $u = 1 \cdot 10^{-4}$ m^2/V$\cdot$h.

The total rate of deposition of suspended charged particles or of discharge of potential-forming ion on the heat-transmitting surface, where the concentration of material in the heat-transfer agent is practically identical over the whole surface (the active zone of a reactor, of a superheater, or the compartments of a cylindrical boiler), is given by the equation

$$A_{av}F = \Sigma A = \frac{\varepsilon_\infty u c q_{cp} F}{\lambda} \text{ (g/h or g-equiv/h).}$$

Since $q_{av}F = Q$, where Q is the thermal power of the area F (kW or kcal/h), then

$$\Sigma A = \frac{\varepsilon_\infty u c Q}{\lambda} \text{ (g/h or g-equiv/h).} \qquad (13)$$

Table 1 gives empirical data on deposition of corrosion products of a heat-transmitting surface of various power-producing and experimental equipment, and also data calculated from Eqs. (11) and (13) for the appropriate conditions. Table 1 shows that there is agreement over a wide range of heat fluxes ($8 \cdot 10^4$–$1.5 \cdot 10^6$ kcal/m$^2 \cdot$h), of concentrations (0.003–2.0 mg/liter), and of pressures, with or without boiling.

Table 1 also shows a small part of the analysis of the empirical material. Deviations outside the limits of accuracy of evaluation are found, as a rule, only in test rigs when artificial or "old" (formed before they played a part in the experiment) particles are used as "corrosion products," and when the heat flux is generated by passing an electric current through the heater section.

The best agreement is observed when average values of the above quantities are reported, values obtained from statistical processing of empirical data taken over a long period of operation, under steady conditions.

It is pointed out in [23] that radiation affects the deposition of corrosion products. For example, in specimens located in a reactor core, deposition is greater than in specimens washed by the water but located outside the core.

Since, because of absorption of radiative energy, a specimen in a reactor becomes itself a source of heat, the observed effect cannot be an unambiguous proof of the special role of radiation in the deposition process in general.

No effect of radiation is observed when a comparison is made of deposition rates calculated from Eqs. (11) and (13) with actually observed deposition rates in fuel elements subjected to a heat flux of at least $1 \cdot 10^5$ kcal/m$^2 \cdot$h.

LITERATURE CITED

1. S. R. de Groot, Thermodynamics of Irreversible Processes [Russian translation], Izd-vo Inostr. Lit., Moscow (1956).
2. K. Denbig, Thermodynamics of Irreversible Processes [Russian translation], Izd-vo Inostr. Lit., Moscow (1954).

3. R. Haase, Thermodynamics of Irreversible Processes [Russian translation], Mir, Moscow (1967).
4. S. S. Kutateladze and V. M. Borishanskii, Heat Transfer Handbook [in Russian], Gosénergoizdat, Moscow–Leningrad (1959).
5. M. I. Temkin and A. V. Khoroshin, Zhurn. Fiz. i Khimii, 26, 500 (1952); 26, 773 (1952).
6. Y. Thouvenin, Effect Peltier Electrolytique: contribution a l'étude teorique et experimentable, Doctoral thesis, University of Paris (1963), p. 1.
7. Yu. A. Zyazev, Investigation of Thermal Electromotive Forces in Living Plant Tissue, Thesis [in Russian], Leningrad (1968).
8. V. G. Levich, Physical and Chemical Hydrodynamics [in Russian], Fizmatgiz, Moscow (1959).
9. N. P. Beskov, Physicochemical Bases of Colloid Science [in Russian], Goskhimitekhniza po NTI, Moscow–Leningrad (1934).
10. V. D. Ganzha et al., At. Énerg., 19, 350 (1965).
11. A. I. Brodskii, Physical Chemistry [in Russian], Vol. 2, Goskhimizdat, Moscow–Leningrad (1948).
12. N. N. Man'kina, Teploénergetika, No. 2, 79 (1959).
13. N. N. Man'kina, Teploénergetika, No. 3, 8 (1960).
14. A. A. Kot, Water Treatment and Cycling in Atomic Power Stations [in Russian], Atomizdat, Moscow (1964).
15. H. Rae and G. Allison, Third Internat. Conf. on the Peaceful Uses of Atomic Energy, Vol. 9, Geneva (1964).
16. G. della Rocca et al., Third Internat. Conf. on the Peaceful Uses of Atomic Energy, Vol. 5, Geneva (1964).
17. I. N. Sokolov et al., COMECON Symposium: "The present state and future development of atomic power plants with water-cooled water-moderated reactors" [in Russian], April 22-27, 1968, Moscow.
18. É. P. Dik, I. I. Nadyrov, and N. N. Man'kina, Teploénergetika, No. 1, 45 (1964).
19. N. N. Man'kina, A. G. Tkachenko, and L. G. Buinovskaya, Teploénergetika, No. 10, 16 (1964).
20. B. N. Ukhin, Teploénergetika, No. 9, 30 (1960).
21. N. N. Man'kina et al., Élektricheskie Stantsii, No. 5, 70 (1967).
22. G. M. Levin and I. M. Blinchevskii, Izv. Vuzov. Énergetika, No. 12, 58 (1965).
23. P. Cohen, Problems in Nuclear Power Engineering [Russian translation], No. 1, IL, Moscow (1958), p. 88.

CONDITIONS FOR THE HYDROMAGNETIC STABILITY OF A PLASMA

L. S. Solov'ev

UDC 533.9

Energy Principle

Under the assumption of an ideal conductivity, a necessary and sufficient condition for the hydromagnetic stability [1] of a plasma configuration retained in equilibrium by a magnetic field B with

$$\nabla p = [\mathbf{jB}], \quad \mathbf{j} = \operatorname{rot} \mathbf{B}, \quad \operatorname{div} \mathbf{B} = 0 \tag{1}$$

is a positive potential energy $\delta W = \delta W_i + \delta W_\Sigma + \delta W_e$ in arbitrary shifts ξ:

$$\delta W_i = \frac{1}{2} \int_{V_i} \{(\mathbf{Q} + [\mathbf{j}\xi])\,\mathbf{Q} + (\gamma p \operatorname{div} \xi + \xi \nabla p) \operatorname{div} \xi\}\, d\tau; \tag{2}$$

$$\delta W_\Sigma = \frac{1}{2} \int_{\Sigma} \{\mathbf{B}(\mathbf{B}\nabla)\,\mathbf{n} - \mathbf{B}_e(\mathbf{B}_e\nabla)\,\mathbf{h}\}\, \xi_n^2\, d\sigma; \tag{3}$$

$$\delta W_e = \frac{1}{2} \int_{V_e} (\operatorname{rot} \delta \mathbf{A}_e)^2\, d\tau; \quad \mathbf{Q} = \delta \mathbf{B} = \operatorname{rot} [\xi \mathbf{B}]. \tag{4}$$

The notation is interpreted as follows: p denotes the plasma pressure; B and $\mathbf{B}_e$ denote the undisturbed magnetic fields inside and outside the plasma, respectively; $\delta\mathbf{B}$ and $\delta\mathbf{B}_e = \operatorname{rot} \delta\mathbf{A}_e$ are the disturbing magnetic fields inside and outside the plasma, respectively; Σ denotes the boundary between the plasma and the vacuum; and **n** denotes the normal to the surface.

When no surface currents exist, i.e., when no tangential discontinuity of B occurs, the surface integral δW_Σ tends to zero and consequently, positive δW_i values guarantee plasma stability.

When Φ and J denote the logitudinal and χ and I the transverse fluxes of the vectors B and **j**, respectively, then, in the natural coordinate system ($d\mathbf{r} = \mathbf{e}_1 d\theta + \mathbf{e}_2 d\xi + \mathbf{e} dV$) which is related to the system of imposed magnetic surfaces by the equilibrium configuration of [2], the vectors B and **j** can be expressed by the derivatives of the fluxes with respect to the volume V:

$$\mathbf{B} = \chi' \mathbf{e}_1 + \Phi' \mathbf{e}_2; \quad \mathbf{j} = I' \mathbf{e}_1 + J' \mathbf{e}_2. \tag{5}$$

When we use the invariant characteristics

$$p' = I'\Phi' - J'\chi'; \quad \Omega = I'\Phi'' - J'\chi''; \quad S = \chi'\Phi'' - \Phi'\chi'', \tag{6}$$

we can represent the equations for δW_i (in the natural coordinates θ, ξ, and V) in the form of [3]:

$$\delta W_i = \frac{1}{2} \int \{(\mathbf{Q} + [\mathbf{je}]\,\xi)^2 + \gamma p\,(\operatorname{div} \xi)^2 - (\Omega + [\mathbf{je}]^2)\,\xi^2\}\, d\tau. \tag{7}$$

The expansion coefficients of the vector **e** expansion in **j** and **B** are

$$\mathbf{e} = \nabla V / |\nabla V|^2 + (\nu \mathbf{j} - \lambda \mathbf{B})/p' \tag{8}$$

and satisfy the following "magnetic" differential equations:

$$\mathbf{B}\nabla\nu = S - \mathbf{Bj}^*/|\quad|^2; \quad \mathbf{B}\nabla\lambda = \Omega - \mathbf{jj}^*/|\nabla V|^2, \tag{9}$$

where

Translated from Atomnaya Énergiya, Vol. 30, No. 1, pp. 14-20, January, 1971. Original article submitted April 3, 1970; revision submitted June 15, 1970.

$$\mathbf{j}^* = \mathbf{j} - 2[\nabla V, (\nabla V \nabla)\mathbf{B}]/|\nabla V|^2. \tag{10}$$

Let us introduce combinations of the displacement components: $\eta = \Phi'\xi^1 - \chi'\xi^2$, $\vartheta = J'\xi^1 - I'\xi^2$. We obtain $\operatorname{div}\xi = \xi' + (\mathbf{j}\nabla\eta - \mathbf{B}\nabla\vartheta)/p'$, where $\xi = \xi^3$, and, hence, δW_i can be written in the form

$$\delta W_i = \frac{1}{2}\int \{([\nabla\eta\nabla V] - (\mathbf{B}\xi)' + (\mathbf{B}\nabla\xi)\mathbf{e} + [\mathbf{je}]\xi)^2 + \gamma p(\operatorname{div}\xi)^2 - (\Omega + [\mathbf{je}]^2)\xi^2\}\, d\tau, \tag{11}$$

where the vector $\mathbf{B}'$ is given by the equation

$$\mathbf{B}' = \chi''\mathbf{e}_1 + \Phi''\mathbf{e}_2 = (\mathbf{B}\Omega - \mathbf{j}S)/p'; \tag{12}$$

the primes denote derivatives with respect to the volume V.

Stability of a Plasma Cylinder

General Relations. It suffices to consider the stability of each helical harmonic $\xi = \xi(r)e^{im(\varphi - \alpha z)}$, $\alpha = k/m$, $k = 2\pi n/L$, where m and n denote integers, for investigating the stability of a plasma cylinder with identical end faces at z = 0 and z = L (toroid model). It follows from the minimization condition [4] that $\xi = 0$, i.e., noncompressed oscillations are most dangerous. We have

$$\delta W_i = \pi L \int_0^a \left\{\frac{1}{\beta r}[y(r\xi)' - 2b_\varphi\xi]^2 + (m^2y^2 - 2b_\varphi j_z) r\xi^2\right\} dr. \tag{13}$$

The following notation is employed: $\beta = 1 + \alpha^2r^2$; $b_\varphi = B_\varphi/r$; $y = \alpha B_z - b_\varphi$; $\xi = \xi_r$; the prime denotes differentiation with respect to r. When we introduce the notation $j_\parallel = j_z + \alpha r j_\varphi$, $j_\perp = j_\varphi - \alpha r j_z$ and use the variable $f = ry\xi$ in place of the radial displacement component, the sum $\delta W_i + \delta W_e = \delta W_V$ is represented by a single integral which must be taken over the plasma region $0 < r < a$ and the external magnetic field region $a < r < b$, where b denotes the radius of a shield with ideal conductivity:

$$\delta W_V = \pi L \int_0^b \left\{\frac{r}{\beta}\left(f' + \frac{j_\parallel f}{ry}\right)^2 + \left(\frac{m^2}{r} - \frac{2j_z b_\varphi}{ry^2}\right) f^2\right\} dr, \tag{14}$$

where we have

$$\delta W_\Sigma = \pi L[\xi^2(B_\varphi^2 - B_{\varphi e}^2)]_a. \tag{15}$$

When current-density discontinuities occur on the radii r_k, we can write for δW_V

$$\frac{\delta W_V}{\pi L} = \int_0^b \left\{\frac{r}{\beta}f'^2 + \left[\frac{m^2}{r} - \frac{1}{\beta y}\left(\frac{2\alpha}{\beta}j_\perp + j_\parallel'\right) + \frac{2\alpha^2 p'}{\beta y^2}\right] f^2\right\} dr + \sum_k \left[\frac{r^2\xi^2}{\beta}(j_\parallel^i y_i - j_\parallel^e y_e)\right]_{r_k}. \tag{16}$$

When the function f satisfies the Euler equation

$$\left(\frac{r}{\beta}f'\right)' - \left[\frac{m^2}{r} - \frac{1}{\beta y}\left(\frac{2\alpha}{\beta}j_\perp + j_\parallel'\right) + \frac{2\alpha^2 p'}{\beta y^2}\right] f = 0 \tag{17}$$

in the space between the discontinuities, then δW_V can be represented in the form of a sum over the discontinuities:

$$\delta W_V = \pi L \sum_k \left[\frac{r^2\xi^2}{\beta}\left(\frac{rf_i'}{f_i}y_i^2 - \frac{rf_e'}{f_e}y_e^2 + j_\parallel^i y_i - j_\parallel^e y_e\right)\right]_{r_k}. \tag{18}$$

It follows from Eq. (16) that plasma instabilities can result from discontinuities of the current density. However, this type of instability does not really occur when a singular point r_s is situated within the plasma so that $y(r_s) = 0$, because in this case, the disturbance drifts to infinity [5]. The expression for δW_V can be written in the form

$$\frac{\delta W_V}{\pi L} = \int_0^a \left\{\frac{r^3y^2}{\beta}\xi'^2 + \left[\left(m^2 - \frac{1}{\beta}\right)\frac{y^2}{r} + \frac{2\alpha^2 r}{\beta^2}(\alpha^2B_z^2 - b_\varphi^2) + \frac{2\alpha^2p'}{\beta}\right] r^2\xi^2\right\} dr + \left[\frac{r^2\xi^2}{\beta}(\alpha^2B_z^2 - b_\varphi^2)\right]_a + \int_a^b \left(\frac{r}{\beta}f'^2 + \frac{m^2}{r}f^2\right) dr. \tag{19}$$

The possible instabilities can be divided into two classes, namely internal instabilities resulting from a negative value of the volume integral in Eq. (16), and surface instabilities or discontinuous instabilities resulting from negative values of the surface integrals in Eqs. (16) and (19). Internal instabilities, which are also present when the plasma boundary is fixed $\xi(a) = 0$, develop with relatively smaller increments (in the ratio B_z/B_φ) when the ratio B_φ/B_z is small.

In the case of a cylindrical geometry, Suydem's criterion [6] is a necessary condition for plasma stability:

$$\mu'^2/4+2\mu^2p'/rB_z^2>0; \quad \mu=B_\varphi/rB_z; \tag{20}$$

this equation is obtained under the assumption that the disturbances are localized in a thin cylindrical layer.

In a low-pressure plasma (for $B_\varphi/B_Z \ll 1$), the solution ξ = const satisfies the Euler equation, and a necessary condition for the absence of surface instabilities for a plasma cylinder without surface currents is obtained from Eq. (18) [7]:

$$LB_\varphi(a)/2\pi aB_z(a)<1. \tag{21}$$

According to Eq. (19), a sufficient condition for the internal stability is obtained from the following two requirements:

$$LB_\varphi(r)/2\pi rB_z(r)<1; \tag{22}$$

$$rp'-\frac{2B_\varphi^2}{m^2-1}\frac{B_\varphi^2}{B_z^2}>0, \tag{23}$$

for m = 1 and m ≥ 2, respectively. When condition (22) is satisfied, only disturbances which are almost constant along the magnetic force lines cause instabilities in the case $B_\varphi/B_Z \ll 1$.

The absence of zeros in the solution of the Euler equation for the function $\xi(r)$ in the interval $0 < r < a$ is a sufficient and necessary condition for the internal stability of a plasma [4].

Plasma Cylinder with Surface Currents. In the absence of distributed currents, when only a tangential discontinuity of **B** exists at the plasma boundary, the condition (21) suffices for the plasma stability in the case $B_{zi} = B_{ze}$, whereas the condition $B_{\varphi e} < B_{zi}$ must be satisfied in the case $B_{ze} = 0$ [8].

Plasma Cylinder with Uniform Current. In the case j_Z = const and B_Z = const, the Euler equation (17) has the exact solution

$$f=\varepsilon J_m(\varkappa r)-\alpha\varkappa rJ'_m(\varkappa r), \quad \varkappa^2=\varepsilon^2-k^2, \tag{24}$$

where $\varepsilon = 2\alpha b\varphi/y$ = const. The configuration under consideration is unstable because Suydem's criterion (20) is not satisfied. The condition of [9],

$$LB_\varphi/2\pi rB_z<1/m, \tag{25}$$

is a necessary condition for the absence of sudden instabilities. However, this condition cannot be satisfied in the case of large m values.

Force-Free Configuration. In the case $\mathbf{j} = \varepsilon\mathbf{B}$, ε = const, $B_Z = B_0J_0(\varepsilon r)$, and $B_\varphi = B_0J_1(\varepsilon r)$, the function stated in Eq. (24) is a solution to Eq. (17). In order to obtain internal stability of the mth mode, the conditions $ja/B < x_{m1}$ [10] must be satisfied, wherein x_{m1} denotes the first root of $J_m(x)$.

When a free boundary is present, an instability caused by a discontinuous current density is possible. In order to stabilize this instability, the singular point $r = r_s$ (where $y = B_0[\alpha J_0(\varepsilon r) - J_1(\varepsilon r)/r] = 0$) must be situated within the plasma. Consequently, in the case of an instability with long-wave oscillations $\alpha r \ll 1$, the relation $\varepsilon a > x_{11}$ must hold, where even the necessary stability condition (25) is satisfied for $\varepsilon a \approx x_{11}$. Thus, the stability conditions for a plasma with a free boundary establish a force-free configuration with $\varepsilon a \approx x_{11} \approx 3.8$ in which B_Z and j_Z change their signs inside the plasma at $r/a \approx x_{01}/x_{11} \approx 0.63$.

Internal Interruption of the Current Density. When $j = j_Z$ = const for $0 < r < r_0$ and $j = 0$ for $r_0 < r < a$, a discontinuity-induced instability of the plasma cylinder with a free boundary at $b \to \infty$ is stabilized when the condition of [7] is satisfied:

$$r_0^2/a^2<1-1/m. \tag{26}$$

In order to satisfy the mode with m = 1, it is necessary and sufficient that inequality (21) be satisfied.

Parabolic Distribution of the Current Density. In the case $j = j_Z = j_0(1-\varepsilon r^2/a^2)$, we obtain for the necessary condition for the surface instabilities to be absent on a plasma cylinder with a free boundary ($b \to \infty$)

$$\left|1-\frac{2m+1}{m+2}\cdot\frac{\varepsilon}{m+1}\right|<\sqrt{1-\frac{1}{m}\cdot\frac{2m+1}{m+2}}. \tag{27}$$

This expression is obtained from Eq. (19) at $\xi = r^{m-1}$. This means that it is necessary to reduce the current density $\varepsilon > 0$. In the case $m \geq 2$, the instabilities under consideration are stabilized for $\varepsilon = 1$ when $j(a) = 0$.

Stabilizing Effect of Conducting End Faces

When in Eq. (11) for δW_i, we neglect the term $\gamma p(\mathrm{div}\,\xi)^2$ and replace the vector in the first bracket with its projection upon ∇V, we obtain

$$\delta W_i \geqslant \frac{1}{2}\int \{(\mathbf{B}\nabla\xi)^2/|\nabla V|^2 - (\Omega + j^2/|\nabla V|^2 - \mathbf{B}\nabla\lambda)\,\xi^2\}\,d\tau. \tag{28}$$

In deriving stability criteria for a plasma configuration whose magnetic force lines can be assumed to be frozen in walls with ideal conductivity, we must postulate that the tangential component of ξ vanishes at the end faces [4]. When we integrate along the force lines, we have $\mathbf{B}\nabla\xi = \Phi\,d\xi/d\zeta$. Taking into account the condition $\xi = 0$ at the end faces $\zeta = 0$ and $\zeta = 1$, we obtain $\int_0^1 (d\xi/d\zeta)^2\,d\zeta \geq \pi^2 \int_0^1 \xi^2\,d\zeta$. Thus, according to Eq. (28), we can obtain from this expression a sufficient condition for stability:

$$\left\langle \frac{\pi}{|\nabla V|^2} \right\rangle \Phi'^2 - \frac{j^2}{|\nabla V|^2} - \Omega + \mathbf{B}\nabla\lambda > 0, \tag{29}$$

where the angular brackets denote averaging over the layer volume between neighboring magnetic surfaces:

$$\langle f \rangle = \frac{d}{dV}\int f\,d\tau. \tag{30}$$

Contrary to the necessary stability condition obtained by B. B. Kadomtsev [4], the criterion stated in Eq. (29) includes a restriction for the longitudinal current. In the case of a plasma cylinder with end faces having ideal conductivity at $z = 0$ and $z = L$, we have $V = \pi r^2 L$, and $\mathbf{B}\nabla\lambda = 0$. In this case, the sufficient stability condition of (29) assumes the form

$$\pi^2 B_z^2/L^2 - 2j_z B_\varphi/r > 0. \tag{31}$$

If $j = j_Z = \text{const}$, we obtain from Eq. (31) a restriction for the longitudinal current:

$$j_z L/\pi B_z < 1.$$

In deriving a necessary stability condition, we restrict ourselves to the case of a plasma cylinder with a uniform current $j = j_Z = \text{const}$ and assume shifts in the form $\xi = \xi(r)\sin m(\varphi - \mu z)\sin kz$, $\eta = \eta(r)\cos m(\varphi - \mu z)\sin kz$, where $k = \pi n/L$. In this case, the tangential components of the electric field $\mathbf{E} = (1/c)(\partial/\partial t)[\xi\mathbf{B}]$ vanish at the end faces $z = 0$ and $z = L$. The minimization of δW_i with respect to η leads to the following expression for a low-pressure plasma

$$\frac{\delta W_i}{\pi L} = B_z^2 \int_0^a \left\{ \frac{\alpha^2 [f'^2 + \mu^2 r^6 (f/r^2)'^2] - 4\mu^2(\mu^2+\alpha^2) f^2}{1 + (\mu^2+\alpha^2) r^2} + \frac{k^2}{r^2} f^2 \right\} r\,dr, \tag{32}$$

where $f = r\xi$. For $\mu^2 a^2 \ll 1$ and $\alpha^2 a^2 \ll 1$, we obtain

$$\delta W_i = \pi L B_z^2 \alpha^2 \int_0^a \{f'^2 + (m^2/r^2 + 4\mu^2 - 4\mu^4/\alpha^2) f^2\}\, r\,dr \tag{33}$$

and the corresponding Euler equation has the solution $f = J_m(2\mu r\sqrt{\mu^2/\alpha^2 - 1})$. This means that the necessary condition for the internal stability at $\xi(a) = 0$ is most restrictive for $m = 1$:

$$\mu a < \sqrt{\pi a x_{11}/2L} \approx \sqrt{2\pi a/L}, \tag{34}$$

and this imposes a restriction on the longitudinal current $j_Z a/B_Z < \sqrt{8\pi a/L}$.

Stability of Closed Toroidal Configurations

Stabilization of the Lowest Modes. A condition for the stabilization of the lowest modes can be easily derived from Eq. (28). For the sake of simplicity, we restrict ourselves to configurations with circular cross sections of the magnetic surfaces and with a small curvature of the magnetic axis. We assume that the longitudinal current decreases in radial direction. Thus, we obtain the following sufficient stability condition for the mode m:

$$jL/4\pi B < 1/(m+2). \tag{35}$$

Analog to Eq. (25), this condition is not satisfied for large m values.

Potential Energy of Helical Harmonics. Let us consider δW_i for a single helical harmonic of a disturbance and assume $\xi = \xi(V)\cos 2\pi \times (n\zeta - m\theta)$. We introduce the notation $u = n\Phi' - m\chi'$, $v = nJ' - mI'$, $\mathbf{c} = n\mathbf{e}_1 + m\mathbf{e}_2 = (ju - vB)/p'$. When we restrict ourselves to a toroidal configuration with axial symmetry, we obtain from the minimization of Eq. (11) with respect to η:

$$\delta W_i = \frac{1}{2}\int \left\{\frac{1}{c^2}(\nabla V (u\xi)' - [\mathbf{c}[\mathbf{je}]])^2 + ([\mathbf{ce}]^2\frac{u^2}{c^2} - \Omega - [\mathbf{je}]^2)\,\xi^2\right\} d\tau. \tag{36}$$

When we assume that ξ and $\mathbf{jc}$ vanish at the plasma boundary, we obtain by partial integration:

$$\delta W_i = \frac{1}{2}\int \left\{\left\langle\frac{|\nabla V|^2}{c^2}\right\rangle (u\xi)'^2 + \left\langle\frac{[\mathbf{ce}]^2}{c^2}\right\rangle u^2 + \left[\frac{v}{\chi'}\cdot\frac{I'+B'e_2}{c^2} - \frac{nI'}{\chi'^2}\cdot\frac{p'+BB'}{c^2}\right.\right.$$
$$\left.\left. - \left\langle\frac{\mathbf{jc}}{c^2}\right\rangle'\right] u + \frac{n^2}{\chi'^2}\left\langle\frac{S\mathbf{jB} - \Omega B^2 - p'^2}{c^2}\right\rangle \xi^2\right\} d\tau. \tag{37}$$

In the case of a cylindrical geometry, this expression transforms into Eq. (16), provided that no tangential discontinuities of the current density are present. It is essential that in the transition to toroidal geometry, the term $\sim p'(r)$ (which is responsible for the internal instability of the plasma cylinder) is replaced, in accordance with the relation

$$\frac{b_\varphi^2 p'(r)}{\beta\pi L} \to S\left\langle\frac{\mathbf{jB}}{c^2}\right\rangle - \Omega\left\langle\frac{\mathbf{B}^2}{c^2}\right\rangle - \left\langle\frac{p'^2}{c^2}\right\rangle, \tag{38}$$

with a quantity which becomes positive for $p' < 0$ and at sufficiently small currents. We note that the two first terms on the right side of Eq. (38) characterize the stabilizing effect of $\min \overline{B}$.

Sufficient Conditions for the Stability of Toroidal Configurations. We represent the vector $\mathbf{B}$ by an expansion in powers of V:

$$\mathbf{B} = \mathbf{B}_0 + \mathbf{B}_0' V + \mathbf{B}_0'' V^2/2 + \ldots;\ \mathbf{B}_0^{(n-1)} = \chi_0^{(n)}\mathbf{e}_1 + \Phi_0^{(n)}\mathbf{e}_2. \tag{39}$$

When we replace the vector in the first bracket of Eq. (11) by its projection upon $[\mathbf{B}_0\mathbf{e}]$ and use the Schwartz inequality, we obtain

$$\delta W_i \geqslant \frac{1}{2}\int \{\langle S(V\xi)' + [\mathbf{je}][\mathbf{B}_0\mathbf{e}]\xi\rangle^2 \langle[\mathbf{B}_0\mathbf{e}]^2\rangle^{-1} - (\Omega + [\mathbf{je}]^2)\,\xi^2\}\, d\tau. \tag{40}$$

Taking into account that, in the case of small currents, the dangerous disturbances are close to constant disturbances along the magnetic force lines so that $\xi \approx \xi_0$, where $\mathbf{B}_0\nabla\xi_0 = 0$, we obtain by partial integration over the variable V the following condition for the positiveness of δW_i:

$$S\langle[\mathbf{je}][\mathbf{Be}]\rangle - \Omega\langle[\mathbf{Be}]^2\rangle - (\langle[\mathbf{je}]^2\rangle\langle[\mathbf{Be}]^2\rangle - \langle[\mathbf{je}][\mathbf{Be}]\rangle^2) > 0. \tag{41}$$

It is assumed in the derivation of Eq. (41) that the current density decreases with the distance from the magnetic axis and that the boundary conditions $\xi_\Sigma = 0$ or $j_\Sigma = 0$ were used. Thus, inequality (41) is a sufficient condition for the internal stability of the plasma configuration. As follows from the above analysis of the stability of a plasma cylinder, when we wish to stabilize a surface instability for $m \geq 2$, it suffices for the stability of a toroidal configuration to satisfy Eq. (41) and the additional condition $|JL/\Phi'V|_\Sigma < 4\pi$ for the first helical disturbance mode.

One can use Mercier's orthogonal coordinates [11] ρ, ω, and s for determining the vector $\mathbf{e} = |\nabla\theta\nabla\zeta|$. After assuming $\theta = \omega/2\pi + \tilde{\theta}$, and $\zeta = s/L + \bar{\zeta}$, we obtain equations for $\tilde{\theta}$ and $\bar{\zeta}$:

$$\mathbf{B}\nabla\tilde{\theta} = \chi' - B_\omega/2\pi\rho, \quad \mathbf{B}\nabla\bar{\zeta} = \Phi' - B_s/h_s L, \tag{42}$$

where $h_s = 1 + k\rho\cos(\omega = \int \varkappa\, ds)$; k and $\varkappa$ denote the curvature and twisting of the magnetic axis s, respectively.

In a configuration with axial symmetry and circular cross sections of the magnetic surfaces, the vector $\mathbf{e}$ is approximated by

$$\mathbf{e} = \frac{\nabla V}{|\nabla V|^2} - \frac{B_\varphi \sin\omega}{\pi^2 R^2 \rho j}\,\mathbf{e}_\varphi, \tag{43}$$

when quasi-homogeneity is assumed. R denotes the radius of the magnetic axis. In this case, criterion (41) reduces to

$$-p'\left[\frac{1}{R^2}\left(1+\frac{\rho p'}{B_\omega^2}\right)-\mu^2\right]>0, \tag{44}$$

where $\mu = B_\omega/\rho B\varphi$. Condition (44) agrees exactly with the sufficient stability condition derived in [12] in another way. As has been shown in [13], the necessary stability criterion of Mercier [14] leads to the restriction

$$\frac{\mu'^2}{4}-\frac{2p'}{\rho B_\varphi^2}\left(\frac{1}{R^2}-\mu^2\right)>0; \tag{45}$$

for the configuration under consideration; the term $1/R^2$ in criteria (44) and (45) characterizes the stabilizing effect of the magnetic bottle which is created when a plasma cylinder is bent into a toroid.

Mechanisms of Hydromagnetic Plasma Stability

It follows from the theory of hydromagnetic stability of plasma configurations that a magnetic bottle (which arises only in configurations with a rather complicated geometry) provides a highly stabilizing effect. Of particular interest in this connection are stability criteria which are not related to an actual plasma geometry.

The concept of a magnetic bottle or well was introduced by Rosenbluth and Longmire [15]. Their stability condition can be reduced to the requirement that a magnetic well $V''(\Phi) < 0$ exists. In configurations with closed magnetic force lines, this condition assumes the form

$$-\Omega>0 \tag{46}$$

in our notation stated in Eq. (6).

B. B. Kadomtsev [16] obtained a necessary and sufficient condition for the stability of a low-pressure plasma under the assumption of closed force lines

$$-\Omega+\gamma p\Omega^2/p'^2>0. \tag{47}$$

Necessary stability conditions were obtained in [17] for configurations with closed force lines under the assumption that the disturbances were constant along the force lines. The corresponding conditions are

$$-\Omega\langle\mathbf{B}^2\rangle-p'^2>0, \qquad \gamma p\Omega-p'^2>0 \tag{48}$$

and the plasma is unstable, if one of the inequalities (48) is not satisfied. The second condition (48) can be satisfied only in configurations without a magnetic well: $\Omega > 0$. This means that the first inequality (48) is a necessary condition for the "convective" stability of configurations with a magnetic bottle or well. The first inequality of (48) can be written in the equivalent form

$$-p'\left\langle\frac{\partial}{\partial V}\left(p+\frac{B^2}{2}\right)\right\rangle>0, \tag{48'}$$

which for $p'(V) < 0$ reduces to the requirement that the average derivative with respect to V is positive from the "full pressure" $p + B^2/2$.

A necessary stability criterion, which is independent of the actual plasma geometry, was obtained in [14, 18, 19] for disturbances localized in a thin layer between neighboring magnetic surfaces. As has been shown in [20], this criterion can be written in the form

$$\frac{S^2}{4}+S\left\langle\frac{\mathbf{jB}}{|\nabla V|^2}\right\rangle-\Omega\left\langle\frac{\mathbf{B}^2}{|\nabla V|^2}\right\rangle-\left(\left\langle\frac{\mathbf{j}^2}{|\nabla V|^2}\right\rangle\left\langle\frac{\mathbf{B}^2}{|\nabla V|^2}\right\rangle-\left\langle\frac{\mathbf{jB}}{|\nabla V|^2}\right\rangle^2\right)>0. \tag{49}$$

A sufficient stability criterion

$$-\Omega-[\mathbf{je}]^2>0 \tag{50}$$

was obtained in [3] with the only assumption that surface currents are absent. In [3], there was also obtained a sufficient criterion for the internal plasma stability under the assumption that the equilibrium configurations considered are quasi-homogeneous:

$$S\langle[\mathbf{je}][\mathbf{Be}]\rangle-\Omega\langle[\mathbf{Be}]^2\rangle-(\langle[\mathbf{je}]^2\rangle\langle[\mathbf{Be}]^2\rangle-\langle[\mathbf{je}][\mathbf{Be}]\rangle^2)>0. \tag{51}$$

Criterion (51) has been generalized in the present article to the case of a decreasing current density. In order to obtain stability, it suffices in this case to satisfy criterion (51) and the additional condition

$$|JL/\Phi' V|_\Sigma < 4\pi. \tag{52}$$

As has been shown in [3], a sufficient condition for internal stability of quasi-homogeneous configurations is identical with criterion (49) without the term $S^2/4$. Assuming that the vicinity of the magnetic axis is the most critical region as far as stability is concerned, it suffices to satisfy criterion (49) (which is less restrictive than criterion (51)) in order to obtain stable configurations with decreasing current densities.

It follows from Eq. (7) that currents in the plasma are a destabilizing factor leading to instabilities. In toroidal configurations without longitudinal currents, a decreasing plasma pressure implies destabilization; in systems with longitudinal currents, the destabilizing effect of the longitudinal current must be added. Consequently, the stability conditions reduce to restrictions for the plasma pressure and the longitudinal current in the plasma. A magnetic bottle, which is characterized by the quantity Ω in the case of configurations with closed force lines, or identical second and third terms in expression (49) for arbitrary configurations, or the spread, which is characterized by the term $S^2/4$ in (49), act as stabilizing factors in criteria (46)-(51).

For the purpose of comparison, we apply criteria (46)-(51) to a "Tokamak" system under the condition that the magnetic field is quasi-homogeneous and that $p'(\rho^2) < 0$. We obtain the following relations from the criteria (46), (48), (49), and (51):

$$\frac{1}{R^2} - \frac{j^2}{4B^2} - \frac{2p'}{j^2R^2} - \frac{p'}{B^2} > 0; \tag{53}$$

$$\frac{1}{R^2} - \frac{j^2}{4B^2} - \frac{2p'}{j^2R^2} > 0; \tag{54}$$

$$\frac{1}{R^2} - \frac{j^2}{4B^2} > 0; \tag{55}$$

$$\frac{1}{R^2} - \frac{j^2}{4B^2} + \frac{2p'}{j^2R^2} > 0. \tag{56}$$

In the case of an extremely small plasma pressure, criteria (53)-(56) reduce to the restrictions stated in (55) for the longitudinal current. The necessary stability conditions (53) and (54) are less restrictive than the necessary condition (55), because the destabilizing effect of a finite plasma pressure was not properly taken into account in (53) and (54). The sufficient condition (56) contains an additional restriction for the plasma pressure (compared to condition (55)).

As has been shown in [21], the sufficient stability condition (50) can be satisfied in systems without a longitudinal current when $\beta_B = 2p/B^2$ is small enough. This means that the mechanism created by a magnetic well is adequate for stabilizing hydromagnetic instabilities in these configurations.

Condition (52) for the length of the system, along with criterion (51), in which the magnetic well is the only stabilizing factor, are sufficient conditions for internal stability of configurations with longitudinal currents. In the case of a free plasma boundary, additional restrictions appear. Condition (52) becomes a necessary condition for the stabilization of helical instabilities (m = 1), for which the finite length of the system plays the role of a stabilizing factor. Apart from this, there arise restrictions for the current distribution, i.e., the current density must decrease rapidly with increasing distance from the magnetic axis.

In configurations with a circular magnetic axis and a circular transverse cross section of the magnetic surfaces (Tokamak type), the depth of the magnetic well is given by the curvature of the magnetic axis. According to the necessary condition (49), in the case of a parabolic pressure distribution, a nonvanishing stability region appears only when the plasma cylinder is folded to a toroid. In more complicated configurations, the depth of the magnetic well depends on the form of the cross section of the magnetic surfaces as well as on both the curvature and the twisting of the magnetic axis [22-25].

A strong stabilizing mechanism resulting from the stress effect created by magnetic force lines [4] arises in certain plasma configurations with magnetic force lines frozen into conductive end faces. As shown by the additional criterion (31), a plasma cylinder with frozen magnetic end sections is a hydromagnetically stable configuration, provided that the longitudinal currents are small enough.

LITERATURE CITED

1. I. Bernstein et al., Proc. Roy. Soc., A244, 17 (1958).
2. S. Hamada, Nucl. Fusion, 1-2, 23 (1962).
3. L. S. Solov'ev, ZhETF, 53, 2063 (1967).
4. B. B. Kadomtsev, Problems of Plasma Theory [in Russian], Vol. 2, Atomizdat, Moscow (1963).
5. W. Newcomb, Ann. Phys., 10, 232 (1960).
6. B. Suydem, Proc. of Intern. Conf. Peaceful Uses Atomic Energy, Vol. 31, United Nations, Geneva (1958).
7. V. D. Shafranov, Zhur. Tekh. Fiz., 40, 241 (1970).
8. V. D. Shafranov, Atomnaya Énergiya, 5, 38 (1956).
9. V. D. Shafranov, Plasma Physics and Problems of Controlled Thermonuclear Reactions [in Russian], Vol. 4, Izd. Akad. Nauk SSSR, Moscow (1958).
10. A. I. Morozov and L. S. Solov'ev, Dokl. Akad. Nauk SSSR, 158, 831 (1964).
11. C. Mercier, Nucl. Fusion, 3, 89 (1963).
12. A. Ware and F. Haas, Phys. Fluids, 9, 956 (1966).
13. V. D. Shafranov and E. I. Yurchenko, ZhÉTF, 53, 1157 (1967).
14. C. Mercier, Int. Conf. Plasma Phys. and Contr. Nucl. Fusion, Salzburg (1961), p. 95.
15. M. Rosenbluth and C. Longmire, Ann. Phys., 1, 120 (1966).
16. B. B. Kadomtsev, Plasma Physics and Problems of Controlled Thermonuclear Reactions [in Russian], Vol. 4, Vol. 4, Izd. Akad. Nauk SSSR, Moscow (1958), p. 16.
17. B. B. Kadomtsev, Plasma Physics and Problems of Controlled Thermonuclear Reactions [in Russian], Vol. 4, Vol. 4, Izd. Akad. Nauk SSSR, Moscow (1958), p. 380.
18. M. Binean, Int. Conf. Plasma Phys. and Contr. Nucl. Fusion, Salzburg (1961), p. 35.
19. J. Green and J. Johnson, Phys. Rev. Letters, 7, 401 (1961).
20. L. S. Solov'ev, ZhÉTF, 53, 626 (1967).
21. V. Shafranov and E. Yurchenko, Nucl. Fusion, 9, 285 (1969).
22. L. S. Solov'ev and V. D. Shafranov, Problems of Plasma Theory [in Russian], Vol. 5, Atomizdat, Moscow (1967).
23. L. S. Solov'ev, Dokl. Akad. Nauk, 182, 1052 (1968).
24. L. Solov'ev et al., Plasma Phys. and Contr. Nucl. Fusion Research (Proc. Conf. Novosibirsk, 1968), Vol. 1, IAEA, Vienna (1969), p. 175.
25. N. M. Zueva and L. S. Solov'ev, Atomnaya Énergiya, 26, 35 (1969).

INVESTIGATION OF THE INSTABILITIES OF THE PLASMA STRING IN THE TOKAMAK-3 SYSTEM BY MEANS OF A CORRELATION METHOD

S. V. Mirnov and I. B. Semenov

UDC 621.039.626:533.933.8

The present article considers instabilities of the plasma string which develop in the Tokamak-3 system when the stability reserve $q = H_z a / H_\varphi R$ is reduced (H_φ denotes the magnetic field generated by the current; H_z is the stabilizing magnetic field; a denotes the small radius of the plasma string; and R is the large radius of the plasma string).

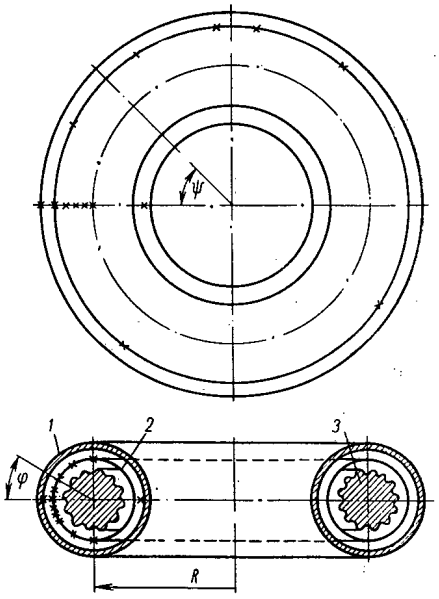

Fig. 1

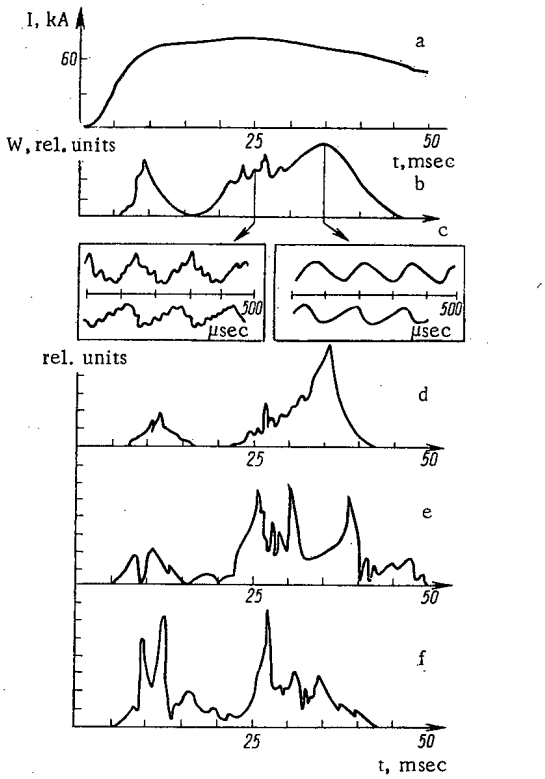

Fig. 2

Fig. 1. Arrangement of the magnetic probes: 1) copper jacket; 2) liner; 3) plasma; ×) magnetic probe.

Fig. 2. Frequency spectrum of the disturbances at q = 3: a) discharge current; b) signal W(t); c) oscillograms of the signals of two magnetic probes placed at angles of 30° in φ direction; d) envelope of the magnetic probe signal after passage through an 8 kc band filter; e) passage through a 10 kc band filter; f) passage through a 15 kc band filter.

Translated from Atomnaya Énergiya, Vol. 30, No. 1, pp. 20-27, January, 1971. Original article submitted September 22, 1969; revision submitted July 8, 1970.

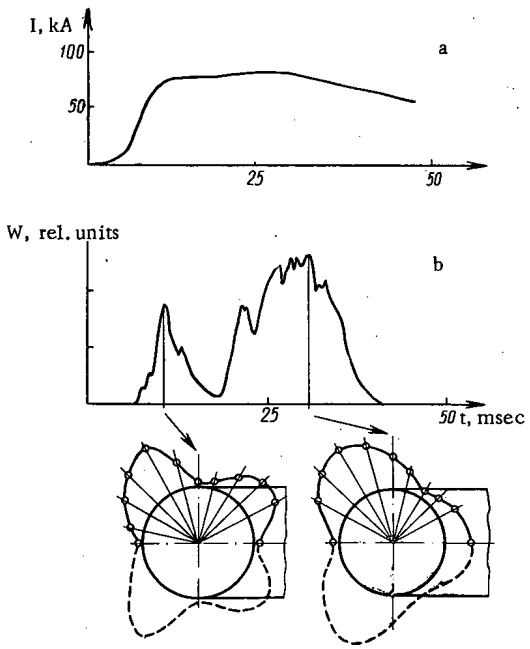

Fig. 3

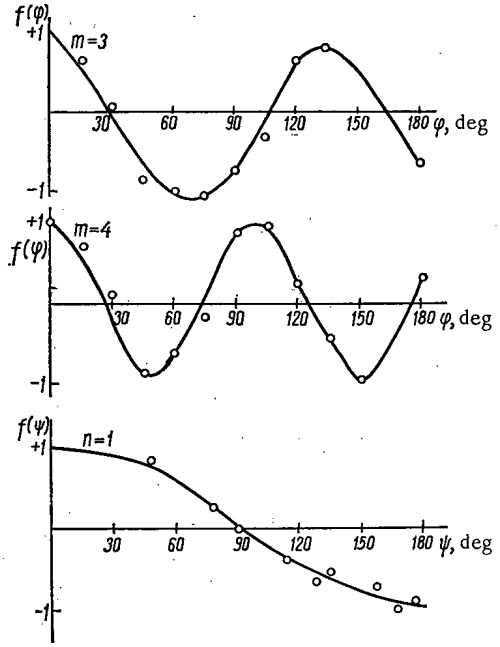

Fig. 4

Fig. 3. Functions $W(\varphi)$ in polar coordinates: a) discharge current; b) oscillogram of W(t). The readings on the circle circumference; the dashed lines denote the mirror image of the curve.

Fig. 4. Dependence of the correlation functions upon φ and ψ in the case of disturbances with m =3 and m =4 (see Fig. 3).

A correlation analysis of the spatial fluctuations of the magnetic field $\tilde{H}_\varphi$ generated by the discharge current was used in investigations of the instabilities. A system comprising 18 magnetic probes on the surface of the discharge chamber (liner) allowed determinations of the spatial structure of the discharge; a set of band filters was used to determine the frequency spectrum.

When one makes the logical assumption that the observed fluctuations of the magnetic field correspond to current-dependent fluctuations of the plasma string's surface, the method used is suitable only for investigating relatively large nonpotential disturbances, i.e., disturbances arising from magnetohydrodynamic instabilities.

It is well known that such instabilities develop in Tokamak systems mainly when q is reduced to 3 [1]. This range of the discharge conditions was investigated in detail. In addition, instabilities arising at q = 2 and in the initial stage of the discharge process at $q \geq 4$ were considered.

All experiments were made with the Tokamak-3 system [2] having the large toroid radius R = 100 cm and the liner radius 20 cm. The stabilizing magnetic field was varied from 17.5 to 26 kOe, the discharge current from 50 to 150 kA, the plasma concentration amounted to $(1\text{-}2)\cdot 10^{13}$ cm^{-3}, and the cross section a of the plasma string was slightly greater than in the preceding experiments; the increased cross section was obtained by increasing the aperture of the limiting diaphragm from 15 to 17.5 cm. The discharge current pulse had a duration of about 70 msec. Hydrogen was used as the test gas.

Observation Method

Figure 1 shows the arrangement of the magnetic probes which consisted of wire coils with a diameter of 10 mm and a length of 30-50 mm oriented parallel to the magnetic field H_φ created by the current. The probes were placed on the outer surface of the toroid, but some additional monitor probes were situated on the inside of the toroid.

The signals derived from the magnetic probes were applied to a four-channel correlation analyzer developed for the experiments. The arriving signals were first subtracted in the analyzer circuits and then

integrated. This procedure resulted in a quantity which is proportional to the difference in the magnetic fields at two points in space. This quantity was squared with semiconductor diodes and averaged over time by integration ($\tau \sim 1$ msec).

The signal $W \sim \bar{H}^2_{\varphi 1} + \bar{H}^2_{\varphi 2} - 2H_{\varphi 1}H_{\varphi 2}$ was then derived from the receiver output and applied to an oscilloscope. We note that for $\bar{H}^2_{\varphi 1} = \bar{H}^2_{\varphi 2} = \bar{H}^2_{\varphi}$, we obtain $W \sim \bar{H}^2_{\varphi}[1 - f(\varphi, \psi)]$, where $f(\varphi, \psi)$ denotes the spatial correlation function of the fluctuations of the magnetic fields [3]; the angular coordinates of the toroid are denoted by φ and ψ (see Figure 1).

The frequency characteristics of the correlation receiver made it possible to conduct measurements in the frequency range 4-40 kc/s. However, the shielding of the magnetic fields by a conductive liner limited quantitative measurements to frequencies below ~15 kc/s.

Since the frequency of the fluctuations was usually below 10 kc/s, a correction taking into account the influence of the liner could not be made.

In the ensuing evaluation of the correlation signals, the correlation functions were calculated when the precise structure of a disturbance had to be determined. In another type of evaluation, the function W was constructed in polar coordinates, which made it possible to estimate the relative magnitude of disturbances in addition to a representation of the disturbance structure.

Structures of the Plasma-String Disturbances

Figure 2b shows one of the oscillograms of W(t). Two different disturbance regions in the plasma string are found in this case. There exists first a region coinciding with the initial part of the discharge; a second region is observed around the maximum of the discharge current. As has been previously described in [4], the first disturbance always occurs. As far as the second region is concerned, it was established that it appears only when the stability reserve q near the boundary of the plasma string decreases to 3 or 2. Under quasi-stationary conditions (growth time of the discharge current approximately 5 msec, plateau length 30 msec, and decline interval 30 msec), a second disturbance region could not be observed at $q \approx 4$.

Let us consider in detail the second disturbance region which arises when q is reduced to 3.

Disturbances of the Plasma String at q = 3. We note that in the case depicted in Fig. 2, the discharge conditions were chosen so that the stability reserve was only slightly greater than 3.

In order to establish the type of disturbances of interest, the signals derived from two magnetic probes placed in φ direction at relative angles of 30° were directly applied to the input of a double-beam oscilloscope.

The horizontal time base had a duration of 500 msec. The triggering occurred at a moment during the development of the discharge. The corresponding oscillograms are shown in Figure 2c for two such moments. One of these moments corresponds to the initial stage of the disturbance, whereas the second moment corresponds to the maximum development stage of the disturbances. Two points are noteworthy: first, the principal component of the observed oscillations has a relatively low frequency; second, the signals of neighboring magnetic probes are shifted in phase. The latter fact indicates that the disturbances under investigation are waves propagating in φ direction. The low frequencies of these waves (4-10 kc/s) imply that the plasma string rotates with a nonuniformly distributed current density $j(\varphi)$ near the boundary. This rotation can result from radial electric fields E_r in that region. One can calculate both the rotation rate v_φ and E_r under this assumption. These quantities vary from $1 \cdot 10^5$ cm/sec to $3 \cdot 10^5$ cm/sec and from 30 V/cm to 75 V/cm, respectively. The rotation occurs as if the plasma were positively charged relative to the walls of the discharge chamber.

Similar disturbances were found in optical observations by N. D. Vinogradova and K. S. Razumova [5] in the TM-2 system. They also assumed a rotation of the plasma string and found, for the corresponding rotation rates, values ranging from $1.5 \cdot 10^5$ cm/sec to $10 \cdot 10^5$ cm/sec.

The band filters, which were put at our disposal by M. N. Shepelev, were used to measure the frequency spectrum of the oscillations recorded by a single magnetic probe.

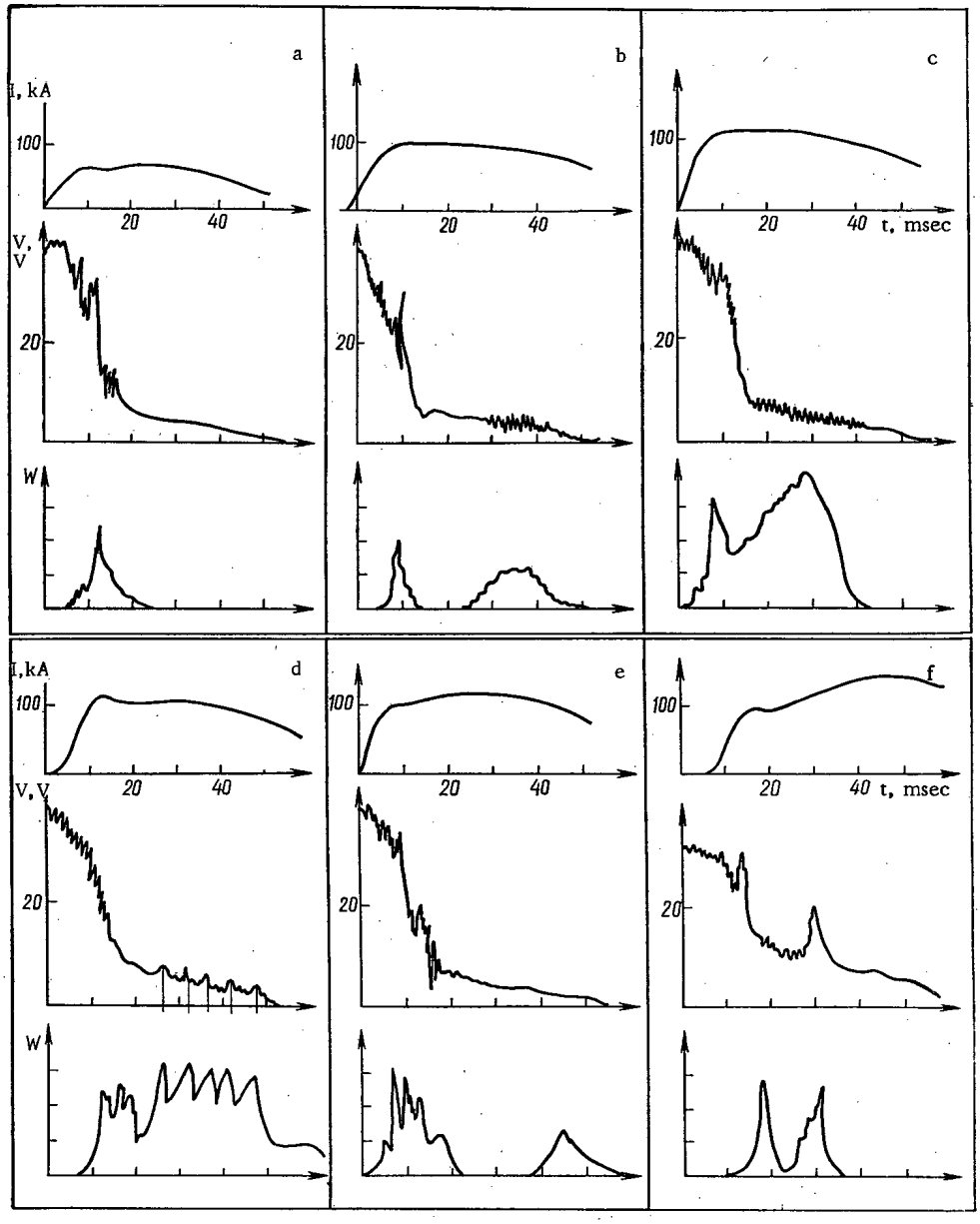

Fig. 5. Development of a resonance disturbance with m = 3 when q is reduced to 3.

Figures 2d, e, and f show as examples the envelopes of the filtered signals for the frequencies 8, 10, and 15 kc/s, respectively. The fact that, in the stage of maximum disturbance development, the spectrum is rather narrow ($\Delta\nu \approx 1$ kc/s) and shifted toward relatively low frequencies (as noticed in the past) is the outstanding feature of the spectrum obtained in this way. In the early development stage of the disturbance, the spectrum extends to 20 kc/s and is less regular. We believe that this behavior can be explained by the generation of a large number of fine disturbances at that stage; the further development of these disturbances results in an accumulation into more powerful and regular disturbance formations.

Some information on the form of these regular disturbances can be obtained from an analysis of the oscillograms shown in Fig. 2c. Since in the case of a constant rotation rate, the signal derived from a magnetic probe is proportional to the derivative of the magnetic field of the disturbance in φ direction, one can conclude from the asymmetry of the oscillograms that the distance between neighboring disturbances in φ direction is much greater than the transverse dimensions of the disturbances. In other words, the disturbances are essentially localized in φ direction.

Our correlation analysis method made it possible to determine the spatial structure of the disturbances. Relationships $W(\varphi)$ for disturbances arising in the initial and medium stages of the discharge are represented in polar coordinates and relative units in Fig. 3. The four-lobe and three-lobe forms mean that the corresponding disturbances have a definite structure with m = 4 and m = 3.

Of particular interest is one feature of the disturbances with m = 3; this feature was more or less typical for all disturbances which we observed. We refer to the asymmetry of the corresponding distribution $W(\varphi)$. The conclusion is that the amplitude of the disturbances decreases from the outer enclosure of the toroid toward the inner enclosure, as one would expect for balloon-type disturbances, i.e., disturbances which develop only on the outer surface of a toroidal plasma string.

However, this conclusion was incorrect. At least two effects could contribute to an apparent attenuation of the disturbances in the measurement system employed. First, the current string could be shifted outward, relative to the center of the liner; second, the correlation function could increase with increasing φ, i.e., the form of the disturbances which were shifted with respect to each other at great angles in φ direction ($\sim 180°$) could be distorted. A measurement of the shift of the current string with the method outlined in [6] revealed that the string's center was shifted, relative to the center of the discharge chamber, by 1-2 cm toward the outside (the configuration of the magnetic probes was concentric to the discharge chamber in the experiments herein described). However, a 2-3 cm inward shifting of the current string by application of magnetic fields transverse to the direction of the discharge current did not change the overall distribution.

On the other hand, direct calculations of the correlation function $f(\varphi)$ show (see Fig. 4) that for m = 3, as well as for m = 4, the form of the disturbances depends only insignificantly upon an increase in φ.

These observations confirm the conclusion that the disturbances develop mainly on the external surface of the plasma string.

A difference amounting to a factor of five was found in direct measurements of the magnetic field fluctuations with the aid of probes placed on the large toroid radius near the internal and external edges of the plasma string (see Fig. 1).

Absolute calculations of the observed disturbances of the magnetic field made it possible to estimate the corresponding disturbances in the discharge current. The disturbances in the discharge current only amount to hundreds of amperes, i.e., they amount to less than 1% of the principal discharge current. Measurements of the correlation function in dependence of the angle ψ (see Fig. 4) reveal that the azimuthal number n = 1 must be ascribed to the disturbances. Since under the discharge conditions considered, the stability reserve along the boundaries is close to 3 (the radius of the string is defined as $d-\Delta$, with d denoting the radius of the diaphragm, and Δ the shift of the current string relative to the chamber's centers), the disturbance under consideration is a resonance disturbance with m = 3 and n = 1 (q = m/n).

It was of interest to observe the further development of the disturbance at increasing discharge currents. When the discharge current is increased in the usual fashion (Fig. 5a to e) without modifying the shape of the discharge pulse, the disturbances with m = 3 become unstable once a certain value $J = J_{cr}$ ($q \approx 3$) is reached (see Fig. 5d). Disruptions occur during the development of the disturbance; the disruptions correspond to not very large, yet noticeable voltage breakdowns. Flashes of the spectral lines of hydrogen are observed, i.e., the string interacts with the walls of the discharge chamber, etc. The maximum current disturbance amounts to 0.5-1 kA at the boundary of the string.

The instability becomes even sharper when the discharge current is increased further on.

However, it turned out that there exists a simple method to reach $q < 3$ without exciting macroscopical instabilities. When the discharge current is increased to values corresponding to $q > 3$ in a stationary discharge characterized by $q < 3$ (see Fig. 5f), a resonance discharge with m = 3 cannot develop into large values, and a stabilization is reached at $3 > q > 2$.

This technique of shaping the discharge current makes it possible to increase the maximum value of the discharge current by 30 to 40%. Though there are indications that discharge conditions involving a rising current can be less favorable than quasi-stationary conditions for the thermal insulation of a plasma [4], we consider it to be an important point that the magnetohydrodynamic instability at q = 3 is not a universal instability in the case of a Tokamak system. An additional increase in the current causes an instability at values as low as q = 2.

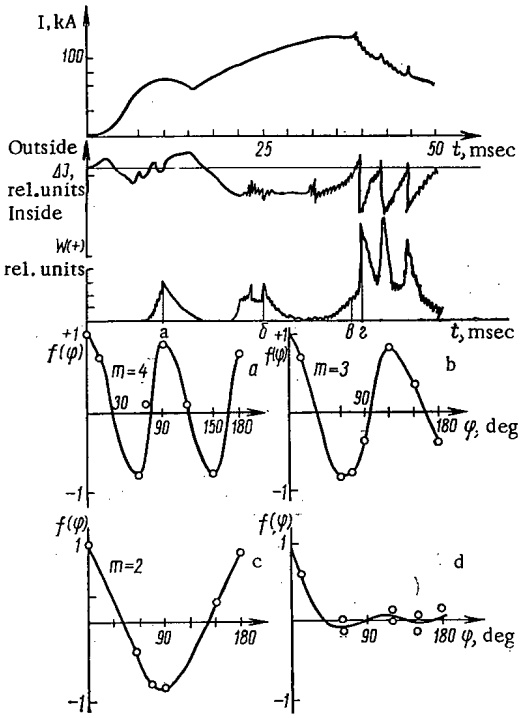

Fig. 6

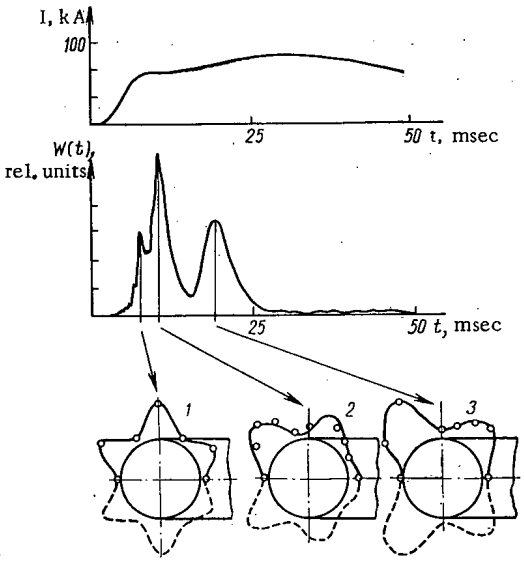

Fig. 7

Fig. 6. Development of the disturbances when q is reduced to 2: a, b, c, d) the function $f(\varphi)$ at various times of the discharge development: a) m = 4; b) m = 3; c) m = 2.

Fig. 7. Development of the disturbances in the initial stage of the discharge: 1) m = 6; 2) m = 5; 3) m = 4.

Disturbances of the Plasma String at q = 2. Figure 6 shows an oscillogram of a quantity which is proportional to the product of the current, times the displacement of the string ($J\Delta$) for the case of a secondary current increase; the figure displays, in addition, an oscillogram of W(t) [6]. The development of the disturbances in dependence of φ of the corresponding correlation functions is shown in the figure for four characteristic moments of time.

In this case, the stabilizing magnetic field had a strength of about 23 kOe, and the rate of increase in the discharge current was chosen so that q decreased to 2 near the current maximum. The curves show that disturbances with m = 4, m = 3, and m = 2 are excited in succession during the discharge process. However, while disturbances with m = 4 and m = 3 are relatively easily suppressed when the current increases, a strong "disruptive" instability occurs during the development of the disturbance with m = 2 [2, 7], and a breakup of the plasma string is the consequence. A correlation analysis of the structure of the powerful disturbances arising on that occasion (see Fig. 6d) reveals that the disturbances are practically unrelated and have a relatively small size. The transverse disturbance dimensions are less than several centimeters. Interestingly enough, similar to the regular disturbances with m = 2, m = 3, and m = 4, the disturbances mentioned above increase from the inner enclosure of the toroid toward the outer toroid enclosure.

At the present time, we are unable to relate the disturbances with m = 2 to the "disruptive" instabilities. But there is reason to assume that the development of the disturbances with m = 2 is more closely related to processes determining the macroscopic state of the plasma string than are the disturbances with m = 3. First, contrary to the disturbances with m = 3, the development of the above-described disturbances is accompanied by an additional outward shift of the entire plasma string (see Fig. 6; ΔJ curve); second, an increase in the growth rate of the discharge current by a factor of almost 2 changes only the time at which the disruptive instabilities start, and shifts that time toward the start of the discharge without suppressing the disturbances with m = 2.

Higher Mode Instabilities Arising in the Initial Stage of the Discharge Development. First results of a correlation analysis involving the angle ψ were published in [4]. It was stated in [4] that under certain

discharge conditions a noticeable group of disturbances with n = 2 to n = 4 cannot be observed near disturbances with n = 1. When one assumes the disturbances to be of the resonance type (m = qn), the surface of the plasma string must split into a large number of small bands.

In the current series of experiments, which differ from previous experiments only in the larger discharge currents and slightly increased dimensions of the plasma string, it was established that similar disturbances are usually small compared to the main disturbances with n = 1. The transition region of the main disturbances is the only exception; in this transition region, the disturbances can be boosted or attenuated. One must therefore assume for resonance disturbances that their mode m must be close to q at the boundary of the plasma string.

Figure 7 shows, in polar coordinates, curves $W(\varphi)$ recorded for three times at a stabilizing discharge current of ~80 kA [as distinct from the usual case (see Fig. 3) it became therefore possible to increase to some extent the initial stage of the discharge]. The times had been chosen so that the amplitudes of the disturbances had clear maxima at particular times.

One can conclude from the curves that regular disturbances with m = 6, m = 5, and m = 4 develop in succession when the discharge current is increased. Since the values ascribed to these disturbances are almost equal to the corresponding q figures near the boundary of the plasma string, one is led to the conclusion that these disturbances, as well as the disturbances considered above (with m = 3 and m = 2), are of the resonance type.

However, these disturbances differ greatly as far as their behavior and influence upon the macroscopic characteristics of the plasma string are concerned. In contrast to the disturbances with m = 3, the disturbances with m = 4 are suppressed under the conditions ruling in a quasi-stationary discharge. This effect may originate either from the narrowness of the plasma parameter region, in which the development of the corresponding instabilities is possible, or from the generation of certain stabilizing factors during the discharge process. According to [8], a sharpening of the distribution of the discharge current density j(r) during the discharge and the increase in the electric conductivity due to plasma heating can have a stabilizing influence.

It is not possible at the present time to point to a definite stabilizing mechanism which could be responsible for the suppression of the disturbances with m = 4. One can only say that a stabilizing effect related to the sharpening of the current distribution during the discharge process (i.e., an actual decrease in the radius of the plasma string) must compete with the destabilizing effect caused by the corresponding decrease in q on the plasma boundary. This effect would explain the fact that at $q \geq 3$, the development of disturbances with m = 3 begins usually in the center section of the discharge (see Fig. 3 and 5b) where the distribution of j(r) is sharper than in the formative stage of the discharge [4].

On the other hand, the suppression of disturbances with m = 3 in a rapidly increasing discharge current seems to indicate that a stabilizing mechanism related to the heating of the periphery of the plasma string plays a very important role under the experimental conditions described.

If this is the case, an additional heating of the boundary regions of the plasma may cause a stabilization of the resonance disturbances with m = 2.

In conclusion, the authors express their gratitude to L. A. Artsimovich, V. S. Mukhovatov, and V. D. Shafranov for useful discussions, and to K. A. Razumova for her interest in the work.

The authors acknowledge the assistance of A. M. Anashin, A. V. Glukhov, A. V. Dedyurin, S. Ya. Dugin, A. I. Nikonorov, and V. G. Shein in the experiments.

LITERATURE CITED

1. L. A. Artsimovich et al., Plasma Physics and Controlled Nuclear Fusion Research, Vol. 1, IAEA, Vienna (1969), p. 157.
2. L. A. Artsimovich, S. V. Mirnov, and V. S. Strelkov, Atomnaya Énergiya, 17, 170 (1964).
3. F. G. Lange, Correlation Electronics [in Russian], Sudpromgiz, Leningrad (1963).
4. S. Mirnov, Nucl. Fusion., 9, 51 (1969).
5. N. D. Vinogradova and K. A. Razumova, Plasma Physics and Controlled Nuclear Fusion Research, Vol. 2, IAEA, Vienna (1966), p. 617.
6. S. V. Mirnov, Atomnaya Énergiya, 17, 209 (1964).

7. E. P. Gorbunov and K. A. Razumova, Atomnaya Énergiya, 15, 363 (1963).
8. V. D. Shafranov, Zhur. Tekh, Fiz., 30, 241 (1970).

SELFACCELERATION IN INTENSE ELECTRON BEAMS

L. N. Kazanskii, A. V. Kisletsov, and A. N. Lebedev

UDC 621.384.6:621.3.038.624

At present direct-action accelerators have been developed by means of which one can obtain electron beams of short duration (of the order of 10^{-8} sec) with currents of tens and hundreds of kiloamperes [1]. Under these conditions the maximum particle energy is limited by the possibilities of creating a high pulse voltage and lies in the range of several megaelectronvolts, which is too low for certain applications of such beams. The use of traditional methods for the subsequent acceleration of high-current beams, even to low energies (10 to 20 MeV), is linked with the solution of complex physics and engineering problems. However, in many cases methods of subsequent acceleration could turn out to be acceptable if they were connected with the reduction of the integrated beam charge while preserving or slightly reducing the instantaneous value of current and total energy of the beam.

In this connection it is of interest to use passive elements which are such that interaction of the beam with them results in a redistribution of energy within the beam (i.e., a portion of the particles is accelerated at the expense of the energy of the remaining ones). This process of selfacceleration may be repeated often for the same original particle bunch (i.e., a cascade connection of passive elements is possible which assures selfacceleration of the beam at the expense of a reduction in its intensity).

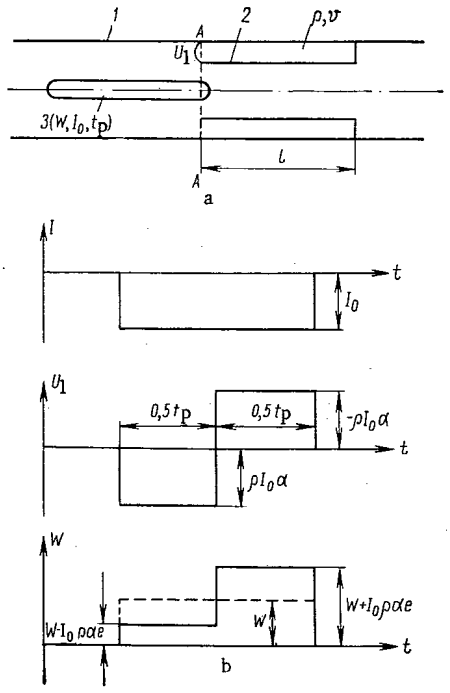

Fig. 1. The process of selfacceleration in a waveguide containing a short-circuited line.

As an example of the method indicated let us consider the scheme shown in Fig. 1a, where 1 is a metallic waveguide with a built-in short-circuited line having a hollow central conductor 2; l is the length of the line; ρ is the wave impedance; v is the propagation velocity of waves in the line. A bunch of relativistic electrons 3 having a pulse length t_u with an energy W and a current I_0 passes through the system. If the length of the line is $l = 0.25 t_u v$, then at the instant at which the bunch reaches the cross section A – A a voltage U_π* appears at the input of the line; this voltage has the form of a bipolar pulse (a randomly initiated modulation pulse) having the amplitude $\alpha\rho I_0$ (α is the coefficient of coupling between the beam and the line). The voltage at the input of the line decelerates the particles in the front half of the beam down to an energy $(W - \alpha\rho I_0 e)$ and accelerates the particles in the second half to energies $(W + \alpha\rho I_0 e)$, where e is the electron charge (see Fig. 1b). In order to avoid breakup of the beam at the input of the line, it is required to choose $\rho < W/I_0 e\alpha$. Thus, in the section considered it is possible for the energy of one half the beam particles to be increased by approximately a factor of two. If the accelerated particles are isolated, then the process may be repeated; this produces a quadrupling of energy at the expense of a further reduction of the pulse length, etc.

* The formation of the voltage U_π across the line is equivalent to the formation of a voltage pulse at the input of a short-circuited line when a pulse from a current source is applied to it [2].

Translated from Atomnaya Énergiya, Vol. 30, No. 1, pp. 27-31, January, 1971. Original article submitted February 20, 1970.

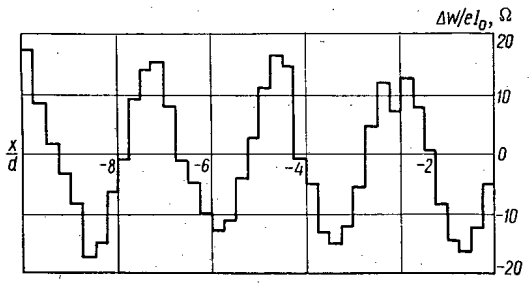

Fig. 2

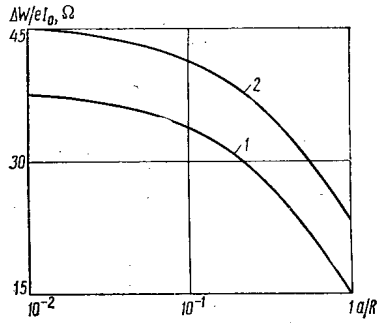

Fig. 3

Fig. 2. The redistribution of the energy along the length of the bunch: $\gamma = 6$, $a/R = 1$, $d/R = 1$, $L/d = 10$. The wavelength of the fundamental excited mode ($m = 0$, $n = 1$) is $\lambda/d = 2.58$.

Fig. 3. Dependence of the impedance $\Delta W/eI_0$ on the relative beam radius a/R ($d/R = 1$): 1) $\gamma = 3$; 2) $\gamma = 6$.

Other passive elements may also be used for selfacceleration of a beam. The passage of a relativistic bunch through a cylindrical resonator having a length d and a radius R is considered below as an example. Unlike [3, 4], in which only the total energy losses of the bunch due to excitation of the resonator were estimated (here the radiation spectrum was cut off fairly arbitrarily), one should be interested in the redistribution of the energy along the length of the bunch with allowance for excitation of higher resonator modes and the action of the Coulomb field of the beam. From these results one may also obtain the total energy losses.

The problem is solved in the stipulated-current approximation; i.e., it is assumed that the velocity v of the charged particles is constant, while the current is uniform over the cross section and has a radius a and a maximum value I_0. For the Fourier components of the current one may write

$$\mathbf{j}(\omega, r) = \frac{I_0}{\pi a^2} f_0(\omega, z)\,\mathbf{e}_z, \tag{1}$$

where $\mathbf{e}_Z$ is the unit vector in the direction of the longitudinal axis of the resonator, while the function $f_0(\omega, z)$ considers the time and space dependences of the current.

Since the dependence of the current on time and on the longitudinal coordinate can be described by the function $f_0(z - vt) = f_0(\xi)$, it follows that

$$f_0(\omega, z) = \frac{1}{2\pi}\int_{-\infty}^{\infty} f_0(z - vt)\,e^{-i\omega t}\,dt = \frac{1}{v}\,e^{-i\omega\frac{z}{v}} f_0(\omega), \tag{2}$$

where

$$f_0(\omega) = \frac{1}{2\pi}\int_{-\infty}^{\infty} f_0(\xi)\,e^{i\omega\frac{\xi}{v}}\,d\xi.$$

In order to determine the fields excited by the bunch, the method of eigenfunctions is used [5]. The electric field is split up into the potential part $\mathbf{E}^l$ (rot $\mathbf{E}^l = 0$, $\mathbf{E}^l = \nabla\Phi$) which has no resonance properties, and the induced part $\mathbf{E}^t$ (div $\mathbf{E}^t = 0$) which does have resonance properties. These fields are respectively expanded in scalar Φ_α and vector $\mathbf{E}_\alpha$ eigenfunctions:

$$\mathbf{E} = \sum_\alpha (A^t_\alpha \mathbf{E}_\alpha + A^l_\alpha \nabla\Phi_\alpha), \tag{3}$$

where α denotes the number of the excited mode (in general, α represents three indices).

After transit through the resonator, a particle situated at a distance x from the beginning of a bunch having the length L and at a distance r from the axis of the bunch receives an energy

$$\Delta W_\alpha(x, r) = e\int_0^d E_{z\alpha}(r, z, t)\,dz \tag{4}$$

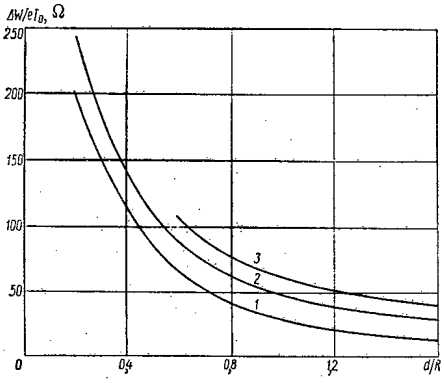

Fig. 4

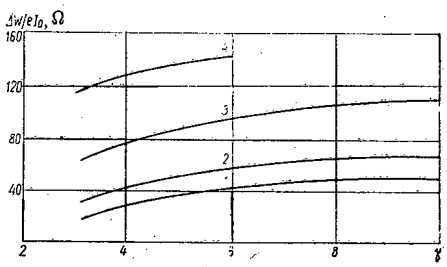

Fig. 5

Fig. 4. Dependence of the impedance $\Delta W/eI_0$ on the relative resonator length d/R ($L \gg R$, $L \gg d$): 1) $\gamma = 3$; 2) $\gamma = 6$; 3) $\gamma = 10$.

Fig. 5. Dependence of the impedance $\Delta W/eI_0$ on the relative energy of the beam: 1) d/R = 1.4; 2) d/R = 1; 3) d/R = 0.6; 4) d/R = 0.4.

from the α-th mode; here $E_{z\alpha}(r, z, t)$ is the longitudinal component of the electric field of the α-th mode. Instead of t it is necessary to substitute the time at which a particle situated at the distance x from the beginning of the bunch reaches the point z: $t = z - x/v$; using the eigenfunctions of a cylindrical resonator, carrying out the inverse Fourier transformation, integrating in (4) with respect to z, and substituting $t = z - x/v$, we obtain

$$\Delta W(x, r) = \sum_{n=1}^{\infty}\sum_{m=0}^{\infty} \frac{4I_0 e \frac{d}{R}\delta_m}{\pi^2 \nu \frac{a}{R}} \frac{\mathcal{J}_1\left(\mu_n \frac{a}{R}\right)\mathcal{J}_0\left(\mu_n \frac{r}{R}\right)}{\mu_n \cdot \mathcal{J}_1^2(\mu_n)} \int_{-\infty}^{\infty} f_0\left(\frac{\xi}{d}\right)\Phi(\nu)\, d\left(\frac{\xi}{d}\right);$$

$$\delta_m = \begin{cases} 2 & m \neq 0, \\ 1 & m = 0; \end{cases}$$

$$\Phi(\nu) = Y(\nu) - \frac{\cos \pi m}{2}[Y(\nu+1) + Y(\nu-1)];$$

$$Y(\nu) = -i\int_{\nu} \frac{\Omega(\beta^2\Omega^2\Omega_\alpha^2 + \pi^2 m^2\Omega^2 - \pi^2 m^2\Omega_\alpha^2)\, e^{i\Omega\nu}\, d\Omega}{\beta^2\Omega_\alpha(\Omega_\alpha^2 - \Omega^2)(\Omega^2 - \pi^2 m^2)^2};$$

$$\Omega = \frac{\omega d}{v}; \quad \Omega_\alpha = \frac{\omega_\alpha d}{v}; \quad \beta = \frac{v}{c}; \quad \nu = \frac{\xi - x}{d}, \tag{5}$$

where μ_n is the n-th root of the zero order Bessel function; ω_α are the natural frequencies of the resonator: $\omega_\alpha^2 = c^2(\mu_n^2/R^2 + \pi^2 m^2/d^2)$ for n = 1, 2, 3 . . . ; m = 0, 1, 2 . . .

The integral in the expression for $Y(\nu)$ is taken with bypassing of the poles of the integrand expression lying on the real axis from below, all poles of the integrand expression being situated above the integration path. If $\nu < 0$, then the integration contour should be closed in the lower half-plane [6] where there are no poles, so that $Y(\nu) = 0$ for $\nu < 0$. For $\nu > 0$ the integral is proportional to the sum of the residues at the point $\Omega = \pm\Omega_\alpha$, $\Omega = \pm\pi m$. After integration, we obtain

$$Y(\nu) = \begin{cases} -F_1\nu\sin\pi m\nu + F_2(\cos\pi m\nu - \cos\Omega_\alpha\nu) & \text{for } \nu > 0, \\ 0 & \text{for } \nu < 0; \end{cases} \tag{6}$$

$$F_1 = -\frac{\pi^2 m(\pi^2 m^2 - \Omega_\alpha^2\gamma^2)}{\beta^2\Omega_\alpha^2(\pi^2 m^2 - \Omega_\alpha^2)};$$

$$F_2 = \frac{2\pi\Omega_\alpha^2}{(\pi^2 m^2 - \Omega_\alpha^2)^2}; \quad \gamma^2 = \frac{1}{1-\beta^2}.$$

Now one may write the following for the nucleus $\Phi(\nu)$:

$$\Phi(\nu)=\begin{cases} F_2\cos\Omega_\alpha\nu\,(\cos\pi m\cdot\cos\Omega_\alpha-1) \\ \qquad\qquad \text{for}\quad \nu\geqslant 1; \\ F_1\sin\pi m\nu\,\dfrac{1-|\nu|}{2}+F_2\left[\dfrac{1}{2}\cos\pi m\nu-\cos\Omega_\alpha\nu\right. \\ \qquad \left.+\dfrac{\cos\pi m}{2}\cos\Omega_\alpha(\nu+1)\right] \\ \qquad\qquad \text{for}\quad 0\leqslant\nu\leqslant 1; \\ F_1\sin\pi m\nu\,\dfrac{1-|\nu|}{2}-\dfrac{F_2}{2}\left[\cos\pi m\nu-\cos\pi m\cos\Omega_\alpha(\nu+1)\right] \\ \qquad\qquad \text{for}\quad -1\leqslant\nu\leqslant 0. \end{cases} \tag{7}$$

Equation (7) describes the contribution made to the energy of the given particle by a field created in the resonator by particles which have traveled ahead by a distance larger than d($\nu \geq 1$), ahead by a distance d($0 \leq \nu \leq 1$) and behind by a distance d($-1 \leq \nu \leq 0$).

Let us assume for simplicity that the bunch has a rectangular distribution, i.e.,

$$f_0\left(\frac{\xi}{d}\right)=\begin{cases} 1 & -\dfrac{L}{d}\leqslant\dfrac{\xi}{d}\leqslant 0; \\ 0 & \dfrac{\xi}{d}>0,\ \dfrac{\xi}{d}<-\dfrac{L}{d}. \end{cases}$$

Let us integrate the kernel of $\Phi(\nu)$ with respect to ξ/d for $0 \leq x/d \leq L/d$, and let us carry out numerical summation over the longitudinal modes (i.e., with respect to the index m) and transverse modes (with respect to the index n). The results of the calculation for particles which have traveled along the resonator axis are shown in Figs. 2-5 for various values of the parameters d/R, a/R and γ. The increment of energy acquired by the particles after passing through the resonator can be characterized by the effective impedance in ohms, i.e., by the quantity $\Delta W/eI_0$ (r, x, d, R, a, γ).

The pronounced periodicity of the energy modulation with the period of the fundamental oscillation mode (m = 0, n = 1), which has a specific effect, is characteristic of the version given (see Fig. 2). Such a picture is characteristic, of course, only for long bunches whose transit duration exceeds the period of the fundamental mode. At the beginning and end of the bunch the Coulomb fields and transients play an important role (i.e., the higher modes are especially essential for short bunches). When the relative beam radius a/R is decreased, the impedance $\Delta W/eI_0$ increases (see Fig. 3). This can be explained by the fact that the electric field of the fundamental mode is maximal on the resonator axis. Consequently, the effect of the field on the beam increases as the beam becomes thinner, the impedance $\Delta W/eI_0$ remaining finite as a tends to vanish.

As is evident from Fig. 4, the function $\Delta W/eI_0$ depends essentially on the ratio between the resonator length d and its radius R. When d/R increases, the effect of interaction between the field and the particle decreases, since the difference between the particle velocity and the phase velocity of those field components with which the particle interacts takes effect. On the other hand, for a stipulated bunch length L/d the ratio d/R cannot be very small, otherwise the longitudinal field of the excited fundamental mode does not have time to change its sign on the resonator axis during the time required for the bunch to traverse the resonator, and the selfacceleration effect will be absent (to a certain extent the case $R \to \infty$ corresponds to radiation departing along a radial line). Evidently, the case in which the acceleration time of the bunch is equal to one-half the period of the fundamental mode will be close to optimal.

From Fig. 5 one may conclude that the dependence of the selfacceleration effect on the energy of the particles is insubstantial for $\gamma \gg 1$.

As follows from the results obtained, the effect of selfacceleration in a cylindrical resonator may be quite considerable. Thus, in a bunch having an initial energy of the order of 3 MeV and a current of 10^5 A a considerable portion of the beam may have an energy of 4.5 to 5.5 MeV after passing through one resonator, while the energy may be increased up to tens of megaelectronvolts after passage through a chain of resonators.

In touching on the prospects for a substantial increase in energy it should be noted that a cylindrical resonator is merely the simplest (and far from the optimal) element for achieving a redistribution of energy within a bunch. From the practical standpoint it is of interest to determine a structural design for self-acceleration which is such that the energy of the largest possible number of particles may be entirely transferred to a comparatively small portion of the beam in the structure.

LITERATURE CITED

1. W. Link, IEEE Trans. Nucl. Sci. (June, 1967).

2. Ya. S. Itskhoki, Pulse Networks [in Russian], Sovetskoe Radio, Moscow (1969).
3. V. N. Lopukhin, Excitation of Electromagnetic Oscillations and Waves by Electron Streams [in Russian], Gostekhizdat, Moscow (1963).
4. O. A. Kolpakov and V. I. Kotov, Zh. Tekh. Fiz., 34, 1387 (1964).
5. L. A. Vainshtein, Electromagnetic Waves [in Russian], Sovetskoe Radio, Moscow (1967).
6. E. T. Whittaker and J. Watson, Course in Modern Analysis, Vol. 1 [Russian translation], Fizmatgiz, Moscow (1962).

SOME RESULTS OF OBSERVATIONS OF UNDERGROUND NUCLEAR EXPLOSIONS

V. N. Rodionov and V. M. Tsvetkov

UDC 621.039.9

The mechanical effects of an underground nuclear explosion can be described, on the one hand, by parameters of the waves generated, and on the other hand, by the dimensions of the regions of irreversible deformation of the medium: the cavity volume and the size of the pulverized zone and the ejection crater.

It is an extremely difficult matter to determine experimentally the maximum volume of the cavity, which is appreciably different from the final volume [1], and also the dimensions of the disintegration zone. However, these parameters are the most important for evaluating the energy liberated in the seismic wave.

It is very important to use information contained in the compression waves in the immediate vicinity of the disintegration zone to determine the parameters of irreversible deformation of the medium in underground explosions.

1. Results of Observations of Explosions in Rock Salt

We consider experimental results obtained for explosions in rock salt, which have been investigated most completely. The literature has reports of two American explosions in salt: "Salmon" [2, 3] and "Gnome" [4]. Data is given below, also, on one explosion in salt conducted in the Soviet Union.

The main parameters of all three explosions are given in Table 1, where they are arranged in diminishing order of energy released. Table 1 also gives the volumes of the cavities formed by the explosions, which were measured after a considerable delay (roughly a month) following the explosion.

Rock salt has quite high uniformity, and in all cases has approximately the same mechanical properties: density $\rho = 2.15$ g/cm^3; longitudinal wave speed c = 4.5 km/sec; Poisson ratio $\nu = 0.25$ to 0.32. The strength of rock salt has not been measured in the natural seam condition. Laboratory crushing tests of salt specimens give a value of ~ 400 kg/cm^2.

The most complete data on the mechanical effect of an explosion in salt were obtained in the Salmon explosion. Figure 1 shows values of the maximum mass velocity as a function of distance, obtained in the Salmon explosion, described by the formula

$$v_{max} = 10\left(\frac{E^{1/3}}{r}\right)^{1.6}. \quad (1)$$

The maximum displacement in the compression wave (Fig. 2) can be approximated by

TABLE 1. Basic Parameters of the Explosions

Explosion number	Explosion energy E, ktons of TNT	Explosion depth, h, m	Conditions of the explosion	Final volume of cavity, V, thousands of m^3
I (Salmon)	5.3	828	In a bore	20
II (Gnome)	3.5	360	In a chamber of volume 30 m^3	23
III	1.1	160	In a bore	10

Translated from Atomnaya Énergiya, Vol. 30, No. 1, pp. 31-36, January, 1971. Original article submitted August 1, 1969; revision submitted December 11, 1969.

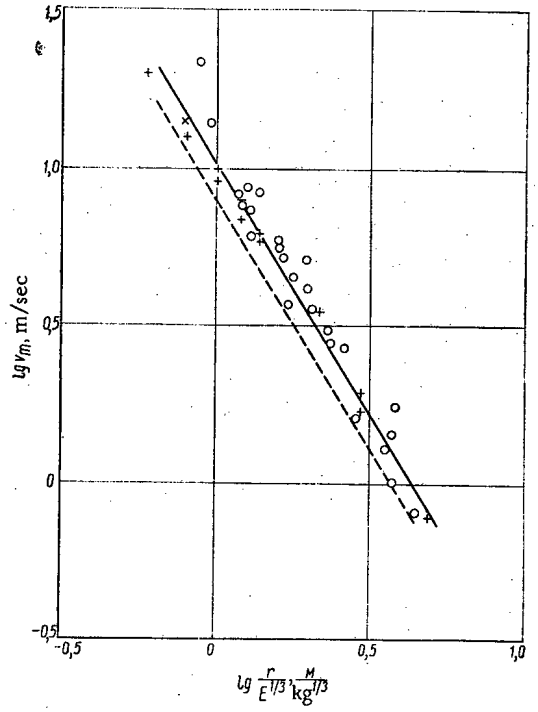

Fig. 1

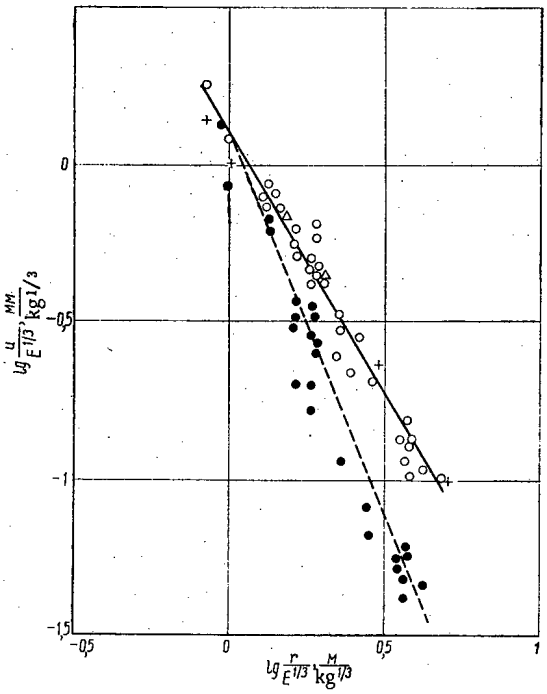

Fig. 2

Fig. 1. The maximum mass velocity of the medium as a function of distance: ○) explosion I; +) explosion III; ——) calculation from Eq. (1); - - - -) average relation for explosion II, from Eq. (3).

Fig. 2. Medium displacement as a function of distance: ○, Δ, +) maximum displacements for explosions I, II, and III, respectively; ●) residual displacements for explosion I; ——) relation calculated from Eq. (2); - - - -) calculation according to section 2.

$$v_{\max} = 1.35E^{1/3}\left(\frac{E^{1/3}}{r}\right)^{1.6}. \tag{2}$$

Here E is the explosion energy, kilograms of TNT; r is the distance from the explosion center, m; v_{max} is the maximum mass velocity, m/sec; u_{max} is the maximum displacement, mm.

Numerous measurements of the residual displacement were made in the Salmon explosion. In spite of the large scatter in the measured values, these data are of very great interest; they are shown in Fig. 2.

Experimental data obtained in the other two explosions are also shown in Fig. 2. They come close to the corresponding results of the Salmon case, but the maximum displacement velocity in explosion II (Gnome) at the same reduced distances is somewhat less:

$$v_{\max} = 8\left(\frac{E^{1/3}}{r}\right)^{1.6}. \tag{3}$$

The volumes of the cavities (see Table 1) reduced to 1 kton TNT are appreciably different for all three explosions.

2. The Compression Wave and the Medium Behavior Outside the Disintegration Zone

The amplitude of the compression wave, which can be evaluated from the formula

$$\sigma_{\max} = \rho v_{\max} c,$$

at distances $r/E^{1/3} > 1$ has a value less than the stresses disintegrating the medium, and it must therefore, apparently, be described using equations of the theory of elasticity.

However, it is easy to observe considerable differences between the compression wave recorded and an elastic wave: attenuation of the displacement velocity with distance occurs considerably faster ($1/r^{1.6}$)

TABLE 2. Parameters of the Medium at the Boundary of the Disintegration Zone

Explosion number	θ, msec	R_p, m	$u(R_p)$, mm	σ^*, kg/cm²
I	23,5	180	220	600
II	25,5	195	138	350
III	14	107	130	600

than it would be in a completely elastic medium; the residual displacements vary with distance (see Fig. 2) also somewhat faster than $1/r^2$, and therefore, there is an irreversible volume compression in the compression wave; the rate of propagation of the maximum amplitude of the compression wave is somewhat less than the rate of propagation of the leading edge. It is important to establish the above interrelated signs of the appearance of nonelasticity of the medium.

We assume that a solid medium is completely elastic and identical, both within the zone encompassed by the compression wave, and outside it. We suppose that only at the front of the wave is there a small irreversible condensation upon compression, proportional to the amplitude, such that the rate of propagation of the wave front differs by a small amount from that of longitudinal waves. To simplify the calculations we consider that at some surface of radius R_0 we assign a displacement, increasing with time and tending to a certain limiting value:

$$U(t, R_0) = \begin{cases} \frac{B}{R_0^2}\left(1-e^{-\frac{t}{\theta}}\right), t \geqslant 0; \\ 0, \quad t < 0. \end{cases} \tag{4}$$

We determine the origin of the motion in a completely elastic medium. For a spherically symmetric case the displacement potential has the form

$$\varphi = \frac{1}{r} f(\xi), \qquad \xi = t - \frac{r-R_0}{c}. \tag{5}$$

From the given function $U(t, R_0)$ we find

$$f(\xi) = -B\left[1 - \frac{e^{-\frac{\xi}{\theta}}}{1-\frac{R_0}{c\theta}} + \frac{\frac{R_0}{c\theta}e^{-\frac{c\xi}{R_0}}}{1-\frac{R_0}{c\theta}}\right]. \tag{6}$$

The rate of displacement v is determined by the expression

$$v = -\frac{f''(\xi)}{cr} - \frac{f'(\xi)}{r^2}. \tag{7}$$

If the wave front propagates with velocity c_Φ, less than that of elastic waves c, the motion of the elastic phase can be expressed using the potential:

$$\varphi = \frac{f_1(\xi)}{r} + \frac{f_2(\bar{\xi})}{r}, \qquad \bar{\xi} = t + \frac{r-R_0}{c}. \tag{8}$$

The appearance of the function f_2 is linked to the fact that the wave front is not a characteristic of the equation of motions, and therefore the front will influence the whole motion. Functions f_1 and f_2 are related by the condition at the wave front

$$u(t, R_f) = -\frac{f_1'(\xi_f)}{cR_f} - \frac{f_1(\xi_f)}{R_f^2} + \frac{f_2'(\bar{\xi}_f)}{cR_f} - \frac{f_2(\bar{\xi})}{R_f^2} = 0. \tag{9}$$

Here

$$\begin{aligned} \xi_f &= \frac{R_f - R_0}{c}\beta; \\ \bar{\xi}_f &= \frac{2(R_f - R_0)}{c} = \frac{2}{\beta}\xi_f; \\ \beta &= \frac{c-c_f}{c_f}; \\ R_f - R_0 &= c_f t. \end{aligned} \tag{10}$$

After transformation of Eq. (9), we obtain

$$\left(\bar{\xi} + \frac{2R_0}{c}\right) f_2'(\bar{\xi}) - 2f_2(\bar{\xi}) = \left(\bar{\xi} + \frac{2R_0}{c}\right) f_1'\left(\frac{\beta\bar{\xi}}{2}\right) + f_1\left(\frac{\beta\bar{\xi}}{2}\right). \tag{11}$$

Hence it can be seen that for $\beta \ll 1$ the function $f_2(\bar{\xi})$ is determined over a wide range of variation of its argument, as long as the behavior of the function $f_1(\xi)$ in the neighborhood $\xi = 0$ is known. This fact

enables us easily to construct a solution by the method of successive approximations. Taking the solution of the problem for a completely elastic medium ($c_f = c$) as a basis, and expanding $f_1(\xi)$ and $f'_1(\xi)$ in a series near $\xi = 0$, we can obtain an equation for determining $f_2(\bar{\xi})$. The solution of this equation is quite laborious, and we do not give it here. Then, knowing $f_2(\xi)$, we can determine the form of the function $f_1(\xi)$, using Eqs. (4) and (8) with $r = R_0$, where $\xi = \bar{\xi} = t$. The functions $f_1(\xi)$ and $f_2(\bar{\xi})$ thus obtained are first approximations. Calculations according to the scheme were carried out for the conditions of explosion I (Salmon), and it was assumed: a) $\beta = 0.1$; b) R_0 corresponds to the point $r/E^{1/3} = 1$ of Fig. 2; c) $R_0/c\theta = 1.7$; d) $B = R_0^2 u(R_0)$.

As the calculations presented have shown, propagation of a front with a speed $c_f = 0.9c$ leads to attenuation of the velocity amplitude with distance according to the law $\sim 1/r^{1.4}$. This attenuation is close to that observed in the experiments. The calculated values of the residual displacements are also in quite good agreement with the experimental data. The dotted line on Fig. 2 shows the calculated relation. The duration of the compression wave (time to move from the center of the explosion) is

$$\tau_+ = 1.2\frac{R_0}{c}, \quad r > 2R_0. \tag{12}$$

From what has been said, we can evidently consider that the various indications of inelastic behavior of the medium during propagation of the compression wave can be considered as a consequence of energy dissipation in a narrow spherical layer near the front. The ratio of the speeds of propagation of the maximum amplitude to that of elastic waves can be taken as a parameter describing the degree of non-elasticity of the rock.

3. One Method of Searching for the Boundary of the Disintegration Zone

It follows from examination of Fig. 2 that there are at least two zones which differ in quality as regards the nature of the motion, at distances $r/E^{1/3} < 1$ (where r is in meters, and E is in kg of TNT) the maximum and the residual displacements coincide, and for $r/E^{1/3} > 1$, following a displacement, a displacement towards the center of the explosion is observed. It is natural to assume that this qualitative difference is linked with disintegration of the medium in the $r/E^{1/3} < 1$ zone. In fact, when disintegration of the medium occurs, the return motion can be due only to stresses at the outer boundary of the disintegrated zone, since the azimuthal stresses $\sigma_{\varphi\varphi} = \sigma_{\theta\theta}$ in the disintegration zone are compressive. On the other hand, in the zone of elastic or almost-elastic deformations, radial displacement leads to the appearance of tensile azimuthal stresses, which tend to return the medium to its original state after the wave passes.

Hence it follows, in particular, that cracks of relatively small extent, associated with shear deformation, should be observed in the disintegration zone. The formation of isolated radial cracks of large extent is possible only outside this zone.

A laboratory experiment [1] has shown that considerable displacement towards the center and in the disintegrated medium are possible under the action of elastic stresses σ_{rr} at the outer boundary of the disintegration zone. However, these displacements take place comparatively more slowly than in the expansion of the cavity, since the stored elastic energy is an order of magnitude less than the explosion energy. These slow motions were not recorded by the instruments, since they had a restricted recording time.

Thus, we shall take the boundary of the disintegration zone R_p to be a spherical surface on which the residual displacements first reach their maximum values (if the displacement is from the periphery towards the center). In other words, at this surface the rate of radial displacement is only positive. It is a pity that direct determination of the boundary of the disintegrated medium from experimental data was possible only for the Salmon explosion. In the other cases either no measurements of residual displacement were conducted, or they were not sufficiently reliable.

For this reason the following method is suggested for seeking the disintegration boundary. The solution of the problem of propagation of a wave in an almost elastic medium, discussed in the previous section, allows us to relate the radius of the disintegration zone or the zone of elastic deformations R_p, assumed equal to R_0, and the duration of the positive phase of the compression wave τ_+, by Eq. (12). However, it is convenient to use a parameter related in meaning to the parameter θ which is determined as follows:

$$\theta = \frac{u_{res}}{u_{max}} = \frac{v_{max}}{v_{max}}, \tag{13}$$

Since for $r = R_p$ the residual displacements have the maximum values,

$$u_{res} = u_{max}.$$

The experiment shows that the maximum velocity and the maximum displacement vary with distance according to a single law. This means that the parameter θ can be found from the measured values of v_{max} and u_{max} at any distances $r > R_p$ from the explosion center. Knowing the parameter θ from experiment, we find the radius of the disintegration zone. For the Salmon explosion the size of the disintegration zone thus calculated agrees with the value corresponding to the point of intersection of the maximum and residual displacements. Knowing the size of the disintegration zone and the medium displacement at $r = R_p$, we can also calculate the strength of the medium $\sigma^* = -\sigma_{rr}|_{r = R_p}$ using an equation from elasticity theory.

The values of σ^* computed (see Table 2) are close, in order of magnitude, to the strength of rock salt, for axial compression of specimens. The somewhat lower strength value in the Gnome test may be connected with certain specific properties of the salt mass. Another non-trivial explanation is possible. We assume that disintegration of the rock salt occurs when a certain limiting shear stress σ_s is reached. Then the condition for disintegration at the boundary of the elastic region can be written in the form

$$\sigma_{rr} - \sigma_{\varphi\varphi} = -\sigma_s.$$

In an elastic medium the relations for radial and azimuthal stresses

$$\sigma_{\varphi\varphi} = -\frac{1}{2}\sigma_{rr}$$

must be satisfied. Taking into account the rock pressure ρgh, we obtain

$$\left.\begin{aligned} \sigma_{rr} &= -\frac{2}{3}\sigma_s - \rho gh; \\ \sigma_{\varphi\varphi} &= \frac{1}{3}\sigma_s - \rho gh. \end{aligned}\right\} \qquad (14)$$

It can be seen from the last expression that the azimuthal stress decreases with depth, and changes from a tensile stress to a compressive one. We can therefore assume that at small depth, disintegration of the medium begins with the formation of radial cracks, and only then does pulverization occur. However, at large depth there is no preliminary rupture of the medium by radial cracks. This means that in the explosion, at a small depth, at the boundary of the disintegration zone, the other conditions

$$\sigma_{\varphi\varphi} = 0 \text{ and } \sigma_{rr} = -\sigma_s$$

are satisfied, which also explains the observed variation of σ^* with depth.

Assuming that radial cracks at the boundary of the disintegration zone are formed only as a result of explosion III, we can determine the average value of $\sigma_s = 520$ kg/cm^2 from the first two explosions.

4. Absence of Compaction of the Medium in the Disintegration Zone

Knowing the size of the disintegration zone and the displacement at its boundary, we can determine the volume displaced in the elastic region:

$$V = 4\pi R_p^2 u(R_p).$$

Using values of R_p and $u(R_p)$ shown in Table 2, we calculate the displaced volume. It turns out to be several times larger than the measured final cavity volume (Table 3).

This effect can result from two causes. First, as the laboratory experiment showed, the cavity can be compressed under the action of stresses at the outer boundary of the disintegration zone. The cavity volume was measured a long time after it was formed, so that, in fact, the maximum cavity dimensions are not known at the time for which the displaced volume was determined. Secondly, one cannot exclude the possibility of reduced compression of the medium in the disintegration zone, since the deformations are large, and the stresses compressing the disintegrated medium are comparable in order of magnitude with the limiting stress. The absence of compaction of the medium in the deformation process was shown experimentally in investigating an explosion in sandy soil [5]. This effect was also noted in laboratory investigations of rock specimens during their disintegration [6].

Simple estimates allow an explanation of the part played by each of these processes.

TABLE 3. Comparison of the Maximum and Residual Cavity Volumes with the Displaced Volume

Explosion number	Displaced volume, V, thousands of m^3	Final volume, V_f, thousands of m^3	$\sigma_{rr} = 2\sigma_{\varphi\varphi}$		$\sigma_{rr} - \sigma_{\varphi\varphi} = -\sigma_s$	
			V_{max}, thousands of m^3	α	V_{max}, thousands of m^3	α
I	90	20	22	0,25	50	0,55
II	65	23	23	0,35	31	0,48
III	20	10	4,5	0,25	10	0,50

It follows from the results of [1], that the maximum cavity volume v_{max} is determined by the explosion energy and the strength and elastic properties of the medium:

$$p_{max} V_{max} = \eta E, \tag{15}$$

where η is the fraction of the explosion energy going to form the explosive cavity; the quantity η is approximately constant and equal to 0.6, both for brittle disintegration and for plastic flow; p_{max} is a characteristic depending on the strength and elastic properties of the medium. It corresponds to the minimum pressure capable of crushing (or plastically deforming) the surrounding medium, and collapsing the cavity walls. At the same time p_{max} is the maximum pressure which can be sustained in a cavity surrounded by pulverized rock.

For the case of Coulomb friction ($\sigma_{rr} = 2\sigma_{\varphi\varphi}$) we have

$$p_{max} = \sigma^* \left[\frac{\frac{4}{3}\pi R_p^3}{V_{max}} \right]^{1/3}. \tag{16}$$

For the case of plastic flow ($\sigma_{rr} - \sigma_{\varphi\varphi} = -\sigma_s$) we have

$$p_{max} = -\sigma_{rr} + \frac{2}{3}\sigma_s \ln \left[\frac{\frac{4}{3}\pi R_p^3}{V_{max}} \right]. \tag{17}$$

Here σ_{rr} is calculated, taking into account the rock pressure from Eq. (14). Equations (15)-(17) have been used to calculate values of the maximum cavity volume shown in Table 3. Table 3 also shows the quantity α, equal to the ratio of the maximum cavity volume to the displaced volume, which describes the condensation of the medium in the disintegration zone (or plastic deformation zone).

Table 3 shows that use of the Coulomb law ($\sigma_{rr} = 2\sigma_{\varphi\varphi}$) to describe flow of crushed rock salt leads to a contradiction with experimental data. For example, for explosion III the maximum cavity volume is considerably less than the final volume.

The results obtained under the assumption that the salt behaves, beyond its strength limit, as a perfectly plastic material, appear more plausible. A comparison of the cavity volumes (maximum and final) shows that the cavity compression is larger, the deeper is the explosion center. It is not possible to estimate conditions for the appearance of motion of the medium towards the center, nor the extent of this process, from the available experimental data. We can only assume that the compression occurs quite slowly, so that redistribution of stresses can occur under the action of the rock pressure in the medium, as time passes.

LITERATURE CITED

1. V. N. Radionov, I. A. Sizov, and V. M. Tsbetkov, Collection: Explosions (Vzryvnoe Delo) No. 64/21, "Seismic details and ejection crater in underground explosions" [in Russian], Nedra, Moscow (1968).
2. G. Werth and Ph. Randolph, J. Geophys. Res., 71, 3405 (1966).
3. L. Rogers, ibid., p. 3415.
4. W. Werth, Bull. Seismol. Soc. America, 52, 981 (1962).
5. V. N. Rodionov, A. N. Romashov, and A. P. Sukhotin, Dokl. Akad. Nauk SSSR, 123, No. 4 (1958).
6. A. P. Stavrogin, "Technology of coal extraction by an underground method," Trudy Tsentr. N.-i. In-ta Inform. i Tekh.-Ékon. Issled. Ugol'noi Prom-sti, No. 5 (17) (1968).

METHODS OF STUDYING NUCLEAR STRUCTURE

V. G. Solov'ev

UDC 539.14

Works on nuclear physics have two objects: the study of nuclear structure as such, and the study of elementary interactions manifesting themselves in nuclear properties. We consider problems related to the study of nuclear structure.

The study of the atomic nucleus is of fundamental scientific interest. This is true for two reasons. The first has to do with the exceptionally important role of atomic nuclei in nature, as appears particularly clearly in stars where nuclear transformations play a decisive role. The second reason is that the study of an elementary interaction between two particles gives inadequate information on the properties of these particles; more complete information can be obtained from the study of systems of strongly interacting particles such as nuclei.

An atomic nucleus is a very complex system characterized by a large number of degrees of freedom. Many different experimental procedures based on physical processes involving strong, electromagnetic, and weak interactions must be employed to study nuclear structure.

The construction of a nuclear theory is beset with great difficulties because of the necessity of describing a finite system of strongly interacting particles in the absence of a series expansion parameter.

Simple models were sought in the early stages of the development of nuclear theory. Then instead of simple models various approximate procedures were used to take account of the forces playing a decisive role in the study of particular nuclear properties.

In modern nuclear theory the many approximate methods used are conventionally divided into three types: phenomenological, semimicroscopic, and microscopic.

In the phenomenological description of the structure of complex nuclei collective coordinates are introduced to characterize the departure of the nuclear shape from sphericity, and the excitation of the nucleus is related to the rotation of the nucleus as a whole and to oscillations of the nuclear surface [1]. In such a description each nucleus is characterized by several parameters. The excitation energies of states, their multipole moments, and the probabilities of electromagnetic transitions are expressed in terms of these parameters. The values of the parameters for each nucleus are determined from appropriate experimental data. Serious limitations and faults are inherent in such a purely phenomenological description.

The semimicroscopic description is based on the selection of an effective nuclear interaction. In the semimicroscopic description the interactions among nucleons in the nucleus are separated into two parts; the average field of the nucleus and the residual interactions. The average field is that nuclear potential which is produced by all the nucleons in the nucleus. A large collection of experimental data obtained in the study of α-, β-, and γ-spectra and nuclear reactions is used to determine the parameters of the average field potential. The residual interactions include the forces not contained in the average field. The residual interactions play a very important role in the nucleus and vary monotonically and slowly from nucleus to nucleus. They are not small and cannot be taken into account by perturbation theory. The average nuclear field plays a very large role; it determines many nuclear properties directly and in addition controls the residual interactions; i.e., it permits the effect of the nuclear forces to show up to some extent. Thus the average field determines specific properties of each nucleus and is responsible for variations in many properties from nucleus to nucleus.

Translated from Atomnaya Énergiya, Vol. 30, No. 1, pp. 37-43, January, 1971. Original article submitted May 12, 1970.

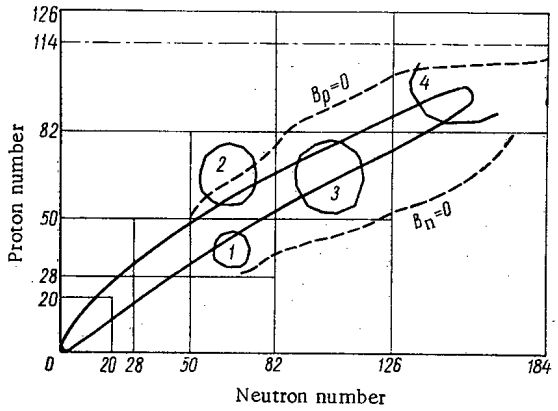

Fig. 1. Neutron – proton diagram of atomic nuclei. The banana-shaped figure denotes the region of known nuclei. The ovals 1-4 are regions in which the deformation energy is greater than 2 MeV. The dashed lines denote zero separation energies of a neutron and a proton.

A form for the residual forces is chosen from an analysis of nuclear spectra, and various properties of a group of nuclei are calculated. As a result of these calculations some of the experimental data are explained and certain predictions are made. The effective forces have many different components and the existing experimental data permit a determination of only part of them.

New experimental facts permit the refining of the effective forces. New calculations are then performed, etc. The semimicroscopic theory claims to describe relative rather than absolute nuclear characteristics. For example it permits a calculation of the energy of an excited state but not the total energy of the nucleus.

Advances in the semimicroscopic theory of the nucleus are linked with the extensive use of mathematical methods developed in the theory of superfluidity [2], superconductivity [3-5], and a Fermi liquid [6].

The semimicroscopic theory which takes account of the average nuclear field, interactions leading to pair correlations of the superconducting type, and multipole – multipole forces is called the superfluid model of the nucleus [7-12]. It has been possible to obtain a rather good description of low-lying excited states of intermediate and heavy nuclei within the framework of the superfluid model. An interesting approach evolves from the theory of finite Fermi systems [13].

The microscopic description uses experimental data on nucleon – nucleon scattering to calculate such fundamental properties as the density of nuclear matter and the binding energy of a nucleon in a nucleus. Development in this direction encounters grave difficulties. Thus nucleon – nucleon scattering yields only part of the necessary data – the values of the functions on the energy surface, when the momenta of the two initial and the two final particles are related by the laws of conservation of momentum and energy. Since the nucleon – nucleon potential is complex and not unique, it is necessary to use certain effective potentials in the calculations, and this reduces the attractiveness of the method from the logical point of view.

Rapid progress in the development of calculational techniques stimulated an extension of the microscopic method to more complicated nuclei and to calculations of nuclear spectra.

Nuclear structure studies are extending in two directions: the measurements of characteristics of ground states and higher and higher excited states, and a broadening of the range of nuclei studied by moving from the β-stable region toward superheavy elements.

Nuclear structure cannot be understood by studying a few nuclei. Many characteristics of even – even nuclei differ from those for neighboring odd – even or odd – odd nuclei. The structure of light nuclei differs from that of intermediate and heavy nuclei. The structure of deformed nuclei is very different from that of spherical nuclei, etc. Deformed nuclei differ greatly from one another. Thus in comparison with nuclei in the $150 < A < 190$ range the peculiarities of deformed nuclei in the actinide region manifest themselves, for example, in fission. It is clear that it is impossible to study fission on the basis of the properties of the rare earth isotopes. While nuclei in the ranges $150 < A < 190$ and $228 < A < 254$ have the form of a prolate ellipsoid of revolution, some of the nuclei in the ranges $50 < Z, N < 82$ and $28 < Z < 50$, $50 < N < 82$ possibly have the form of an oblate ellipsoid of revolution, etc.

The list of those nuclear characteristics which change from one nucleus to another could be continued. However it is already clear that in spite of the fact that forces between nucleons are the same in all nuclei, nuclear structure differs, and it is impossible to investigate it without significantly broadening the range of nuclei studied.

The modern period of development of nuclear physics is a period of intensive collection of experimental facts, since the existing quantitative information on nuclear structure is still small. Figure 1 shows the neutron – proton diagram of nuclei. Naturally occurring nuclei (with times appreciably larger than the

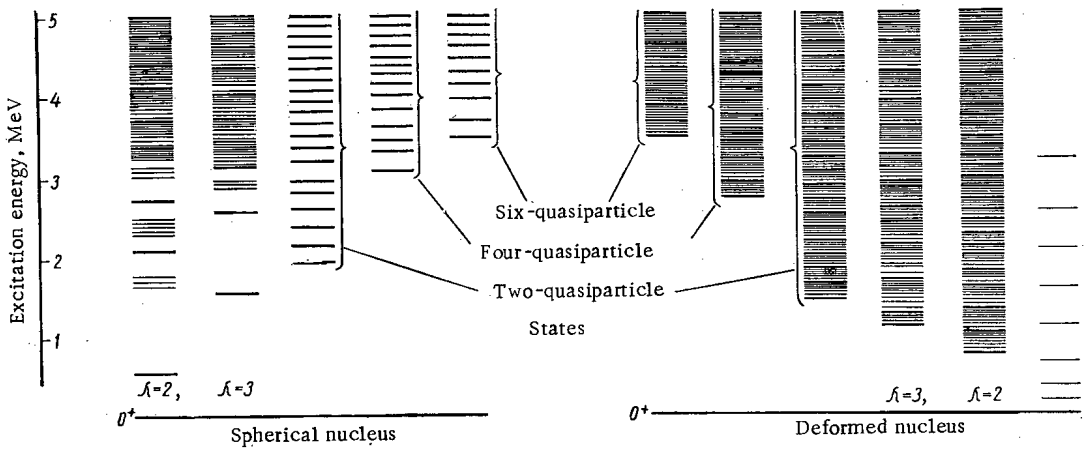

Fig. 2. Scheme of excited states of spherical and deformed even – even nuclei. The heavy lines denote ground states, one-phonon, and two-, four-, and six-quasiparticle states. The thin lines indicate multiphonon and rotational states; $\lambda = 2$ denotes quadrupole, and $\lambda = 3$ octupole states. The ground-state rotational band is shown on the right-hand side.

nuclear time) must exist between the lines $B_p = 0$ and $B_n = 0$; i.e., nuclei with positive separation energies of a neutron and a proton.

It is clear from Fig. 1 that the region of nuclei observed experimentally comprises only a quarter of all possible nuclei. Low-lying excited states have been studied in only about one tenth of the known nuclei. The construction of particle beam mass separators of the Isolda type at CERN [14] and YaSNAPP at JINR [15], and the wide use of heavy ion accelerators extend the range of known nuclei both by moving away from the β-stable region, and by advancing toward superheavy elements. A very intense experimental search is being conducted for the island of long-lived superheavy elements [16].

Studies of the characteristics of ground states and higher and higher excited states occupy a fundamental place in nuclear physics. Low-lying excited states are described within the framework of the semimicroscopic procedure by means of quasiparticles and phonons. Rotational bands in deformed nuclei are built on ground, quasiparticle, and phonon states. Figure 2 shows schematically the excited states in even – even spherical and deformed nuclei. The lower levels are of a collective nature and then the two-, four-, etc., quasiparticle states occur. With an increase in excitation energy the interactions of quasiparticles with phonons, the Coriolis interaction, and other forces complicate the structure of excited states.

Let us consider strongly deformed nuclei for example. β- and γ-spectroscopy and the results of $(n\gamma)$ and direct reactions have led to the following: 1) ground state and low-lying excited state rotational bands have been studied and values of moments of inertia, quadrupole moments, and gyromagnetic ratios have been obtained; 2) the energies of quadrupole and octupole states, and the magnitudes of B(E2) and B(E3) have been found; 3) spins I, their projections K, and parities π have been determined for a large number of levels. In addition to these characteristics it is necessary to obtain more detailed information on the structure of the states. It is necessary to determine sets of asymptotic quantum numbers $[N, n_z, \lambda]$ for the quasiparticle states and the component composition of the vibrational states, since the wave functions of the vibrational states are superpositions of two-quasiparticle wave functions.

Let us consider how the asymptotic quantum numbers and the purity of the quasiparticle states can be determined experimentally. The asymptotic quantum numbers can be reliably determined by α- and β-spectroscopy for an allowed unretarded β-decay and a favored α-decay. In the $150 < A < 190$ region, however, allowed unretarded transitions occur only between two pairs of states, and in the $228 < A < 254$ region they do not occur at all. The number of favored α-transitions is also small. Therefore the methods of α- and β-spectroscopy give insufficient information on the asymptotic quantum numbers of the quasiparticle states and practically no information on their purity.

Let us turn to direct reactions involving the transfer of a single nucleon. Table 1 shows the relative intensities of the population of the $1/2^-$ [521] and $1/2^-$ [510] state rotational bands and the values of

TABLE 1. Relative Intensities and Values of $\left(\sum_{\Lambda} a_{l\Lambda}\,(l\Lambda\,1/2\sum|jK)\right)^2$ for Population in (d, p) and (d, t) Reactions of $1/2^-[521]$ and $1/2^-[510]$ State Rotational Bands*

	Spin I	Population of $1/2^-[521]$ band levels							Population of $1/2^-[510]$ band levels			
		in (d, t) reactions				in (d, p) reactions			in (d, p) reactions			
		theory	experiment			theory	experiment		theory	experiment		
			^{171}Yb	^{173}Yb	^{175}Yb		^{159}Gd	^{161}Gd		^{171}Yb	^{173}Yb	^{175}Yb
Relative intensities at $\theta = 90°$	1/2	100	100	100	100	100	100	100	2,4	—	3,3	—
	3/2	9,3	24	6,3	6,5	9,8	12	8,8	100	100	100	100
	5/2	26		17	21	37	32	50	35	43	51	45
	7/2	31	32	27	27	47	65	50	25	16	25	20
	9/2	5,0	3	2,5	3,5	7	8	7,6	1,4	4,4	4,2	5,5
	11/2	0,7	1,4	1,7	1,2	1,2	—	—	0,2	—	—	—
Values of $\left(\sum_{\Lambda} a_{l\Lambda}\,(l\Lambda\,1/2\sum|jk)\right)^2$	1/2	0,249	0,284	0,300	0,282	0,25	0,23	0,25	0,01	—	0,01	—
	3/2	0,024	0,018	0,020	0,019	0,02	0,03	0,02	0,40	0,34	0,31	0,31
	5/2	0,182	0,142	0,142	0,165	0,18	0,15	0,24	0,29	0,31	0,33	0,29
	7/2	0,231	0,272	0,243	0,228	0,23	0,29	0,19	0,19	0,10	0,15	0,12
	9/2	0,269	0,185	0,164	0,216	0,27	0,30	0,29	0,09	0,24	0,21	0,28
	11/2	0,045	0,097	0,130	0,09	0,05	—	—	0,01	—	—	—

* Data from [17].

$\left(\sum_{\Lambda} a_{l\Lambda}\,(l\Lambda\,1/2\,\Sigma\mid jK)\right)^2$, where the $a_{l\Lambda}$ are the expansion coefficients of the Nilsson potential in terms of the wave functions. The relative intensities are normalized to 100 for the $1/2-1/2[521]$ and $3/2-1/2[510]$ levels. It is clear from Table 1 that the intensity distributions over the rotational bands are different for these two states. A comparison with calculations permits a unique assignment of asymptotic quantum numbers to these states with $K^\pi = 1/2^-$. By studying the intensity distributions of the level population of the rotational bands in direct reactions involving the transfer of a single nucleon extensive data on asymptotic quantum numbers of one- and two-quasiparticle states have been obtained.

A combination of the methods of β- and γ-spectroscopy with direct reactions involving single-nucleon transfer has given the characteristics for a rather large number of quasiparticle states in deformed nuclei. The measurement of cross sections for the excitation of one-phonon vibrational states permits the determination of their component composition. The first analysis showed that the theory gives correct values of the largest components of the γ-vibrational states in a number of nuclei.

As the excitation energy rises the density of states increases and their structure becomes more complex [18]. The study of complex states requires supplementing the values of $I^\pi K$, given by α-, β-, and γ-spectroscopy, by information on the component composition of these states. Therefore a comprehensive study of nuclear structure must be performed using the methods of α-, β-, and γ-spectroscopy and nuclear reactions; this has so far not been adequately developed. In some cases it is found that laborious β- and γ-spectra studies actually give no new information on the structure of the nucleus being studied.

Studies using α-, β-, and γ-spectroscopy and nuclear reactions gave a large amount of experimental material on energies, spins, and many integral characteristics of low-lying states in spherical and deformed nuclei. These data have been used to determine the parameters of the average field potentials and other nuclear characteristics such as moments of inertia, quadrupole moments, etc.

The question of the accuracy of the assumed description of nuclear states or the magnitude of the admixture of higher configurations in quasiparticle and phonon states is very important. The simplest answer to this question can be obtained by studying nuclei which are nearly doubly magic. Since in magic nuclei the average field is chosen so that the density matrix is practically diagonal, residual interactions must be minimal. Low-lying states of nuclei differing by one nucleon from a doubly magic nucleus must be single-particle (single-hole) states or states of a particle (hole) plus a phonon, etc. Experimental data obtained from single-nucleon transfer reactions [19] have shown that states up to 1.5-2.0 MeV in ^{207}Tl, ^{207}Pb, ^{209}Pb,

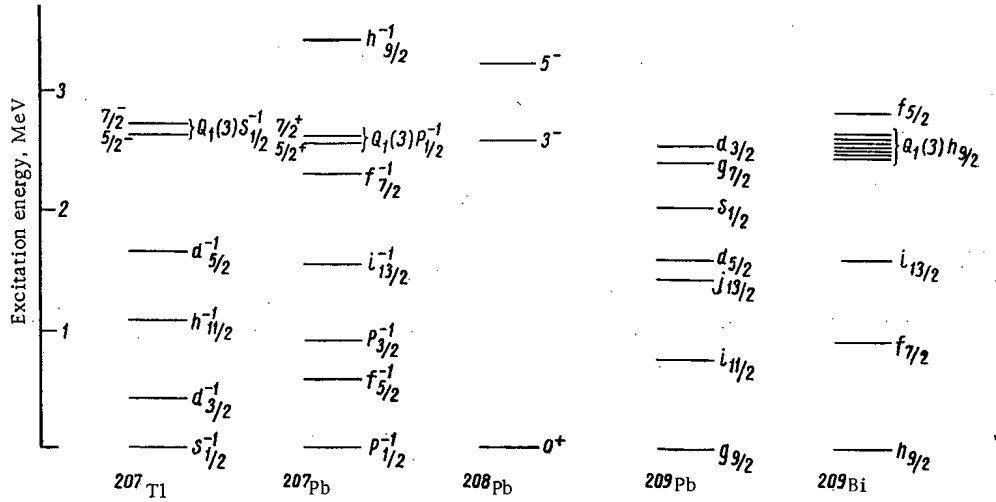

Fig. 3. Experimental data on low-lying excited states in ^{208}Pb and in neighboring nuclei differing by one nucleon. $g_{9/2}$, $i_{11/2}$, $h_{9/2}$, etc., denote particle excited states while $S^{-1}_{1/2}$, $d^{-1}_{3/2}$, and $p^{-1}_{1/2}$ denote hole excited states. $Q_1(3)S^{-1}_{1/2}$, $Q_1(3)p^{-1}_{1/2}$, and $Q_1(3)h_{9/2}$ denote multiplets—octupole phonon plus particle.

and ^{209}Bi are practically pure single-particle states; for higher excitation energies some states remain single-particle and others exhibit a mixture of higher configurations. For example, in ^{207}Pb the states $p^{-1}_{1/2}$, $f^{-1}_{5/2}$, $p^{-1}_{3/2}$, and $i^{-1}_{13/2}$ are pure single-hole states while the states $f^{-1}_{7/2}$ and $h^{-1}_{9/2}$ contain admixtures of 20 and 35% respectively. The level of these odd nuclei and of ^{208}Pb are shown in Fig. 3. The experimental data on magnetic moments do not contradict the fact that the ground states of these nuclei are practically single-particle (single-hole) states.

The lowest state in ^{208}Pb is an octupole single-phonon 3^--state with an energy of 2.615 MeV. Multiplets consisting of a particle (hole) plus an octupole phonon should be observed in neighboring odd nuclei. Those multiplets for which the particle (hole) is in the subshell corresponding to the ground state of the odd nucleus should have the lowest energy.

Actually ^{207}Tl shows a doublet $I^\pi = 5/2^-$ and $7/2^-$ with an energy of about 2.6 MeV consisting of an octupole phonon plus a $S^{-1}_{1/2}$ hole. In ^{207}Pb there is a doublet $I^\pi = 5/2^+$ and $7/2^+$ with energies of 2.625 and 2.664 keV consisting of an octupole phonon plus a $p^{-1}_{1/2}$ hole. Since the proton is in the $h_{9/2}$ subshell in the ground state of ^{209}Bi, the septet of octupole phonon plus $h_{9/2}$ particle has spins and parities of $3/2^+$, $5/2^+$, $7/2^+$, $9/2^+$, $11/2^+$, $13/2^+$, and $15/2^+$ and an energy close to the energy of the 3^- phonon in ^{208}Pb. All levels of this septet have been observed experimentally, and the energy splitting is about 250 keV.

In nuclei differing from ^{208}Pb by one nucleon one should expect higher energy states consisting of a phonon plus a particle (hole) in an excited state. In addition there should be three-particle, five-particle, etc., states, and also states consisting of a particle (hole) plus two phonos, etc. It is of very great interest to find all single-particle states in these nuclei and to trace the complication of the structure of three-particle, particle plus phonon, etc., states with increasing excitation energy.

The problems of the amounts of admixtures of higher configurations in quasiparticle states, the structure of phonon states, etc., in nonmagic spherical and deformed nuclei still await solution. There is great interest in the study of the behavior of quasiparticle and phonon states and their interweaving with increasing excitation energy.

The experimental data have shown that low-lying nuclear states are appreciably more complex than predicted by recent theories. Therefore the further study of the structure of low-lying nuclear states and progress to higher excitation energies requires a comprehensive study combining the methods of α-, β-, and γ-spectroscopy (including $(n\gamma)$ reactions) with direct nuclear reactions using monochromatic beams of particles of various kinds including heavy ions.

There have been many studies of the equilibrium shape of nuclei in ground and excited states. While the equilibrium shape of the ground states of most nuclei in the β-stable region are known, the study of

equilibrium deformations of ground states of nuclei far from the β-stable region, and of equilibrium deformations of nuclei in excited states, is in the initial stage. There are interesting questions connected with the study of the shapes of isomers, especially of the structure of spontaneously fissionable isomers [20], nuclei with the shape of an oblate ellipsoid [21] (regions 1 and 2 of Fig. 1), etc. The study of nuclear fission, including the appearance of characteristic features of nuclear structure, is very important.

The study of nuclear structure is inseparably linked with the explanation of the mechanism of nuclear reactions. Progress in the treatment of direct nuclear reactions has given valuable information on nuclear structure. Thus the method of distorted waves has yielded data on the principal components of nuclear wave functions. A more complete determination of the component composition of nuclear states requires a refinement of the mechanisms of nuclear reactions.

So far we have discussed the ground and low-lying states of nuclei. Let us now consider the situation with respect to the study of the structures of more highly excited nuclear states. The region of excitation from 2 or 3 MeV to the binding energy of a nucleon in intermediate and heavy nuclei has received slight attention.

The existence of mass separators of the Isolda and YaSNAPP types and proton emitters offers a very great possibility of studying levels with excitation energies of 2 MeV and more in intermediate neutron-deficient nuclei. With a displacement from the β-stable region toward neutron-deficient isotopes the energies of β-transitions increase greatly, making it possible to study levels with excitation energies from 2 to 5 MeV. It should be noted that it is of interest to study the structure of very short-lived isotopes displaced from the β-stable region by 15 and more neutrons, and short-lived isotopes displaced from the β-stable region by 8-14 neutrons. It is very important that the advance to larger excitation energies be gradual and take place over a wide front.

The methods of neutron spectroscopy led to information on the average characteristics of compound states close to the binding energy of a neutron. Explaining the nature of these states (how different are the structures of levels with identical spins and parities, how do the shells manifest themselves, etc.,) is an important scientific problem. Here the greatest interest lies in the study of $(n\gamma)$ and $(n\alpha)$ reactions by resonances [22].

In the quasicontinuous spectral region great interest centers on the study of analogous states and a different type of giant resonances. It is hardly necessary to say that the study of analogous states and the fine structure of giant resonances is in the initial stage.

Every year there is an increase in information on nuclear structure from experiments on the interaction of intermediate and high energy particles with nuclei. Thus the scattering of fast electrons indicates the deviation of the electric charge density in nuclei from the Fermi distribution. The absorption of kaons by nuclei indicates a possible enrichment of the nuclear surface by neutrons.

The study of muon capture in nuclei gives valuable information on nuclear shapes, the structure of the dipole and quadrupole excitations, and partial transition rates. Interactions of pions with nuclei give information on the short-range correlations of nucleons in nuclei. The cross sections for the forward expulsion of fast light nuclei in the interaction of protons with nuclei give some information on clusters in nuclei. There is great interest in the study of the mechanism of the interaction of high energy particles with nuclei.

Obtaining data on the density distribution of nuclear matter in nuclei, the structure of phonon states, and many other characteristics, requires nearly mono-energetic beams of protons, deuterons, electrons, and other particles over a wide range of energies. Intense beams of kaons are also required.

We have higher hopes for the study of hypernuclei. In hypernuclei the interactions of hyperons with nucleons and with one another are not greatly weakened by the operation of the Pauli principle and therefore there is the possibility of studying new aspects of nuclear structure. At the present time students of hypernuclei are paying particular attention to the determination of the characteristics of nucleon–hyperon (spin – spin dependence, tensor components, etc.,) and hyperon – hyperon potentials, the role of three-particle forces in hypernuclei, etc. Information on bound excited states of hypernuclei is still inadequate, and advancement into the region of heavier hypernuclei is very slow.

In spite of the increase in the contributions of high-energy physics to the study of nuclear structure, it is not expected that the contributions during the next few years will be either very large or very valuable.

LITERATURE CITED

1. A. S. Davydov, Excited States of Atomic Nuclei [in Russian], Atomizdat, Moscow (1967).
2. N. N. Bogolyubov, Lectures on Quantum Statistics [in Russian], Sovetskaya Shkola, Kiev (1949).
3. J. Bardeen, L. Cooper, and J. Schriefer, Phys. Rev., 108, 1175 (1957).
4. N. N. Bogolyubov, V. V. Tolmachev, and D. V. Shirkov, A New Method in the Theory of Superconductivity [in Russian], Izd-vo AN SSSR, Moscow (1958).
5. N. N. Bogolyubov, Usp. Fiz. Nauk, 67, 549 (1959).
6. L. D. Landau, Zh. Éksp. Teor. Fiz., 35, 97 (1958).
7. V. G. Solov'ev, The Effect of Pairing Correlations of the Superconducting Type on the Properties of Atomic Nuclei [in Russian], Gosatomizdat, Moscow (1963).
8. S. T. Belyaev, Mat. Fys. Medd. Dan. Vid. Selsk, 31, No. 11 (1959).
9. V. G. Solov'ev, The Structure of Complex Nuclei [in Russian], Atomizdat, Moscow (1966), p. 38.
10. V. G. Solov'ev, Atomic Energy Review, 3, No. 2, 117 (1965).
11. D. R. Bes and R. A. Sorensen, Advances in Nucl. Phys., 11, 129 (1969).
12. V. G. Solov'ev, Prog. in Nucl. Phys. 10, 239 (1968).
13. A. B. Migdal, Theory of Finite Fermi Systems and Properties of Atomic Nuclei [in Russian], Nauka, Moscow (1965).
14. P. G. Hansen, Proc. Inter. Conf. Properties of Nuclear States, Les Presses de l'Université de Montreal, Montreal (1969), p. 189.
15. G. Muziol', V. I. Raiko, and Kh. Tyroff, JINR Report [in Russian], R6-4487 (1969).
16. G. N. Flerov, V. A. Druin, and A. A. Pleve, Usp. Fiz. Nauk, 100, 45 (1970).
17. D. H. Burke et al., Mat. Fys. Medd. Vid. Selsk, 35, No. 2 (1966); P. O. Tjom and B. Elbek, Mat. Fys. Medd. Dan. Vid. Selsk, 36, No. 8 (1967).
18. V. G. Solov'ev, Nuclear Structure (Dubna Symposium), Vienna, IAEA (1968), p. 283.
19. N. Stein, Proc. Inter. Conf. Properties of Nuclear States, Les Presses de l'Université de Montreal, Montreal (1969), p. 337.
20. S. M. Polikanov, Usp. Fiz. Nauk, 94, 44 (1968).
21. D. A. Arseniev, A. Sobiozewski, and V. G. Solov'ev, Nucl. Phys., A 126, 15; A 139, 296 (1969).
22. F. L. Shapiro, Nuclear Structure (Dubna Symposium), Vienna, IAEA (1968), p. 283.

ANALOG STUDIES OF THE DYNAMICS OF A POWER PLANT CONTROL SYSTEM INCORPORATING A 440 MW(e) REACTOR

L. N. Golyand, S. Ya. Dunaevskii, V. F. Ostashenko, and T. M. Afanas'eva

UDC 621.039.51

Results of analog simulation studies of the dynamics of the control system for a power plant unit incorporating the V-440 reactor are presented. The reliability of the results obtained in the analog simulation* are confirmed by experiments conducted on real equipment (the first and second power units of the Novaya Voronezh' nuclear power plant). Transients in the control system of the first and second power units are compared to the simulation results, with the power output brought down to 70 and to 120 MW respectively. The simulation accuracy was estimated in neutron flux at 3-5% rating, in terms of pressure to about 1 atm, in terms of coolant temperature to within 1-2°C.

The static characteristics of the third power unit of the Novaya Voronezh' nuclear power plant (with the V-440 reactor) are presented along with the dynamic characteristics of the unit, the latter including the speed at which the reactor is brought up to full power, the extent to which reactor parameters are smoothed out automatically, and delay times, in response to reactivity surges and turbogenerator loads. The characteristics are reported for different power output levels and different reactivity coefficients with respect to coolant temperature.

The dynamic characteristics of the third power unit in the Novaya Voronezh' nuclear power plant in response to a stepwise drop in station power output from 100% to 50%, with a relay type controller acting on the reactor control rods in a constant-speed mode, are discussed.

The relationship between the maximum pressure deviation in the secondary loop, and of the control response time on the one hand, and the rate of change in reactivity by action of the control rods on the other, were obtained in the case of a reactivity surge. These relationships were obtained at different temperature coefficients of reactivity, with pressure relief devices (discharging steam to the condensers of turbogenerators) operating or nonoperative. The relationship can be discussed as the limiting dependences in estimates of the performance quality of control systems designed for the third power unit of the Novaya Voronezh' nuclear power plant.

Two arrangements for power control are cited for the power unit: pressure control in the secondary loop and average coolant temperature control in the primary loop, with automatic correction of the coolant temperature to match the turbogenerator loads. The two arrangements are compared with commensurate adjustments made, including adjustments with the identical stability margin in terms of modulus.

The dependence of the control response time with power cut to the 50% level and a different rate of reactivity change by the action of the control rods was also obtained. This dependence was then used to estimate the operating efficiency of the controller. The control response time with the pressure controller operating in a constant-speed mode was used as the lower limiting estimate. An estimate of the reactor power overcontrol was also made for that control mode.

The dependence of the maximum pressure deviation in the secondary loop, and of the control response time, on changes in turbogenerator loads, on the rate of change of reactivity by action of the control rods, and on the control setup of the power unit, is investigated.

*The details of the model were described in the authors' paper presented for the USSR at the COMECON symposium "Control and management of atomic reactors and nuclear power plant facilitities" in Budapest, 1969.

Translated from Atomnaya Énergiya, Vol. 30, No. 1, p. 44, January, 1971. Abstract No. 453/5856. Original article submitted April 20, 1970; revision submitted July 30, 1970.

These investigations revealed that the various control arrangements discussed are equivalent in their dynamic characteristics. But the pressure control approach is more reliable in the performance of the transducers. The secondary-loop pressure control concept is therefore recommended for the application.

SWELLING OF CYLINDRICAL DISPERSION TYPE FUEL ELEMENT IN NONUNIFORM TEMPERATURE AND NEUTRON FIELDS

Yu. I. Likhachev

UDC 621.039.517

Axisymmetric swelling of a long cylindrical dispersion type fuel core in radially nonuniform temperature fields and neutron fields has been discussed. It is suggested that the fuel consists of regularly spaced

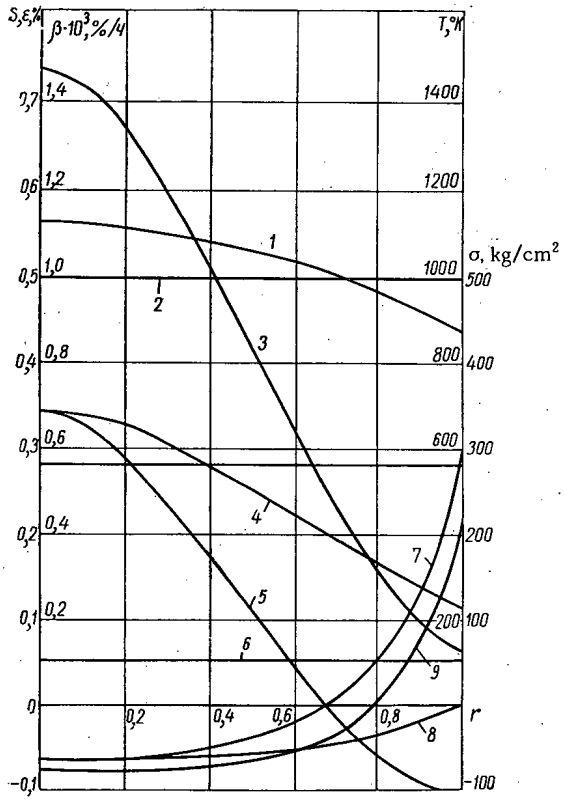

Fig. 1

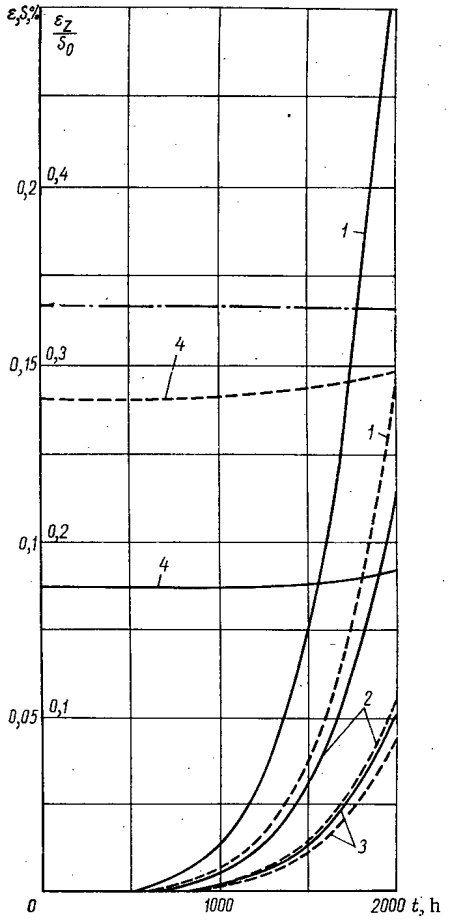

Fig. 2

Fig. 1. Distribution of parameters over the cross section of the core of the fuel element in a fast reactor: 1) temperature, 2) fission density, 3) swelling, 4-6) peripheral, radial, and axial strains respectively, and respective stress σ_θ, σ_r, σ_z (7-9 respectively), for time 2000 h.

Fig. 2. Time variation of average amount of swelling (1), peripheral (2), and axial (3) strains in equivalent fuel elements, for the case of a fast reactor (continuous curves) and thermal reactor (broken curves). Curve 4 indicates the fraction of axial deformation due to average swelling (dot-dash curve corresponds to the case of isotropic swelling of fuel elements).

Translated from Atomnaya Énergiya, Vol. 30, No. 1, pp. 44-45, January, 1971. Abstract No. 454/5638. Original article submitted October 11, 1969; abstract submitted July 28, 1970; revision submitted July 28, 1970.

identical spherical cells in the form of hollow thick-walled spheres with spherical granules of fissionable materials inside. Swelling of individual cells S(r, t) is determined by the creep experienced by hollow spheres loaded by the internal pressure of gaseous fission products building up, and by the external pressure which is picked up by equal components of the spherical macroscopic stress tensor which originate in the interaction between volumes of the fuel element core swelling at different rates. The macroscopic stresses are determined by solving the problem of the creep experienced by a fuel core in the case of the bulk strain varying over the core cross section and increasing with time, and equal to the swelling S(r, t) of the spherical cells.

A method of numerical solution of the system of integro-differential equations obtained has been worked out by V. V. Vakhromeeva.

Figures 1 and 2 show results of calculations of the swelling of a disperse type fuel core with a matrix of austenitic steel (type 1Kh18N9T) and grains of uranium dioxide, for cases where the fuel element does service in fast reactors and in thermal reactors. The fact that swelling and increased fuel-element diameter in a thermal reactor are substantially less than in a fast reactor (in the case of equivalent fuel elements in which the temperature on the surface of the core, the average amount of heat release over the cross section, the thermal conductivity of the fuel composition, and the core radius, are assumed identical) is explained by the smaller temperature drop over the cross section of the fuel element in a thermal reactor.

LOWERING THE RATE OF HYDROGEN DIFFUSION THROUGH Kh18N10T STEEL WHEN THE STEEL SURFACE IS OXIDIZED IN A TONNAGE HYDROGEN ATMOSPHERE

V. I. Subbotin, V. N. Bykov,
F. A. Kozlov, N. N. Ivanovskii,
and V. V. Kazarnikov

UDC 53.3.15

A study of the penetration of hydrogen through a Kh18N10T steel membrane of thickness 0.2 ± 0.01 mm has shown that the permeability of the membrane decreases 50 to 100 times after oxidation in an atmosphere of tonnage hydrogen (≈ 0.5 vol. % O_2).

The amount of hydrogen diffusing through a volume that had already been roughed out to a vacuum was determined from changes in pressure occurring over a specified time span. The hydrogen pressure was measured with the aid of an LT-2 thermoelectric pressure gage, with irregularities of the temperature, in the volume, and changes in the characteristics of the pressure gage brought on by the enhanced thermal conductivity of the gas [1] taken into account. The temperatures were monitored by Chromel–Alumel thermocouples. The hydrogen diffusion rate was measured over the 600-750°C temperature range at a 760 mm Hg hydrogen pressure drop. The membrane was oxidized at 650°C for 16 h in an atmosphere of tonnage hydrogen at 1 atm pressure. Preliminary outgassing of the entire system in a vacuum of at least $1 \cdot 10^{-4}$ mm Hg at 850°C for 50 h cut the gas inleakage to the working volume down to $1.45 \cdot 10^{-4}$ N · cm³ · mm/cm² · h.

The energies of activation of the process by which the hydrogen penetrated the oxide film and the Kh18N10T steel were respectively 16.4 ± 3.2 kcal/mole and 12.0 ± 3.0 kcal/mole. The results obtained imply that hydrogen diffuses through the oxide lattice not in monatomic form (as in materials with a metallic type bond [2]) but in molecular form (as in enamels and glasses [3]).

Translated from Atomnaya Énergiya, Vol. 30, No. 1, p. 46, January, 1971. Abstract No. 455/5188. Original article submitted December 18, 1968; abstract submitted February 12, 1970.

The difference in the rates of hydrogen diffusion through the oxide films on the Kh18N10T steel, obtained when the steel was oxidized in air and in an atmosphere of tonnage hydrogen, seem to be due, in our opinion, to the effect of the environment and of the oxidation conditions on the quality of the film forming. Under the oxidation conditions prevailing in our experiments, the oxide formed became alloyed with the chromium. As a consequence, the plasticity of the oxide film increased, stresses were reduced, and the number of flaws in the oxide layer decreased as a result.

These factors result in a more continuous oxide film forming when the Kh18N10T steel oxidizes in an atmosphere of tonnage hydrogen, a film which is of complex composition and less permeable to hydrogen than the oxide film that forms in air.

LITERATURE CITED

1. L. G. Khorkin, ZhTF, XXV, 726 (1955).
2. O. M. Bérrer, Diffusion in Solid Bodies [Russian translation], IL, Moscow (1948).
3. A. A. Appen, Temperature-Stable Inorganic Films [in Russian], Khimiya, Leningrad (1967).

CHANGE IN REACTIVITY DURING SHUTDOWNS OF A HIGH-FLUX REACTOR

T. S. Zaritskaya

UDC 621.039.516.2

The change in reactivity during shutdown of a high-flux reactor due to I^{135}, Xe^{135}, Pm^{149}, and Sm^{149} is calculated. The dependence of this process on the steady-state operating power before shutdown is studied.

The general nature of the reactivity change is as follows: there is first a rapid buildup of Xe^{135} from the decay of I^{135}, then the decay of Xe^{135}, and finally the slow buildup of stable Sm^{149} due to the decay of Pm^{149}. It is established that for a neutron flux of $2.6 \cdot 10^{14}$ neutrons/cm^2 · sec the asymptotic value of the reactivity for infinitely long shutdown is the same as the steady-state reactivity before reactor shutdown, and for a flux of $3.2 \cdot 10^{14}$ neutrons/cm^2 · sec the steady-state value of the reactivity agrees with the minimum in the shutdown process when Xe^{135} has decayed and Sm^{149} has not yet been formed.

The results of the calculations serve as reference material in choosing shutdown procedures for high-flux reactors.

Translated from Atomnaya Énergiya, Vol. 30, No. 1, p. 46, January, 1971. Abstract No. 456/5481. Original article submitted July 10, 1969; revision submitted September 21, 1970.

EFFECT OF EMPTY CYLINDRICAL CHANNELS ON NEUTRON MIGRATION*

I. S. Grigor'ev

UDC 621.039.51.12

Measurements of the elongation factors of the squares of the diffusion length $\mathscr{L}_i = L_i^2/L_0^2$ and migration length $\mathscr{M}_i = M_i^2/M_0^2$ in water are reported for different lattices of empty cylindrical reactor channels. All the experimental $\mathscr{L}_{\parallel}$ values for guide channels parallel to the axis were found to be below those computed on the basis of Behrens's formula [1]. These discrepancies are practically entirely eliminated when corrections for the anisotropy in neutron scattering, and specific to the heterogeneous medium [2], are taken into consideration.

The $\mathscr{L}_{\perp}$ measurements disclosed a need to pay attention to angular correlations of the mean free neutron paths $\delta_{q\perp}(\mu\rho)$ [3]. Experimental $\sigma_{q\perp}$ values were obtained and a semiempirical formula for computing $\mathscr{L}_{\perp}$, which yields excellent agreement with experimental $\mathscr{L}_{\perp}$ values measured in our work and those published earlier by other authors, is proposed.

The $\mathscr{M}_i$ measurements were conducted with the use of neutron sources having different spectra (fission spectrum and spectrum of the polonium–beryllium source) and shape (plane source and "point" source). The measurements showed that the use of the equation $M_i^2(p) = L_i^2(p) + \tau_i(p)$ to calculate $M_i^2(p)$ values in a medium containing voids does not contradict available experimental data.

LITERATURE CITED

1. D. Behrens, Proc. Phys. Soc., A62, 607 (1949).
2. B. M. Novikov, Atomnaya Énergiya, 21, 272 (1966).
3. P. Benoist, Nucl. Energy, A13, 97 (1961).

INFLUENCE OF INSTRUMENT-DEPENDENT QUANTITIES UPON THE FORM OF THE β-RADIATION ABSORPTION CURVE†

V. G. Belashov and A. M. Bogachev

UDC 539.12:621.039.538

The aim of the present work is to investigate the analog and discrete recording methods for β radiation and the influence of instrument-dependent quantities (resolving time and relative recording efficiency) upon the form of the absorption of β radiation fluxes, because the available data are inconsistent.

A theoretical analysis of the influence of the recording method was made by modeling the interaction of the allowed Fermi spectrum of β particles with relatively thin foils. It was found that the absorption curve recorded with an analog method (γ_I) is given by the expression

$$\gamma_I(x \simeq b) = 1 - \left[\frac{5\cdot 7\cdot 9}{16} b^{5/2}\left(\frac{2}{5} - \frac{4}{7}b + \frac{2}{9}b^2\right)\right],$$

*Translated from Atomnaya Énergiya, Vol. 30, No. 1, pp. 46-47, January, 1971. Abstract No. 457/5708. Original article submitted January 4, 1970.

†Translated from Atomnaya Énergiya, Vol. 30, No. 1, p. 47, January, 1971. Abstract No. 458/5732. Original article submitted January 23, 1970; abstract submitted August 25, 1970; revision submitted August 25, 1970.

where x denotes the absorber thickness and $b = E_{max}/E_x$, the ratio of the maximum energy of the β spectrum to the maximum energy of the electrons which are not recorded by the detector when an absorber of thickness x is introduced. The curve recorded by a discrete method (γ_N) is given by the equation

$$\gamma_N (x \simeq b) = 1 - \left[\frac{3 \cdot 5 \cdot 7}{16} b^{3/2} \left(\frac{2}{3} - \frac{4}{5} b + \frac{2}{7} b^2\right)\right].$$

The curves obtained with the various recording methods were compared. The influence of the resolving time τ of the counting equipment was considered under the assumption that the true absorption curve has exponential form. The excess of the relative slope φ_{rel} of the true curve over the slope of the instrument-dependent curve is related to the quantity τ by

$$\varphi_{rel} = 1 + N(0)\,\tau \exp -\mu x,$$

where N(0) denotes the flux density of the radiation when no absorber x is inserted and μ is the attenuation coefficient. The instrument-dependent curve is always situated above the real curve and the distance increases with increasing $N(0)\tau$. The relative efficiency of a recording has a similar influence. Theoretical conclusions confirm the experimental results.

The following conclusions can be drawn from the investigations:

1) the absorption curve can have exponential form or nonexponential form. The form of the curve depends upon the change of β spectrum by the absorber and upon the above-described instrument-dependent influences;

2) the slope of the absorption curve recorded with a discrete recording method for the radiation flux is steeper (at least in the initial section) than the curve recorded with an analog method under otherwise equal conditions;

3) use of discrete recording methods of the radiation flux in radioisotope instruments makes it possible to considerably increase the sensitivity with which a parameter is recorded.

The results obtained can be used for optimization of radioisotope instruments and for improvements in dosimetry, activity determinations, estimates of the thermal effect caused by radioactive samples, etc.

THE EQUILIBRIUM DISTRIBUTION OF HYDROGEN ISOTOPES IN THE LIQUID – VAPOR SYSTEM FOR AMMONIA

V. M. Bakin and Ya. D. Zel'venskii

UDC 621.039.322.3

The available experimental data of the value of α, the separation factor for hydrogen isotopes in the rectification of ammonia, apply to the temperature range below 20°C, and the data given by different authors are markedly different. In the past the values of α for the temperature range above 20°C have been estimated by extrapolation. It therefore seems of interest to make direct measurements of the value of α in the $NH_3 - NH_2D$ system for the uninvestigated temperature range.

TABLE 1

Temperature, °C	10	20	30	40	50
α	1,0246	1,0216	1,0187	1,0161	1,0136
Temperature, °C	60	70	80	90	
α	1,0112	1,0090	1,0070	1,0050	

The separation factor for hydrogen isotopes in the liquid–vapor system for ammonia was measured in the 10-90°C temperature range, using an instrument equivalent to one theoretical separation stage, by distilling off and analyzing specimens of the vapor phase which is in

Translated from Atomnaya Énergiya, Vol. 30, No. 1, pp. 47-48, January, 1971. Abstract No. 459/5809. Original article submitted March 12, 1970.

equilibrium with a large quantity of the liquid phase. The article describes the design of the instrument, which can be used for studying the liquid–vapor equilibrium at pressures up to 100 atm abs. In order to determine the value of α more accurately, we used ammonia enriched with deuterium (approximately 4 molecular percent when converted to ND_3). The conditions for experiments capable of yielding reliable data are the following: rate of stirring of liquid phase, approximately 200 rpm; rate of vapor-phase sampling, not more than $1 \cdot 10^{-4}$ g/cm^2 · sec.

An isotope analysis of the ammonia samples was carried out by burning the ammonia over copper oxide at 600°C to form water and then determining the deuterium content by the float method. The error in the method of analysis used was no more than 2-3 μg, which corresponds to a deviation of ± 0.0015 in the value of α.

Knowing the concentration of the vapor and liquid phases in the equilibrium state, we calculated the separation factor of hydrogen isotopes in the liquid–vapor system as the ratio of the relative concentrations of deuterium in the liquid and vapor phases, respectively.

The resulting experimental values of α for the 10-90°C temperature range under investigation can be described, with a mean absolute error of ± 0.0010, by the equation

$$\lg \alpha = \frac{10.796}{T} - 0.02756, \quad (1)$$

found by the method of least squares. Table 1 shows the values of α calculated from Eq. (1). In the temperature range under investigation, our experiments did not indicate any inversion in α (which is assumed by some authors to exist at 75-85°C, on the basis of extrapolation of the data obtained in the temperature range from −70 to +20°C). Calculations using Eq. (1) indicate that $\alpha = 1$ at 118-119°C.

From the variation of α as a function of temperature, we calculated the difference between the heats of vaporization of ammonia molecules containing different hydrogen isotopes and obtained a value of $\Delta L = \Delta H_{NH_2D} - \Delta H_{NH_3} = 49.4 \pm 1.5$ cal/mole.

The results of the experiment to determine the separation factor of hydrogen isotopes in the liquid–vapor system for ammonia are evaluated and are compared with the known literature data.

THE SIMULATION OF HYDRODYNAMIC PROCESSES IN THE SEPARATION OF ISOTOPES IN PACKED COLUMNS

V. A. Kaminskii, N. A. Giorgadze, R. Sh. Vartapetyan, and M. P. Dzhodzhua

UDC 621.039.3+532.5

In order to obtain formulas for calculating the hydrodynamic parameters of columns filled with an effective wire packing, we propose the use of a geometrically simple model based on the statistical characteristics of actual packings.

In the model the vapor moves in a narrow channel between two parallel surfaces inclined at some angle to the horizontal, while the liquid runs off as a film on the two interior faces of the channel. The width of the model is equal to the perimeter of the packing in a unit cross section of the column, while the space for the passage of the gas is determined from the condition that equivalent diameters in the packing and the model must be equal.

In the case of such a model we obtain a formula for the thickness of the liquid film by solving the hydrodynamic equations in the form of boundary-layer equations, taking account of friction on the boundary

Translated from Atomnaya Énergiya, Vol. 30, No. 1, pp. 48-49, January, 1971. Abstract No. 460/5459. Original article submitted July 7, 1969; abstract submitted August 6, 1970; revision submitted August 6, 1970.

separating the phases. Together with the known expression for the pressure gradient in the gas channel, this formula will give us a system of algebraic equations from which we can simultaneously determine φ_d, the retentive capacity of the packing, and ∇P, its hydrodynamic resistance:

$$\Gamma = \frac{i\rho_l g - \nabla P}{3\mu_l a_k^2}\varphi_d^3 - \frac{V_{og}\rho_g f_g \varphi_g^2}{16\mu_l a_k^2 (F-\varphi_{st}-\varphi_d)^2};$$

$$\nabla P = \frac{V_{og}^2 \rho_g \rho_k}{8(F-\varphi_{st}-\varphi_d)^2} f_g.$$

Here Γ is the amount of liquid retained per unit of perimeter; a_k and i are the width of the model and the sine of its angle of inclination, respectively.

In order to explain the mechanism of phase inversion in columns with fine packing, we started from the premise that it is hardest to keep the film unbroken at places where the liquid flows along the lower surfaces of the packing elements. In the model the corresponding liquid flow takes place along the upper surface of the channel.

For a fixed value of the load, when the sum of pressure and frictional forces acting on an element of the liquid film will be equal and opposite to the component of the force of gravity in the direction of flow, the liquid will stop flowing in the direction in which it has been moving. As a result, there will be a sharp increase in the thickness of the film, and it will separate from the surface of the wall and spill out into the vapor phase.

The corresponding limiting velocity for the vapor is of the form

$$V_{og}^* = \left[\frac{i\rho_l g}{\frac{\psi}{(F-\varphi_{st}-\varphi_d)^2\varphi_d} + \frac{\psi}{(F-\varphi_{st}-\varphi_d)^3}}\right]^{0.73},$$

where

$$\psi = \frac{130\rho_g a_k}{8\left(\frac{4\rho_g}{a_k\mu_g}\right)^{0.64}}.$$

For a packing consisting of segments of a triangular spiral used for the separation of boron, nitrogen, and carbon isotopes by chemical exchange and distillation, and also for the air–water system, we obtained good agreement between the calculated and experimental data.

SOME REGULARITIES IN THE SPUTTERING OF A THIN LAYER OF FISSIONABLE MATERIAL ONTO A METALLIC SUBSTRATE BY FISSION FRAGMENTS

V. K. Gornikov and P. A. Petrov*

UDC 539.2:539.12.04

As had been shown in an earlier article, sputtering of thin layers of fissionable isotopes onto metallic substrates (thin sources) is achieved through the action of fission fragments traversing the surface. The amount of sputtering (emission) then depends on the topography of the surface of that layer [1]. This topography undergoes some changes through the bombardment by the fission fragments, which acts to reduce emission from thin sources with increased radiation exposure dosage.

* Deceased.

Translated from Atomnaya Énergiya, Vol. 30, No. 1, p. 49, January, 1971. Abstract No. 461/5312. Original article submitted March 21, 1969; abstract submitted August 5, 1970; revision submitted August 5, 1970.

The sources used for further research on these phenomena, as described in this paper, were in the form of thin layers of the spontaneously fissioning isotope Cm^{244} coated onto different metallic substrates. It was found, in this experiment, that emission by these sources on which the fission fragments impinged is completely restored through thermal annealing of the sources in the atmosphere and at normal pressure. The recovery temperature is related to the recrystallization temperature of the substrate material.

On the basis of these and other experimental data, it is inferred that the decrease in the emission of the thin sources is brought about by fragments penetrating deeper into the metallic substrate. The thin layer of fissionable material coated onto the surface of the solid specimen may be acting, therefore, as a sensitive indicator of microscopic deformations in the surface of the material under investigation. In particular, a new method of investigating radiation damage in solid media becomes possible on that basis. The great sensitivity of the method makes it possible to conduct this research at low exposure doses and during the irradiation process, and also makes it possible to study the effects of radiation in their dependence on the state of the material under investigation.

LITERATURE CITED

1. V. K. Gorshkov and L. N. L'vov, Atomnaya Énergiya, 20, 327 (1966).

MULTIPOSITION TARGET CHAMBER FOR A NEUTRON GENERATOR

D. V. Viktorov, I. M. Rozman, and A. M. Shcherbakov

UDC 621.039

The target chamber was developed for experiments investigating the effect of neutrons produced in the reactions H^2 (d, n) He^3 and H^3 (d, n) He^4 on the performance of semiconductor instruments, and is designed to accommodate standard deuterium or tritium targets 14 mm in diameter. The objects to be irradiated can be placed at a 90° angle to the deuteron beam, at a distance $L \geq 23$ mm from the center of the active layer of the target, or at a 55° angle at a distance $L \geq 7.5$ mm. The chamber offers three positions. The target can be replaced twice without disturbing the vacuum in the accelerator tube. This is achieved through the way the working target and the spare targets are soldered to a cooled copper disk, and the targets are replaced by rotating this disk through 90° (control is either manual or remote).

The chamber is adjusted through the bellows-sealed joint of the ion guide. There is a connection for mounting a counter to detect accompanying particles (at a 90° angle to the beam). The target chamber is electrically insulated from the other parts of the generator, so that the deuteron current can be measured.

The disk carrying the targets is cooled by water flowing down a channel of rectangular cross section 30×0.8 mm^2. The dependence of heat transfer on the water flowspeed ($w \geq 3.8$ m/sec) was measured. The production of the heat transfer coefficient α (W/cm^2 · deg) by the effect heat extraction surface area S (cm^2) is in agreement with the theoretical dependence $\alpha S = Bw^{0.8}$, at the value B = 5.6. Comparison with theoretical predictions shows that the high value of B stems from the large heat extraction surface area: S is about five times greater than the target area.

When w = 6.8 m/sec (water pressure at entry 3 atm), the temperature drop between the active layer of the target and the cooling water is about 100°C by 400 W of the deuteron beam, or about $1 \cdot 10^{11}$ cm^{-1} by the intensity of the neutrons generated in the reaction H^3 (d, n) He^4.

Translated from Atomnaya Énergiya, Vol. 30, No. 1, pp. 49-50, January, 1971. Abstract No. 462/5581. Original article submitted July 14, 1970.

RESONANT ACCELERATION OF PARTICLES BY FAST ELECTROMAGNETIC WAVES PROPAGATING PARALLEL TO AN INCREASING MAGNETIC FIELD

A. N. Didenko and V. K. Kononov

UDC 621.384.62

We are concerned here with the possible continuous acceleration of charged particles in a smooth waveguide of rectangular or circular cross section along whose axis a TE_{n1} wave is propagating with a phase velocity $v_p = \beta_p c$ ($\beta_p > 1$). The wave guide is placed in an external axisymmetric magnetic field. If the magnetic field is constant along the length, the phase shift of the particle which arises with respect to the wave will lead to the disruption of self-resonant acceleration. For continuous acceleration of the particles, the magnetic field must change along the wave guide in a specific manner. In this case, the acceleration will not be self-resonant, so the trajectory of the equilibrium particle and the stability of the motion about this trajectory must be studied.

The problem was solved in the following manner. The equation of motion of a charged particle in the field of left-rotating travelling TE_{11}-wave is written in a cylindrical coordinate system (r, θ, z) (z is along the waveguide axis), and is solved under the following conditions:

1) $\varphi = \omega t - k_z z - \theta = \varphi_s = \text{const}$; this means that the phase of the equilibrium particle with respect to the wave is constant (k_z is the z-component of the wave vector);

2) $r = r_s = \text{const}$.

From the solutions of the equations of motion, we find the required behavior of the external magnetic field along the waveguide axis:

$$h_z = e_0 \frac{\mathcal{J}_1(\varkappa r)}{\varkappa r \mathcal{J}_1'(\varkappa r)} \frac{1-\varkappa^2 r^2}{kr} \sin\varphi_s - \frac{k\gamma\left(\beta_p^2 - \sqrt{(k^2r^2+\beta_p^2)(1-\gamma^{-2}) - k^2r^2\beta_p^2}\right)}{k^2r^2+\beta_p^2}; \tag{1}$$

$$h_r = \frac{e_0}{\beta_p}\cos\varphi_s \frac{\beta_p^2 - k^2r^2(\beta_p^2-1)}{k^2r^2+\beta_p^2} \frac{\beta_p^2 - \sqrt{(k^2r^2+\beta_p^2)(1-\gamma^{-2}) - k^2r^2\beta_p^2}}{\sqrt{(k^2r^2+\beta_p^2)(1-\gamma^{-2}) - k^2r^2\beta_p^2}}, \tag{2}$$

where

$$h = \frac{eH}{m_0c^2}; \quad e_0 = \frac{eE_0}{m_0c^2}\mathcal{J}_1'(\varkappa r); \quad \varkappa^2 = k^2 - k_z^2; \quad \gamma = \frac{\mathcal{E}}{m_0c^2};$$

$\mathcal{E}$ is the energy of the particle, E_0 is the electric field intensity of the wave, and $\mathcal{J}_1$ and $\mathcal{J}_1'$ are Bessel function and its derivative with respect to r. The length over which a particle acquires an energy $\Delta\gamma = \gamma - \gamma_H$ is found from

$$ze_0kr(\beta_p^2-1) = \beta_p\left\{\gamma - \gamma_H + \left(\gamma\sqrt{(k^2r^2+\beta_p^2)(1-\gamma^{-2}) - k^2r^2\beta_p^2} - \right.\right.$$

$$-\gamma_H\sqrt{(k^2r^2+\beta_p^2)(1-\gamma_H^{-2}) - k^2r^2\beta_p^2} - \beta_p(\beta_p^2-1)^{-\frac{1}{2}}\left[\operatorname{arctg}\frac{\sqrt{\beta_p^2-1}(\gamma-\gamma_H)}{1+(\beta_p^2-1)\gamma\gamma_H} + \right.$$

$$\left.\left.+\operatorname{arctg}\frac{\beta_p^{-1}\sqrt{\beta_p^2-1}\left(\gamma\sqrt{(k^2r^2+\beta_p^2)(1-\gamma^{-2}) - k^2r^2\beta_p^2} - \gamma_H\sqrt{(k^2r^2+\beta_p^2)(1-\gamma^{-2}) - k^2r^2\beta_p^2}\right)}{1+\frac{\beta_p^2-1}{\beta_p^4}\gamma\gamma_H\sqrt{(k^2r^2+\beta_p^2)(1-\gamma^{-2}) - k^2r^2\beta_p^2}\sqrt{(k^2r^2+\beta_p^2)(1-\gamma_H^{-2}) - k^2r^2\beta_p^2}}\right]\right\}. \tag{3}$$

According to these calculations, we can select parameters such that the particle moves along a helix of constant radius and constant spacing over essentially the entire length of the acceleration. The stability of the motion was also treated in a linear approximation. Quite simple inequalities were found. It turned out that the stable motion in the field of a TE_{11}-wave, the conditions $\sin\varphi_s > 0$ must be satisfied.

Numerical calculations show that such accelerators may be useful for producing highly intense beams of electrons with energies of the order of several (or tens of) megaelectron volts.

Translated from Atomnaya Énergiya, Vol. 30, No. 1, p. 50, January, 1971. Abstract No. 463/5773. Original article submitted February 13, 1970.

CALCULATION OF LOW-CURRENT BEAMS IN DIRECT-ACTION ACCELERATORS

R. P. Fidel'skaya

UDC 621.384.64

We treat the formation of low-current beams in direct-action accelerators with an account of the finite phase volume and relativistic effects. An analytic solution is found for the equation derived by Kapchinskii [1] for the envelope of a beam with a finite phase volume for the case of a uniform electric field E. This equation is used to derive the basic equations for the optics of low-current direct-action accelerators, which are valid for both ionic and electronic (relativistic) beams. Equations are obtained for the minimum beam radius R_{min} and the corresponding distance from the entrance to the tube Z_{min} for given values of the radius R_0, the electric field potential U_0, and the beam convergence angle α_0 at the entrance to the tube:

$$R_{\min}=\frac{F_0R_0}{\sqrt{F_0^2+4\eta c^2U_0(1+\eta U_0)\alpha_0^2R_0^2}}; \tag{1}$$

$$Z_{\min}=\frac{\{[1+2\eta U_0+\sqrt{4\eta U_0(1+\eta U_0)}]\exp A-1\}^2}{4\eta E[1+2\eta U_0+\sqrt{4\eta U_0(1+\eta U_0)}]\exp A}-\frac{U_0}{E}, \tag{2}$$

where

$$A=\frac{-4\eta c^2ER_0^3\alpha_0\sqrt{\eta U_0(1+\eta U_0)}}{4\eta U_0(1+\eta U_0)c^2R_0^2\alpha_0^2+F_0^2};$$

$\eta = e/2m_0c^2$, πF_0 is the area of the two-dimensional phase volume of the beam, and c is the velocity of light.

The inverse problem, i.e., that of determining for a given R_{min} and corresponding U_0 the beam parameters R and α for a particle energy eU, has been solved:

$$R^2=R_{\min}^2+\left[\frac{F_0}{2c\eta ER_{\min}}\ln\frac{1+2\eta U+\sqrt{4\eta U(1+\eta U)}}{1+2\eta U_0+\sqrt{4\eta U_0(1+\eta U_0)}}\right]^2; \tag{3}$$

$$\alpha=\frac{F_0}{2cR_{\min}\sqrt{\eta U(1+\eta U)}}\sqrt{1-\frac{R_{\min}^2}{R^2}}. \tag{4}$$

The condition is found for the optimum initial angle at which the beam can be focused at a maximum distance from the entrance to the tube:

$$\alpha_{opt}=\frac{-F_0}{2cR_0\sqrt{\eta U_0(1+\eta U_0)}}. \tag{5}$$

The method of calculating the optics of low-current direct-action accelerators by means of the envelope equation is compared with the Elkind method [2], based on geometric optics. In particular, it is shown that the size and position of the crossover of the charged-particle flux depend on the magnitude F_0 of the beam phase volume and are equal to the corresponding values calculated by means of geometric optics only as $F_0 \to \infty$ (more precisely, for F_0 bounded by an arbitrary paraxial part of the beam).

LITERATURE CITED

1. I. M. Kapchinskii, Particle Dynamics in Linear Resonant Accelerators [in Russian], Atomizdat, Moscow (1966).
2. M. Elkind, Rev. Sci. Instrum., 24, 129 (1953).

Translated from Atomnaya Énergiya, Vol. 30, No. 1, p. 51, January, 1971. Abstract No. 464/5796. Original article submitted March 3, 1970.

LETTERS TO THE EDITOR

THE REDUCTION OF HEXAVALENT URANIUM BY HYDROGEN SULFIDE IN AQUEOUS SOLUTIONS AT INCREASED TEMPERATURES AND PRESSURES

R. P. Rafal'skii and B. S. Osipov

UDC 550.4:541.123:546.791

In connection with a study of the conditions of transport and deposition of uranium by hydrothermal solutions in the formation of uranium deposits, experiments were conducted earlier on the reduction of hexavalent uranium with hydrogen sulfide at temperatures up to 300°C in sulfate and carbonate solutions [1]. However, the amount of hydrogen sulfide in these experiments was not particularly monitored; in addition, the results of experiments in carbonate medium proved to be poorly reproducible, apparently as a result of the formation of colloids.

Below are cited the results of experiments conducted under strictly controlled conditions. Hydrogen sulfide was introduced into a quartz ampoule, and the ampoule with solution (degree of filling f = 0.5) was then frozen by immersion in liquid nitrogen. * The necessary amount of H_2S was measured by volume with a gas burette, to which hydrogen sulfide was delivered from a Kipp's apparatus after purification and drying (H_2O, I, $CaCl_2$). The burette was sealed with mercury. At room temperature the latter reacts with hydrogen sulfide too slowly to appreciably change the measurable amount of H_2S. Evidently the sorption of hydrogen sulfide by the rubber of the hoses connecting the main burette and the ampoule can lead to substantial errors. To minimize the possibility of sorption, the glass tubes were butt-jointed. On the whole, the method developed ensures the obtaining of quite reliable data.

The duration of experiments with a solution of UO_2SO_4 with an initial concentration of 9.8 g/liter uranium was 75, 30, and 10 h at 100, 150, and 200°C, respectively. From the data obtained earlier [1] it is evident that this time is more than sufficient for the reaching of equilibrium in the system. After exposure at the set temperature, the ampoules were removed from the furnace, cooled in cold water, opened, and the solution separated from the precipitate by vacuum filtration. During work it was found that these operations in this case can serve as a source of substantial errors.

As was established by special experiments, in the formation of uranium dioxide in the precipitate in the form of crystals, its dissolution during cooling and after it proceeds extremely slowly. However, as a result of the interaction of uranyl sulfate with hydrogen sulfide, dispersed precipitates are formed, consisting of rounded particles [2]. When the equilibrium is disturbed, their dissolution proceeds far more rapidly and can substantially distort the results. It was established that in the case of simultaneous cooling of 10-15 ampoules and their successive opening, the uranium concentration in solution is higher the later the ampoule is opened. Therefore, the ampoules were subsequently removed from the furnace in turn; from the time of removal of the ampoule from the furnace until a collection of the sample of the filtrate for analysis 5-7 min elapsed. The dissolution of the precipitate during this time was negligible and did not lead to any appreciable distortion of the equilibrium concentrations.

Below are cited all the results obtained at the concluding stage of the work, after complete development of the method and elimination of possible sources of errors. The convergence of the results of parallel experiments is quite satisfactory (Fig. 1). In all the experiments an appreciable amount of elementary sulfur was formed.

* Air was preliminarily evacuated from the ampoule and the line connecting the ampoule with the gas burette.

Translated from Atomnaya Énergiya, Vol. 30, No. 1, pp. 52-53, January, 1971. Original letter submitted May 13, 1970.

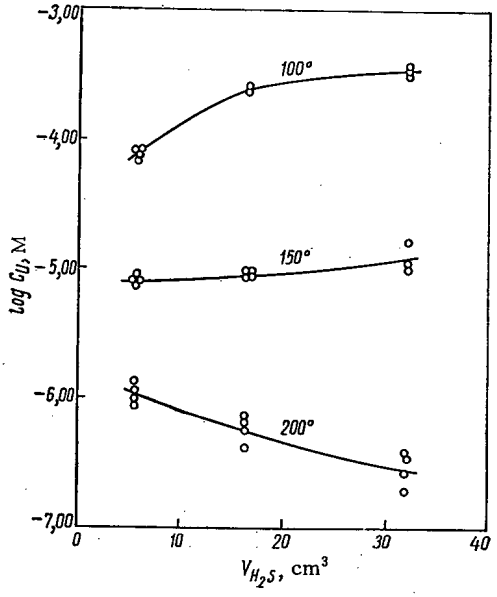

Fig. 1

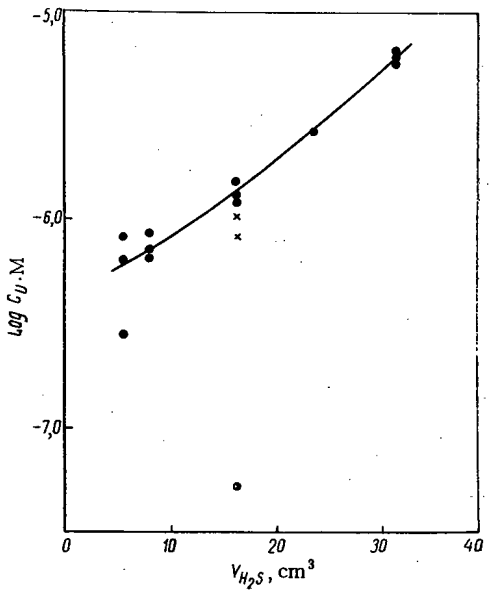

Fig. 2

Fig. 1. Dependence of the uranium concentration in sulfate solution on the amount of hydrogen sulfide in the ampoule.

Fig. 2. Dependence of the concentration in a 0.1 N solution of $NaHCO_3$ on the amount of hydrogen sulfide in the ampoule at 200°C (●); ×) results of experiments with uraninite.

The change in the equilibrium concentration of uranium in solution as a function of the amount of H_2S in the ampoule at various temperatures is shown in Fig. 1, along the x-axis of which the volumes of hydrogen sulfide under normal conditions, converted to V_{amp} = 6 cm^3, are plotted. On Fig. 1 are plotted the results of all the parallel experiments obtained for each point. The curves were constructed according to the average values. Contrary to expectations, at 100 and 150°C the uranium concentration increases with increasing amount of hydrogen sulfide in the ampoule. It may be assumed that this is due to the formation of hydrosulfide, or, more correctly, hydrogen sulfide complexes of uranium. Such complexes of this metal have not been described in the literature, insofar as we know, but the existence of such complexes of the basic heavy metals can be considered firmly established. The available experimental data are insufficient to judge the composition of the above-mentioned uranium complexes.

A "normal" dependence is observed at 200°C: with increasing concentration of the reducing agent, the uranium concentration in solution decreases. The temperature dependence of $C_{U_{eq}}$ is of the same nature as the dependence established for other systems containing uranium and reducing agents.

In experiments with bicarbonate solutions, a 0.1 N solution of $NaHCO_3$ was used as the initial solution. The uranium concentration in it, comprising 0.05 g/liter, was created by dissolving UO_3. When the ampoules were loaded in these experiments, the operation of thawing of the solution after unsealing of the ampoule and its removal from liquid nitrogen was quite unpleasant. In this case many of the ampoules broke down, which was expressed in the appearance of cracks in the quartz glass, sometimes accompanied by a slight explosion.

Below are cited the data of the last series of experiments conducted at 200°C* (Fig. 2), obtained after elimination of possible sources of errors. The convergence of the results of parallel experiments in this series, if we consider methodological difficulties, should be considered excellent. Exceptions are the clearly lowered data of one experiment, obtained for V_{H_2S} = 16.4 cm^3.

In addition, an attempt was made to approach equilibrium from the other side. A weighed sample of uraninite, synthesized by the method described earlier [3], was placed in the ampoule, which was then filled with a 0.1 N solution of $NaHCO_3$. After the introduction of hydrogen sulfide and sealing, the ampoule was heated for 76 h at 200°C. The results of two experiments (see Fig. 2) are in good agreement with the data obtained when equilibrium was approached "from above."

* Duration of experiments 48 h, degree of filling f = 0.5.

In bicarbonate solution the same dependence of the uranium concentration on the amount of H_2S is observed as in acid medium. However, although C_U in the latter case increases with increasing amount of hydrogen sulfide only at 100 and 150°C, such an effect is observed in $NaHCO_3$ solution at 200°C. In the presence of small amounts of H_2S, the uranium concentrations in acid and carbonate media are very close, but when $V_{H_2S} = 32$ cm^3, the concentration in bicarbonate solution is more than an order of magnitude higher than in sulfate solution. If the effect of hydrogen sulfide on C_U is actually due to the formation of complexes, then it can be concluded on the basis of the experimental data that a bicarbonate medium is more favorable for this process.

LITERATURE CITED

1. R. P. Rafal'skii, Physicochemical Investigation of the Conditions of Formation of Uranium Ores [in Russian], Gosatomizdat, Moscow (1963).
2. R. P. Rafal'skii and Yu. M. Kandykin, Geologiya Rudnykh Mestorozhdenii, 1, 98 (1960).
3. R. P. Rafal'skii, A. D. Vlasov, and K. F. Kudinova, At. Énerg., 13, 181 (1962).

RATE OF GROWTH OF HELIUM PORES DURING ANNEALING OF IRRADIATED BERYLLIUM OXIDE

A. V. Khudyakov

UDC 621.039.532.5:621.039.553

The fortunate combination of nuclear and physicomechanical properties possessed by BeO has given rise to intensive research on the radiation stability of beryllium oxide at high temperatures. It is known [1] that in BeO components with irradiation temperatures > 800°C, the effects of anisotropic expansion of the lattice parameters, which lead to failure of components at lower temperatures, become negligible. This means that at temperatures > 800°C BeO components would have longer service lives in a reactor if helium-filled pores did not form at the grain boundaries. Much research on the formation of helium pore in BeO has failed to establish the laws of development of pores when helium is evolved from the crystalline lattice; in particular, the rate of pore growth has not been measured.

EXPERIMENTAL METHOD

A concentration of about $1.2 \cdot 10^{19}$ helium atoms per cubic centimeter was created in beryllium oxide specimens [2] by irradiation at about 70°C with an integral flux of $5 \cdot 10^{20}$ neutron/cm^2 ($E \geq 1$ MeV). Then the irradiated specimens were annealed at 1400 or 1500°C in isothermal conditions. After each annealing session the specimens were broken apart; from the fresh chips we prepared chromium-shadowed carbon replicas. These were examined in UÉMB-100 and UÉMB-100V electron microscopes. Analysis of possible errors and control experiments established that the relative error of mean pore diameter determination was less than 10%.

From each chip we prepared two or three replicas; the area examined was usually 1.5-3 mm^2. The mean pore dimension was found from the pore dimension distribution (Fig. 1). The appearance of pores only at the grain boundaries is confirmed by the form of the chips (Fig. 2). By microscopic pycnometry on polished sections [3] we measured the total pore volume in the annealed specimens.

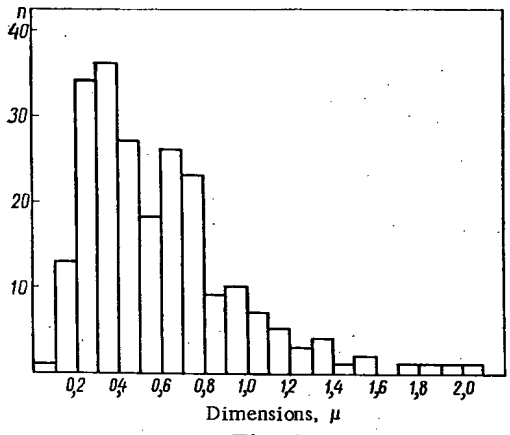

Fig. 1

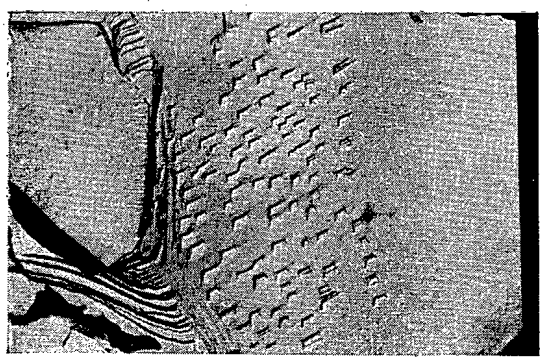

Fig. 2

Fig. 1. Distribution of pore diameters (annealing for 81 min at 1400°C).

Fig. 2. Helium pores in irradiated BeO (annealed for 5 min at 1500°C; magnification × 10,000).

Translated from Atomnaya Énergiya, Vol. 30, No. 1, pp.54-55, January, 1971. Original letter submitted July 24, 1969; revision submitted August 14, 1970.

TABLE 1. Changes in Dimensions of Helium Pores during Isothermal Annealing

Anneal temperature, °C	Anneal time, min	Area of chip, μ^2	Number of pores	Mean pore diameter, μ
1400	25	108	328	0,23
1400	30	355	802	0,28
1400	35	775	768	0,29
1400	81	630	223	0,61
1500	4	314	833	0,28
1500	15	319	36	0,72

RESULTS

Analysis of electron micrographs of the specimens annealed at 1400°C reveals that we can distinguish three time intervals with different porosity developments. In the first interval (up to about 20 min) there is a vigorous separation of fine pores, the dimensions of which could sometimes not be exactly measured. Then (up to 100 min) the pores are mainly larger than 0.2 μ; however, at the grain boundaries vanishingly small pores (50-100 Å) continue to appear. Subsequently all the pores grow; the growth rate slows down and the appearance of new fine pores ceases. After 15 h of annealing the total porosity of the specimens increases from 8 to 12%. Further annealing (up to 28 h) does not lead to an increase in the porosity (within the error of measurement which was ± 0.5%). At 1500°C we were unable to detect the first stage of pore development, because even after only 4 min of annealing the pores were already as large as after 30-35 min of annealing at 1400°C. The last stage begins after about 10-15 min and finishes after 4 h, when the total porosity is 12%; it does not change appreciably on further annealing. The pore dimensions were measured in the 1400°C replicas in the second stage of pore development and in the 1500°C replicas at the boundary between the second and third stages (see Table 1).

The variation of the mean pore dimension is represented by an empirical equation of the form

$$\bar{l} = \bar{l}_0 t^x, \quad (1)$$

where at 1400°C, $\bar{l}_0 = 0.016\ \mu$, x = 0.8 ± 0.1, and at 1500°C, $\bar{l}_0 = 0.1\ \mu$, x = 0.7 ± 0.2, where $\bar{l}$ is the mean pore dimension and t is the time in minutes.

DISCUSSION

The three stages of pore formation are evidently due to changes in helium emission rate from the crystal lattice at the grain boundaries. In the third stage new fine pores are not formed: emission of helium from the lattice gradually stops. In the second stage the pores most probably grow by receiving fresh portions of gas from the interiors of the grains. This supply of gas also explains the high pore growth rate, which exceeds the value theoretically predicted by (1) [4, 5], $x \leq 0.5$. The growth of the pores is due to the high gas pressure in them. Thus for similar BeO specimens [6] it was found that at anneal temperatures of 1400-1500°C the helium pressure in the pores reaches 5000 atm. Pore growth is much influenced by the grain boundaries which are sources of vacancies. Some part is played by mechanical stresses at grain boundaries, due to their anisotropic expansion during heating. In any case, we must try to give a theoretical explanation of the experimentally measured pore growth rates.

Although the kinetics of pore development during high-temperature irradiation will be different from those in the present case, the results lead us to certain conclusions on the nature of the pore development process during irradiation. In the first place, we can reckon that in reactors at 1400-1500°C practically all the helium will be concentrated in the pores. In the second place, at any time during irradiation, the helium pressure in the pores will be balanced by the surface tension. There should not be marked stresses round the pores.

These conclusions follow from the fact that pore development from the moment of nucleation until cessation of growth occurs in a very short time at the temperatures in question.

The author thanks Z. E. Ostrovskii, N. V. Sudakova, and G. S. Balandin for help with the work, and V. I. Klimenkov for useful advice.

LITERATURE CITED

1. B. S. Hickman and A. V. Prior, Beryllium Oxide [Russian translation], Atomizdat, Moscow (1968), p. 41.
2. A. V. Khudyakov, Z. E. Ostrovskii, and V. I. Klimenkov, At. Énerg., 23, 226 (1967).
3. A. V. Khudyakov, N. V. Sudakova, and G. S. Balandin, ibid., 28, 157 (1970).
4. Ya. E. Geguzin, Macroscopic Defects in Metals [in Russian], Metallurgizdat, Moscow (1962).
5. R. Nelson, D. Mazey, and R. Barnes, Phil. Mag., 11, 109 (1965).
6. L. Weil and J. Aslanian, Kältetechnik, 14, 397 (1962).

MEASUREMENT OF THE CROSS SECTION FOR FISSION OF U^{238} BY 2.5 MeV NEUTRONS, BY DETERMINING THE NEUTRON FLUX BY THE METHOD OF ACCOMPANYING PARTICLES

I. M. Kuks, V. I. Matvienko,
Yu. A. Nemilov, K. A. Petrzhak,
Yu. A. Selitskii, and V. B. Funshtein

UDC 539.173.84

Despite the large number of publications [1-3] on determination of the fission cross section of U^{238} in the region of the first plateau, the data on this question are unreliable, because the scatter of the measured cross sections exceeds the error of measurement. Most of the results are presented in the form of a ratio to the fission cross section of U^{235} without determination of the neutron flux. Absolute measurements, in which the neutron flux is measured by means of the recoil protons, are rarer. The most direct method of monitoring the neutron flux – the method of accompanying particles – was used in measurements of the fission cross section only for neutrons with energies of 14-15 MeV from the reaction T(d, n)He^4 [4, 5]; it was not used for lower-energy neutrons from the reaction D(d, n)He^3. Nevertheless, it is the cross sections in the region of the first plateau which are of greatest practical interest in reactor construction, because they correspond to the region of maximum neutron yield from the fission of heavy nuclei. For this reason we have attempted to use the most direct method of accompanying particles to determine σ_f at $E_n = 2.5$ MeV, in the same way as that used earlier at $E_n = 14$ MeV.

Figure 1 shows a schematic diagram of the experiment. A beam of deuterons was limited by diaphragm D, 5 mm in diameter, and fell on target M. We used a thin deuterium–titanium target on a molybdenum base 0.3 mm in thickness. To separate He^3 nuclei with energies of about 0.8 MeV, arising in the reaction D(d, n)He^3, from the products of the mirror reaction D(d, p)T, we used a proportional counter C, 20 mm in diameter, filled with argon at 40 mm Hg. The advantage of a proportional counter filled with low-pressure gas was that protons and tritons lost only a little of their energy in the counter gas, whereas He^3 was completely slowed down. As a result, pulses from He^3 had the greatest amplitude and could be reliably absolutely counted. To reduce scatter in the He^3 energy due to emergence from various depths in the target, the energy of the irradiating deuterons had to be reduced to 50-70 keV. Deuterons scattered by the target were absorbed by a nickel film glued to diaphragm O, 1 mm in diameter, and simultaneously serving as the vacuum window of the counter. Complete absorption of deuterons with energies of 70 keV corresponded to a film thickness of 350 $\mu g/cm^2$.

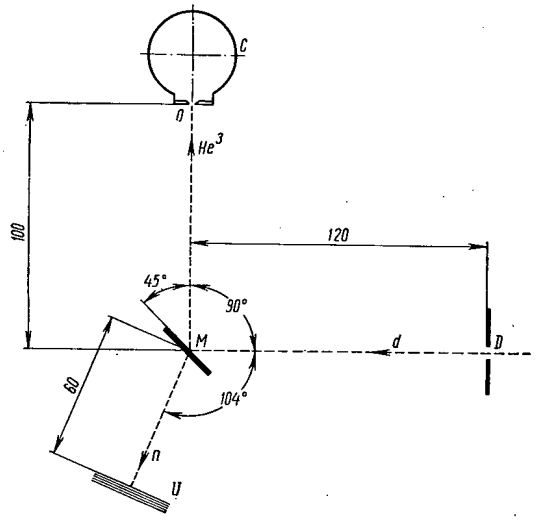

Fig. 1. Schematic diagram of experiment.

Figure 2 illustrates the distribution of pulses from tritons and He^3 nuclei. As we see from this figure, the resolution of the peaks decreases somewhat with the passage of time, owing to formation of scale on the target. With the amplification used, the proton peak fell in the first few channels of the pulse analyzer (not shown in Fig. 2).

The relative positions of the uranium target and proportional counter (Fig. 1) were so chosen that the determination of the neutron flux to the target was insensitive

Translated from Atomnaya Énergiya, Vol. 30, No. 1, pp. 55-57, January, 1971. Original letter submitted June 30, 1970.

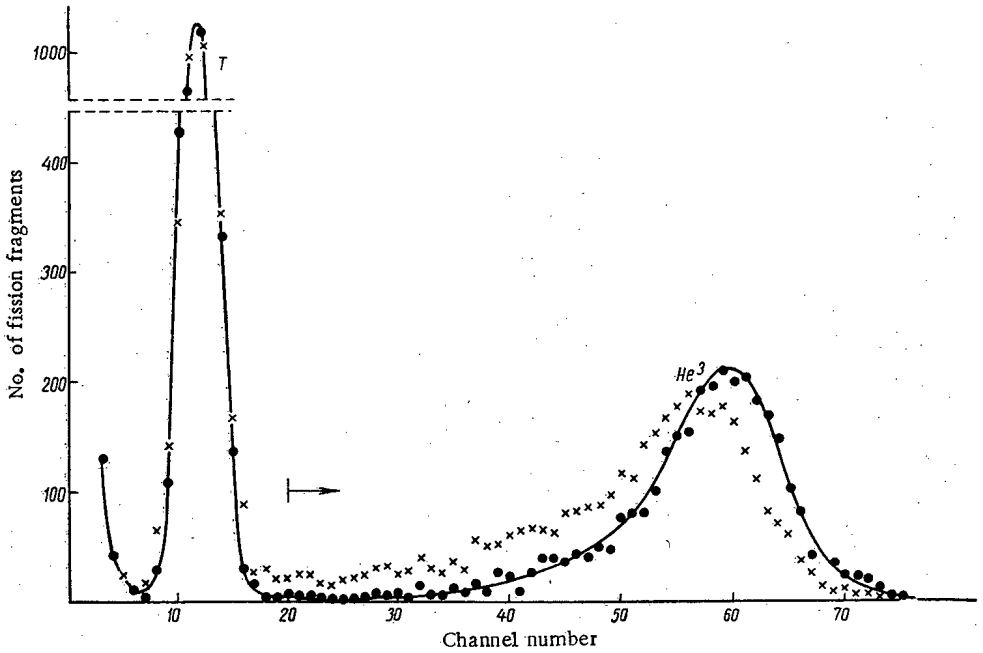

Fig. 2. Distribution of amplitudes of pulses in counter. ●) Fresh target; ×) target after 1.5 h of operation with current of 0.7 mA to target. Arrow indicates registration threshold.

to the angular distribution parameters, since the latter were not accurately known. He^3 ions registered by the counter corresponded to neutrons incident only in the central part of the uranium target. If the deuteron energies are low, the angular distribution of the neutrons in the center-of-mass system is given [6] by the formula

$$\sigma(\Theta) \sim 1 + A\cos^2\Theta.$$

We arranged the center of the target at an angle $\Theta \approx 90°$, where the variation of $\sigma(\Theta)$ is minimal, so that, within the solid angle used, the correction for flux inhomogeneity was 2%.

The fission-fragment detector was of mica. This combined high track registration efficiency [7] with minimum mass of the substance scattering the neutrons. A stack of ten layers of uranium and five layers of mica was composed so that each layer of mica registered fragments from the two layers of uranium pressed against it.

The targets were prepared by vacuum deposition of uranium fluoride (natural isotope mixture) on polished aluminum foil 0.1 mm thick and 19 mm in diameter. The isotope mixture of the uranium in the target was checked by special measurements on an α-spectrometer. The total weight of uranium in all ten layers was about 10 mg and was determined from the α-activity of the layers, measured in an ionization chamber, and the known specific activity of natural uranium which is $1501/\text{min} \cdot 4\pi \cdot \text{mg}$ [8].

In constructing the device we paid special attention to reducing elastic scattering of neutrons by the components in the direction of the uranium layers. Our calculations revealed that the main role here is played by the parts close to the target M. In the working version of the device, the deuterium–titanium target was the vacuum-atmosphere boundary and had no fastening device. Vacuum sealing was achieved by laying the target on a thin indium ring and covering the outer edge with picein. The target was cooled by a fine water spray from a thin capillary. All the walls near the target were less than 0.5 mm thick.

In a series of control experiments, we estimated the contributions made to the number of registered fragments by (i) fissions due to neutrons from the tamped target formed by the deuteron-beam-limiting diaphragm, and (ii) fissions of U^{235} in the natural uranium, due to thermal and subthermal neutrons. We found that the first of these factors can be neglected. To estimate the role of the second factor we performed an experiment with U^{235}. The result of this experiment was subsequently allowed for in the form of a correction of 2% to the cross section value. In addition, to check the workability of the apparatus as a whole we

made preliminary measurements of the fission cross section of U^{238} for neutrons from the reaction T(d, n)He^4. The value found, 1.13 ± 0.04 barn at E_n = 14.1 MeV, agrees with the latest data [3].

In all, during the exposures we registered 1300 fragments. In calculating the fission cross section we made the following assumptions:

i) the efficiency of registration of fission fragments by mica is 96 ± 1% [7];

ii) the contribution from fragments due to U^{235} fission is 2%;

iii) the geometrical correction associated with the finite dimensions of the deuteron beam and the uranium layers in the stack is 1%;

iv) the difference between the neutron beam density in the uranium layer and the density at its center is 2%;

v) the correction for neutrons, elastically scattered in the components of the apparatus, and incident on the uranium target, is 4 ± 1%;

vi) a correction was made for the efficiency of monitoring the neutron flux and for changes due to formation of scale on the target.

We analyzed the counter pulse amplitudes three times, namely, before, during, and after exposure. We estimated the relative number of pulses from He^3 with amplitude below the threshold of registration by smoothly extrapolating the α-particle peak towards zero amplitude. The mean relative correction averaged over three graphs was 2 ± 1%.

Finally we found the cross section for fission of U^{238} by 2.5 MeV neutrons to be 0.55 ± 0.02 barn, which agrees with the latest values recommended in the literature [3].

LITERATURE CITED

1. J. Stehn et al., Neutron Cross Sections, BNL-325, Vol. III, Brookhaven (1965).
2. W. Davey, Nucl. Sci. Engng, 32, 34 (1968).
3. W. Hart, Authority Health and Safety Branch, UKAEA, R. (1969), p. 169.
4. A. N. Protopopov, Yu. A. Selitskii, and S. M. Solov'ev, Trudy Radievogo in-ta im. V. G. Khlopina AN SSSR, 9, 55 (1959).
5. A. A. Berezin et al., At. Énerg., 5, 659 (1958).
6. J. Marion and J. Fowler, in: Physics of Fast Neutrons [Russian translation], Vol. 1, Atomizdat, Moscow (1963), p. 27.
7. O. V. Rumyantsev, Yu. A. Selitskii, and V. B. Funshtein, Pribory i Tekhnika Éksperimenta, No. 1, 51 (1968).
8. E. Hyde, I. Perlman, and G. Seaborg, Nuclear Properties of Heavy Elements [Russian translation], No. 4, Atomizdat, Moscow (1969), p. 131.

SPECTRA OF PROTONS FROM (t, pf) REACTIONS OF THE ISOTOPES U^{233}, U^{238}, AND Np^{237}

M. F. Andreev, V. A. Zavgorodnii, V. A. Pereshivkin, and V. I. Serov

UDC 539.125.4:539.173

The (t, p) reaction with subsequent fission of the compound nucleus is convenient for determining the fission characteristics of nuclei formed from an initial nucleus by addition of two neutrons. By means of this reaction we can obtain nuclei with excitation energies much lower than the binding energy of a neutron in the fissionable nucleus. The neutron emission channel is thus closed, which facilitates study of subbarrier fission, a process of special interest in the light of Strutinsky's model of the two-humped fission barrier [1].

In this letter we describe the results of measurements of the spectra of protons from the (t, pf) reaction of the isotopes U^{233}, U^{238}, and Np^{237}; this is the first stage in our study of the fissionabilities of these nuclei in the reaction (t, pf).

The shapes of the proton spectra enable us to draw some conclusions on the fissionabilities of the nuclei U^{235}, U^{240}, and Np^{239}.

The work was carried out in a tandem electrostatic generator with tritons accelerated to 13.23 ± 0.07 MeV. A schematic diagram of the experiment is shown in Fig. 1.

The target was a layer of oxides of uranium and neptunium isotopes, deposited by vacuum evaporation on to aluminum substrates with a thickness of about 100 $\mu g/cm^2$, or on gold substrates with a thickness of about 400 $\mu g/cm^2$ (NpO_2). The thicknesses of the targets used for the measurements were ~300 $\mu g/cm^2$ for U^{233}, ~400 $\mu g/cm^2$ for U^{238}, and ~700 $\mu g/cm^2$ for Np^{237}.

The protons were detected by a telescope of silicon semiconductor $\Delta E-E$ counters with a solid angle of 0.14 sr at the target. The thickness of the sensitive layer of the ΔE detector was 100 μ, and that of the E detector 2 mm. The resolving power of the $\Delta E-E$ counter telescope for protons was 120 keV at a working detector temperature of −55 to −65°C. To reduce contamination of the "proton" channel by fission fragments and α-particles, a 30 μ aluminum foil was placed in front of the telescope.

The fission fragments were registered by a silicon semiconductor detector of the surface-barrier type with a solid angle of 2.45 sr at the target. The fission fragment detector operated at 0-5°C, and its resolving power for α-particles with energies of about 5 MeV was 150 keV.

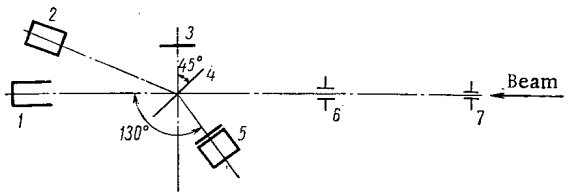

Fig. 1. Scheme of experiment. 1) Faraday cylinder; 2) monitor for particles scattered elastically by the target; 3) fission fragment detector; 4) target; 5) $\Delta E-E$ semiconductor counter telescope; 6, 7) collimating diaphragms.

When the triton beam current was 0.010-0.015 μA, the total count rate in the "proton" channel for the energy range 4-20 MeV was $(5-7)\cdot 10^2$ sec^{-1}, and that in the fission-fragment channel was $(5-7)\cdot 10^3$ sec^{-1}; the coincidence count rates were ~0.6 sec^{-1} for U^{238}, ~1.6 sec^{-1} for U^{233}, and ~3.5 sec^{-1} for Np^{237}.

As a logical circuit for separating the charged particles (P, d, t, α) according to their masses, we used a multichannel pulse analyzer, the AI-4096, operating in two-dimensional mode. The memory cube of the analyzer was divided up into 16 planes (ΔE) with 256

Translated from Atomnaya Énergiya, Vol. 30, No. 1, pp. 57-59, January, 1971. Original letter submitted April 16, 1970.

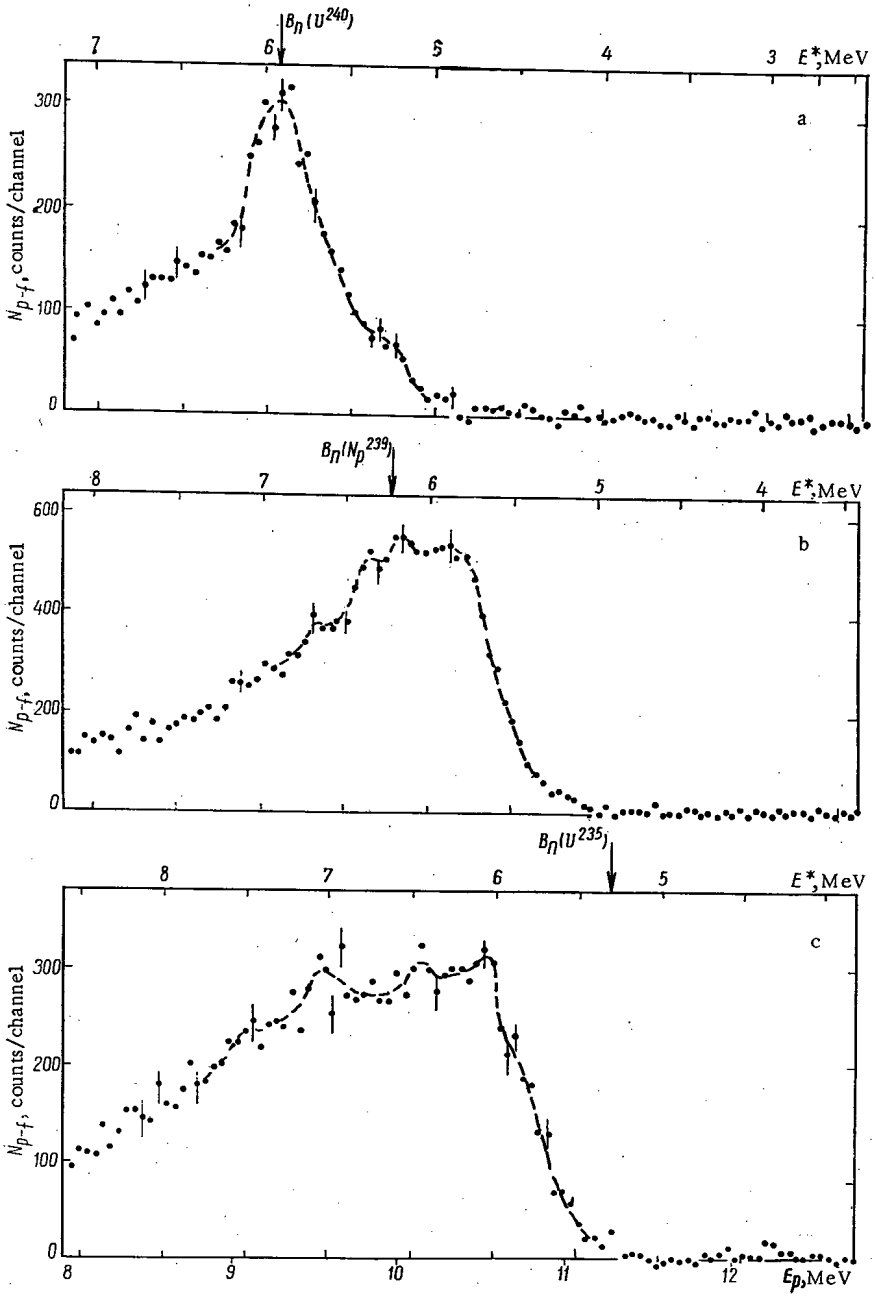

Fig. 2. Spectra of protons from the (t, pf) reactions of the isotopes U^{238} (a), Np^{237} (b), and U^{233} (c).

channels (E + ΔE) in each. The resolving time of the coincidence circuit was 60 nsec. The spectrum of random coincidences of protons with fission fragments was measured by the same spectrometric channel after a 250 nsec delay line had been switched into the fission-fragment registration channel.

The spectra of protons formed by the (t, pf) reactions of the isotopes U^{233}, U^{238}, and Np^{237} are plotted in Fig. 2. The dashed curves were plotted by five-point smoothing of the spectra by the method of least squares [2].

From Fig. 2 we see that fission of the compound nuclei U^{240} and Np^{239} occurs at excitation energies below the binding energy of neutrons in these nuclei. This means that fission of U^{239} and Np^{238} nuclei can be induced by thermal neutrons. A distinguishing feature of the fission of these nuclei in the (d, pf) and (t, pf) reactions [3-6] is that, at excitation energies equal to the binding energy of a neutron in the fissionable

nucleus, the fissionability curve displays a sharp change of slope or even a maximum, due to opening of the channel with emission of a neutron. The same maximum is observed, as a rule, in the spectra of protons from the same reactions [3-6]. In the spectra of protons from the (t, pf) reactions of the isotopes U^{238} and Np^{237} (see Fig. 2), these maxima occur at excitation energies of 5.92 MeV (U^{240}) and 6.18 MeV (Np^{239}), which are close to the known binding energies of a neutron in these nuclei, namely, Bn = 5.92 MeV for U^{240} [7] and Bn = 6.23 MeV for Np^{239}. Furthermore, in the spectrum of protons from the reaction Np^{237}(t, pf) we observe a peak at $E^*(Np^{239})$ = 5.9 MeV, and in the reaction U^{238}(t, pf) we observe a weak peak at $E^*(U^{240})$ = 5.3 MeV. These peaks may correspond to quasistationary states in the second well of the two-humped potential barrier [8]. However, their natures may be accurately determined after the fissionability curves of the Np^{239} and U^{240} nuclei have been plotted and the angular distribution of fission fragments from the (t, pf) reaction has been studied.

In the spectrum of protons from the reaction U^{233}(t, pf) the peaks at $E^*(U^{235})$ equal to 6.06 and 7.06 MeV correspond to capture of 0.75 and 1.75 MeV neutrons by the U^{234} nucleus. Within the accuracy of this experiment (± 0.12 MeV), the positions of these peaks agree with those of the peaks appearing in fission of U^{234} by neutrons (0.84 and about 1.9 MeV) [9]. This conclusion is based on the fact that the resonances in the spectra of protons from the reactions (d, pf) and (t, pf) [3-6] have practically the same excitation energy of the fissionable nucleus as those on the fissionability curves found from the same reactions.

The authors are grateful to B. D. Kuz'minov for kindly making available the large-area semiconductor detectors.

LITERATURE CITED

1. V. Strutinsky, Nucl. Phys., A95, 420 (1967); A122, 1 (1968).
2. A. Savitzky and M. Golay, Anal. Chem., 36, 1627 (1964).
3. J. Northrop et al., Phys. Rev. 115, 1277 (1959).
4. M. F. Andreev et al., Izv. Akad. Nauk SSSR, Seriya Fiz., 33, 726 (1969).
5. J. Pedersen and B. Kuzminov, Phys. Letters, 29B, 176 (1969).
6. H. Britt et al., Phys. Rev., 175, 1525 (1969).
7. A. Wapstra et al., Proceedings of the Third International Conference on Atomic Masses, Winnipeg (1967).
8. V. Strutinsky and S. Bjornholm, Int. Symp. Nucl. Structure, Dubna (1968); C. Wong and J. Bang, Phys. Lett., 29B, 143 (1969).
9. R. Lamphere, Nucl. Phys., 38, 561 (1962); Phys. Rev., 104, 1654 (1956).

AN INTERMEDIATE NEUTRON DETECTOR

V. I. Fominykh and O. A. Migun'kov

UDC 539.1.074.88

Intermediate energy neutrons are commonly counted by slowing them down and recording them with thermal neutron detectors. Such detectors record intermediate and fast neutrons. It is of interest to develop detectors which have a neutron sensitivity limited to the energy range around 1 MeV and are insensitive to γ-radiation.

In the detector described the moderator consists of two plastic hemispherical shells 114 mm in diameter with a wall thickness of 12 mm (Fig. 1). The moderator wall thickness was computed from results in [1, 2].

The use of SNM-13 corona counters with backgrounds of no more than 2 counts per minute in γ-fields of 2000 R/h [3] gives the instrument a low γ-sensitivity. The detector was calibrated by using neutron sources with various average neutron energies.

TABLE 1. Detector Sensitivity ε and Error $\Delta\varepsilon$ as Functions of Neutron Energy $\bar{E}$

$\bar{E}$	ε, counts/neutron	$\Delta\varepsilon$, counts/neutron
0,025eV	$1{,}71\cdot10^{-3}$	$0{,}12\cdot10^{-3}$
25keV	$2{,}29\cdot10^{-4}$	$0{,}34\cdot10^{-4}$
300keV	$1{,}76\cdot10^{-4}$	$0{,}19\cdot10^{-4}$
1,4MeV	0	$\leqslant 2{,}3\cdot10^{-5}$
2,8MeV	0	$\leqslant 2{,}3\cdot10^{-5}$

An SbBe(γ, n) source consisting of a standard Sb^{124} γ-source (type SU-11) surrounded by a cylindrical layer of powdered beryllium 1 cm thick and 3 cm long and having a density of 0.86 g/cm^3 supplied 25 keV neutrons. The γ-source was placed in an aluminum capsule with a magnetic cap which made possible the remote assembly and disassembly of the neutron source and also permitted the assembled source to be shifted. At the time the detector was calibrated the total neutron flux was $5\cdot10^5$ neutrons/sec for a γ-source activity of 0.4 g·eq of Ra.

A RaBe (γ, n) source supplied neutrons with an average energy of 300 keV, and a PoB (α, n) source supplied neutrons with an average energy of 2.8 MeV. The total

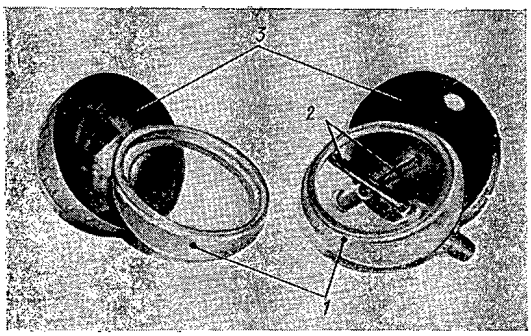

Fig. 1

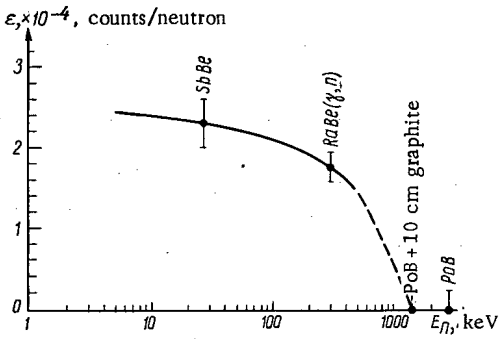

Fig. 2

Fig. 1. Intermediate neutron detector. 1) Spherical moderator; 2) SNM-13 counters; 3) cadmium shell.

Fig. 2. Sensitivity of intermediate neutron detector as a function of neutron energy.

Translated from Atomnaya Énergiya, Vol. 30, No. 1, pp. 59-60, January, 1971. Original letter submitted December 12, 1969; revision submitted March 31, 1970.

neutron flux emitted by the sources was determined by the activation of manganese. The results of these measurements are shown in Table 1 and Fig. 2.

In order to obtain an accurate value of the upper energy limit of the sensitivity the detector was calibrated with a PoB source placed in a graphite sphere 10 cm in radius. According to [4] the average energy of the neutrons from such a source is 1.4 MeV. Figure 2 shows that the upper limit of the sensitivity of the detector is about 1 MeV.

The sensitivity of the detector to thermal neutrons was determined by removing the cadmium shell and placing the instrument in the thermal neutron flux from a PoBe source placed in a paraffin sphere 15 cm in diameter [5]. The sensitivity determined in this way was $1.71 \pm 0.12 \cdot 10^{-3}$ counts/neutron. The correction to the neutron temperature from the paraffin sphere was neglected. Assuming that there are no singularities in the 25 keV to 0.025 eV range the curve of Fig. 2 can be extrapolated to the thermal region.

The intermediate neutron detector developed permits a measurement of intermediate neutron fluxes of more than 7 neutrons/sec $\cdot$ cm^2 in γ-fields up to 2000 R/h.

LITERATURE CITED

1. T. Bonner et al., Phys. Rev., 100, 84 (1955).
2. R. Fräki et al., AE-91 (1962).
3. Yu. M. Tolchenov and V. G. Chaikovskii, in: Nuclear Physics Dosimetry Apparatus [in Russian], Gosatomizdat, Moscow (1962), p. 16.
4. R. Nobles et al., Rev. Sci. Inst., 25, 334 (1954).
5. R. D. Vasil'ev et al., Izmeritel'. Tekh., 8, 74 (1968).

USE OF A Ge(Li) γ-SPECTROMETER FOR MONITORING COOLANT ACTIVITY IN NUCLEAR REACTORS

A. M. Demidov, G. A. Kotel'nikov, and A. A. Oskerko

UDC 621.039.534:681.2

This paper presents the results obtained by monitoring the activity of the coolant in the pool loop, the primary loop, the PVO loop, and the PVK loop of the MR reactor at the I. V. Kurchatov Institute of Atomic Energy [1]. The measurements were made with a sample collector and a germanium–lithium γ-spectrometer.

Corrosion Product Content. The sample volume collected for analysis from the pool loop and the primary loop was about one liter. To speed up the analysis and to remove excess Na^{24} activity, the sample was first concentrated to a volume of ~20 cm^3 by passage through AV-17 resin. In the case of the channel loops, a sample of ~30 cm^3 without preliminary treatment was sufficient. The specific isotopic activities found by spectral analysis are given in Table 1. As an illustration, a portion of the γ-ray spectrum from the coolant in the pool loop is shown in Fig. 1.

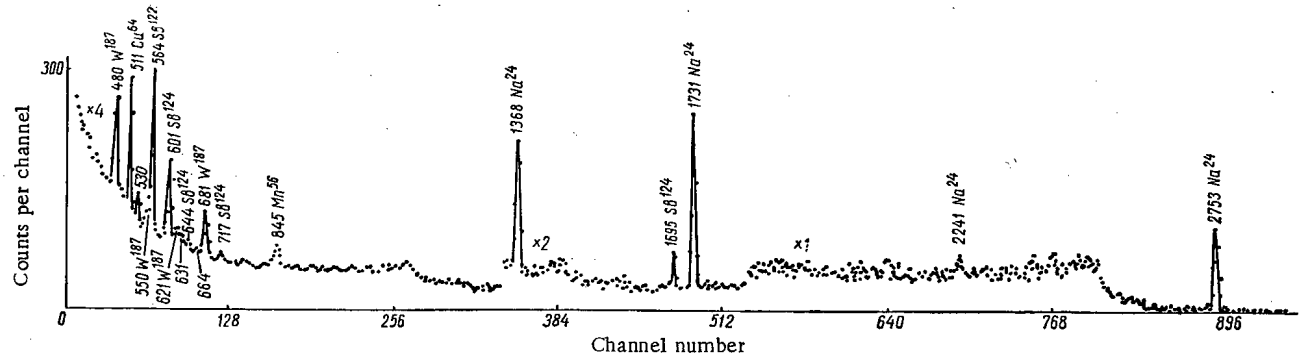

Fig. 1. Portion of the γ-ray spectrum of the pool loop during steady operation.

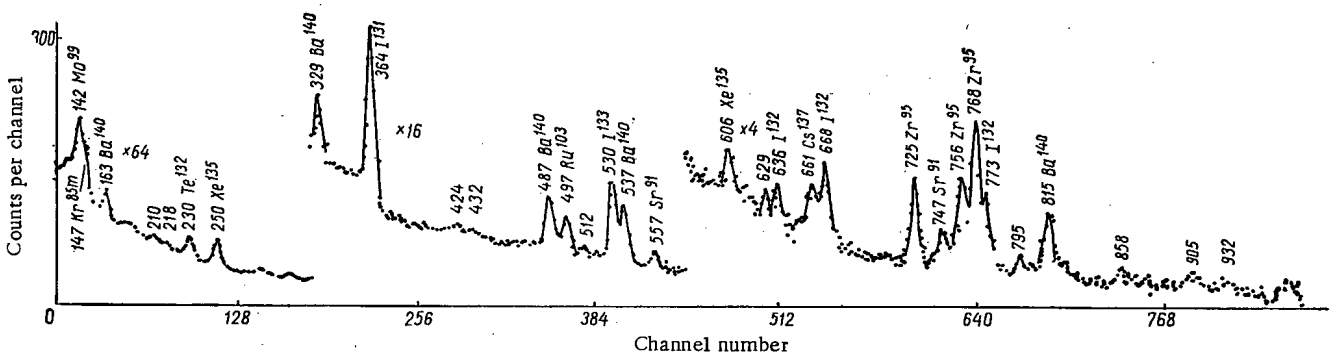

Fig. 2. Portion of the γ-ray spectrum from PVO loop during breakdown of fuel-element-cladding integrity.

Translated from Atomnaya Énergiya, Vol. 30, No. 1, pp. 60-62, January, 1971. Original letter submitted November 16, 1969; revision submitted August 3, 1970.

TABLE 1. Isotopic Composition of MR Reactor Coolant

Isotope	$T_{1/2}$	Specific activity, dis/sec · liter				Isotope	$T_{1/2}$	Specific activity, dis/sec · liter			
		pool loop	primary loop	PVK loop	PVO loop			pool loop	primary loop	PVK loop	PVO loop
Na^{24}	15 h	10 000	30 000	35 000	—	Zr^{95}	63 days	—	—	130	—
Cr^{51}	28 days	2000	100	400	3000	Mo^{99}	67 h	40	—	70	5000
Mn^{54}	291 days	6	—	60	1000	Sb^{122}	2,8 days	500	30	—	—
Mn^{56}	2,6 h	500	—	60 000	40 000	Sb^{124}	60 "	150	7	15	80
Co^{58}	71 days	5	10	160	1700	I^{131}	8 "	20	20	300	7000
Fe^{59}	44 days	5	—	130	620	I^{133}	21 h	50	40	1600	36 000
Co^{60}	5,25 yr	20	380	2600	3900	Ba^{140}	13 days	—	70	80	—
Cu^{64}	13 h	4000	—	—	—	W^{187}	24 h	700	—	1000	10 000

The appearance of Na^{24} results mainly from the $Al^{27}(n, \alpha)Na^{24}$ reaction, and the chromium, copper, antimony, tungsten, and rhenium isotopes result from thermal neutron activation of stable isotopes.

Monitoring Ion-Exchange Filters. By measuring the γ-ray spectrum at the entrance and exit of purification devices, a filtration factor was calculated for several elements; it was 5 for chromium, 8 for cobalt, 20 for copper, 12 for zirconium, 13 for cerium, 5 for iodine, and 6 for barium.

In one case when exhausted filters were replaced, it appeared that the fresh filters began to contaminate the loop with certain elements, among which copper was especially prominent. In the primary loop, for example, the Na^{24} concentration increased by a factor of 10, the chromium concentration by a factor of 200, and the copper concentration by a factor of $1.6 \cdot 10^6$. In addition, Br^{82} and W^{187} activities appeared.

Monitoring Transition Processes. The variation in isotopic composition resulting from a sharp pressure drop in a loop was recorded. In this case, the Na^{24} activity was practically unchanged, and the chromium, cobalt, tungsten, and tantalum activities increased by factors of 50-200, which most likely resulted from the increase in sludge.

Breakdown in Integrity of Fuel Element Cladding. A portion of the γ-ray spectrum from coolant which flowed over a ruptured fuel element in the PVO loop is shown in Fig. 2. Loss of integrity occurred when Fe^{59} and Co^{60} corrosion activity was being removed from the loop. The energies of the peaks and their identifications are indicated on the figure. A comparison of the specific activities of volatile and nonvolatile fission fragments (iodine, barium) and also of corrosion products (sodium, cobalt) enables one to reach some conclusions about the state of the fuel element cladding. In the case under discussion, the ratio of iodine, zirconium, and barium pointed to direct contact of coolant with the nuclear fuel and the washing out of the fuel. There was surface contamination in the cases of the pool loop and the primary loop. In the PVK loop, there was gas flow through microcracks in the fuel element cladding.

The authors are grateful to E. N. Babulevich for providing staff assistance during the work at the reactor.

LITERATURE CITED

1. V. V. Goncharov et al., Paper No. P-323 presented by the USSR at the Third International Conference on Peaceful Uses of Atomic Energy, Geneva (1964).

RADIATION YIELD OF Mn^{3+} IN DOSIMETRIC GLASSES

V. M. Trofimov,* D. G. Galimov,
I. N. Dobretsova, N. F. Orlov,
and D. M. Yudin

UDC 621.387.46:621.386.82:535.345.1

One problem in dosimetry of large γ-ray and electron fluxes is to devise dose indicators in the dose range up to $3 \cdot 10^8$ MR at temperatures from –200 to +200°C. A promising material for dosimetry of this type is glass [1]; in particular, recent work has been done with phosphate glass with various activators creating an induced absorption band (IAB) under the action of ionizing radiation. The doses of γ-rays and electrons are measured by means of the change in intensity of the IAB. In phosphate glasses, the most suitable activator is manganese [2], which has an IAB with λ_m = 560 nm, stable at high temperatures (400°C). The IAB is due to the reaction

$$Mn^{2+} + h\nu = Mn^{3+} + e.$$

Unstable hole centers [3, 4], formed at nonbridging oxygen atoms in pentavalent phosphorus sites, lead to formation of an IAB in the main glass, partly overlapping the IAB of Mn^{3+}.

As a result of competition from manganese, at comparatively low manganese concentrations the IAB of the base is suppressed. To choose the optimal initial concentration of manganese in phosphate glasses so as to give a stable IAB, we studied the radiation yield of Mn^{3+}. We studied two glass compositions based on sodium–calcium (0157) and potassium–calcium (0160) metaphosphate.

The IAB is more intense in irradiated 0160 glass than in 0157 glass. To these bases we added Mn^{2+} as activator in the following concentrations: 0.2, 0.4, 0.8, and 2 mole % above 100 mole %.

* Deceased.

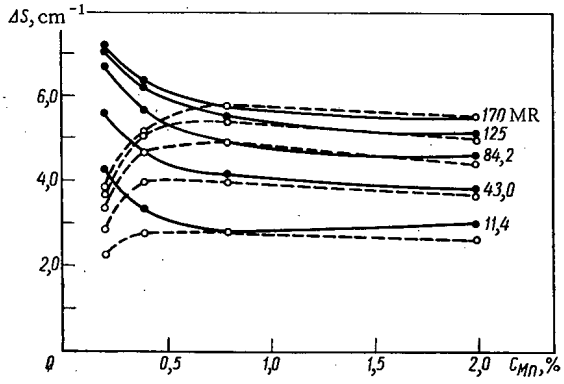

Fig. 1

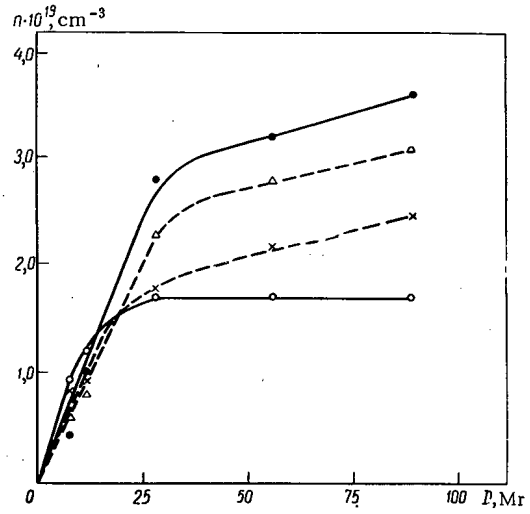

Fig. 2

Fig. 1. Intensity of IAB with λ_m = 560 nm, versus Mn^{2+} concentration.

Fig. 2. Number of Mn^{3+} ions versus dose, according to EPR data, for glass 0160. Initial manganese concentrations (in mole %): 0.2 (○); 0.4 (×); 0.8 (Δ); 2 (●).

Translated from Atomnaya Énergiya, Vol. 30, No. 1, pp. 63-64, January, 1971. Original letter submitted July 29, 1969.

TABLE 1. Radiation Yield of Mn^{3+} Ions (According to Fig. 2)

C_{Mn}, mole %	Dose range, MR	G_I, ions/100 eV	Dose range, MR	G_{II}, ions/100 eV
0,2	0—10	1,03	25—100	0
0,4	0—15	0,74	25—100	0,08
0,8	0—30	0,75	35—100	0,098
2,00	0—30	0,67	35—100	0,08

Figure 1 plots the intensity of the IAB with λ_m = 560 nm versus the Mn^{2+} concentration for glass 0157 (dashed curves) and 0160 (solid curves). We see that in glass 0157, the IAB of the base is practically entirely suppressed at concentrations of Mn^{2+} above 0.2 mole % (the IAB intensity increases with the Mn^{2+} concentration). In glass 0160, the IAB of the base is suppressed only at concentrations of Mn^{2+} above 0.8 mole %; at Mn^{2+} concentrations below 0.8 mole % ΔS is greater than for Mn concentrations above 0.8 mole %, because the coloration process is made up of two processes, namely, coloration at hole centers of the base, and coloration at Mn^{3+} ions; the former is the more intense process.

From Fig. 1 we see that the maximum radiation yield of Mn^{3+} ions is to be expected at manganese concentrations near 0.8 mole %.

The results of EPR investigations confirm the presence of maximum radiation yield of Mn^{3+} ions at the stated activator concentration in glass 0160 (Fig. 2). Measurements of the amount of Mn^{3+} formed during irradiation of the glasses were made by measuring the difference between the EPR signal amplitudes due to Mn^{2+} ions before and after irradiation. The number of Mn^{3+} ions increases with the activator concentration up to 0.8 mole %, and then tends to decrease. The explanation is apparently that manganese can occur in the glass network in two ways.

At small concentrations, isolated Mn^{2+} centers are formed, at which migration of holes in the base terminates. Owing to the nonuniform distribution of the activator, when its concentration increases there is a rise in the probability that two manganese ions will adjoin one another. In this case there is an increased probability of exchange of charge carriers between manganese ions, which promotes acceleration of the recombination processes and reduces the radiation yield of Mn^{3+}. These effects are revealed when we analyze the changes in intensity of the optical and paramagnetic absorption spectra of manganese versus its concentration in the glasses.

The data on the radiation yield of Mn^{3+} ions, taken from Fig. 2, are listed in Table 1, where G_I and G_{II} are the radiation yields of Mn^{3+}, for activator concentrations of 0.2, 0.4, 0.8, and 2.0 mole %, for the given dose ranges. These results can be used to plot S versus D by means of the Smakula formula [5].

Thus we find that Mn^{3+} ions are responsible for the formation of an IAB with λ_m = 560 nm in phosphate glass; the intensity of this IAB is a maximum when the initial manganese concentration is about 0.8 mole %. This manganese concentration secures complete suppression of the unstable IAB of the base, and this improves the dosimetric characteristics of the glass – i.e., its ability to retain the information for a long time and its capacity for operation at high temperatures. In addition, as we see from Fig. 1, this concentration avoids saturation of the (S, D) curves over a wide range of doses (~200 MR).

LITERATURE CITED

1. G. V. Byurganovskaya et al., Action of Radiation on Inorganic Glasses [in Russian], Atomizdat, Moscow (1968).
2. V. M. Trofimov, N. F. Orlov, and N. Z. Andreeva, At. Énerg., 27, 155 (1969).
3. D. M. Yudin, Fiz. Tverd. Tela, 7, 1733 (1965).
4. G. O. Karapetyan, A. I. Sherstyuk, and D. M. Yudin, Optika i Spektr, 23, 44 (1967).
5. L. Spurny, Person. Dosimetry Radiat. Accidents, Proc. Sympos. (Vienna, 1965), Vienna (1965), pp. 131-147.

COMPARISON OF COMBINATION AND DISPERSE AIR-EQUIVALENT SCINTILLATORS

M. I. Arsaev, V. A. Krasnikov, and B. G. Margulis

UDC 535.373.1:539.1.083:537.531:539.122

The basic, and most widely used, method for producing air-equivalent scintillators is the introduction of a compensator which has an effective atomic number greater than that of air into a scintillator with $Z_{eff} < Z_{eff\ air}$ [1-3]. The compensator can be introduced into the base scintillator in the form of organometallic chemical compounds; it can enter into solution with the base scintillator or can be dispersed in the form of fine granules within the base. This type of air-equivalent scintillator we shall call a disperse scintillator. If the compensator is a scintillating compound, one can create another type of scintillator – the combination scintillator, in which the compensator is located above (with respect to the incident γ-ray flux) and the base scintillator is below [4].

An advantage of the disperse scintillators is their uniform composition and consequent excellent isotropy. However, the introduction of a compensator leads to a deterioration of the optical properties of a detector, which reduces its sensitivity and increases the energy dependence of the sensitivity because of changes in the light collection coefficient resulting from nonuniform distribution of the specific energy absorption for soft and hard radiation over the length of the scintillator.

The main advantage of combination scintillators over disperse scintillators is the smaller energy dependence, other conditions being equal. This is because it is energetically more advantageous if the γ-radiation is directly absorbed in the high-Z material (compensator) and absorption of the attenuated flux then occurs in the base scintillator as compared with the case where the γ-ray flux is absorbed in a disperse scintillator. Consequently, a smaller amount of compensator is required for compensation of the change in energy sensitivity of the base scintillator, and the γ-ray flux attenuation factor over the length of the scintillator is reduced leading to an improvement in this detector parameter. Combination scintillators also have better sensitivity because the compensator is not introduced into the base scintillator and

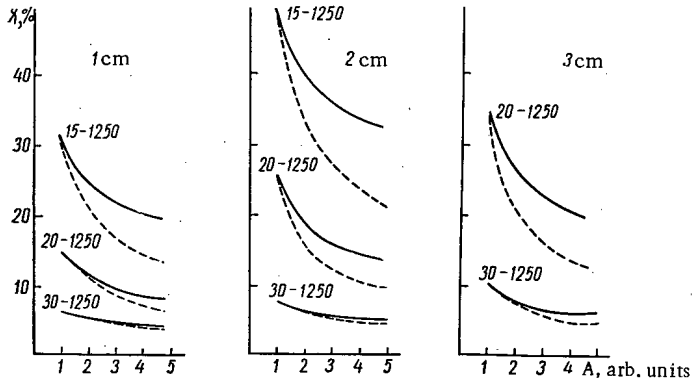

Fig. 1. Variation in energy sensitivity, χ, as a function of A for three scintillator thicknesses: ——) disperse scintillator; – – –) combination scintillator.

Translated from Atomnaya Énergiya, Vol. 30, No. 1, pp. 64-66, January, 1971. Original letter submitted October 24, 1968; revision submitted January 4, 1970.

TABLE 1. Values of A and Relative Light Yield

Type of scintillator	Coefficient A		Relative light yield	
	1 cm	2 cm	1 cm	2 cm
Combination	5,0	4,75	1,2	1,25
Disperse	3,0	3,0	1,0	1,0

thus does not degrade the transparency of the base. Among the deficiencies of the combination scintillators, one should note their anisotropy with respect to the direction of γ-ray fluxes.

For a quantitative evaluation of the parameters of combination and disperse scintillators, calculations were made of the minimum possible values of the variation in energy sensitivity for given thicknesses of the scintillators mentioned; the calculations were experimentally checked using a scintillating plastic with Z = 5.6 as the base scintillator and ZnS(Ag), with Z = 27, as the compensator. Quantitative changes in sensitivity were calculated on the basis of published data [4, 5], where expressions were obtained for the relative efficiencies $\eta(E)$ of combination and disperse scintillators, and where it was shown that, other conditions being equal, the variation in energy sensitivity of disperse scintillators depended on the ratio of the conversion efficiencies of compensator and base, $A = G_{comp}/G_{base}$, and that of the combination scintillators on the ratio $A = G_{comp}K_{comp}/G_{base}K_{base}$, where K_{comp} and K_{base} are factors which determine the fractions of the light energy arriving at the photomultiplier photocathode produced respectively in the compensator and in the base.

Figure 1 shows the optimal values of the variation in sensitivity, which is defined as $\chi = (\eta_{max} - \eta_{min}/\eta_{max} + \eta_{min}) \cdot 100\%$, as a function of A (calculated for a special case; the energy dependence of G_{comp} and G_{base} was not taken into account, nor was the energy exchange between compensator and base because of the escape of secondary electrons). As is clear from the figure, the variation in sensitivity is considerably less for combination scintillators than for disperse scintillators, with the degree of advantage depending significantly on the energy range of the γ-rays detected, on the value of A (for sufficiently small A), and, to a lesser extent, on the scintillator thickness. To obtain a minimum variation in the sensitivity of combination and disperse scintillators, therefore, it is necessary to use the optimal values of A for each type of scintillator, which may differ significantly for the identical compensators and bases because of differences in the optical characteristics of the scintillators and differences in construction.

It has been shown [6] that for disperse scintillators using ZnS(Ag) as a compensator and a scintillating polystyrene plastic as a base, the best results with respect to this detector parameter are obtained with type K-430 ZnS(Ag), for which $G_{comp}/G_{base} = 3$. Type FS-4 ZnS(Ag) phosphor, although it has a light output 35% greater than that of K-430, gives much the same results because the small size of the phosphor

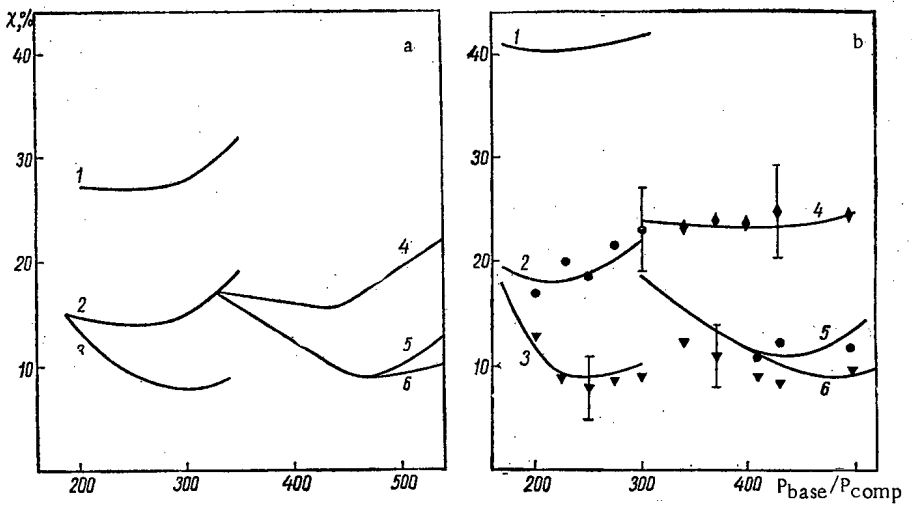

Fig. 2. Dependence of variation in energy sensitivity on the ratio P_{base}/P_{comp} for combination and disperse scintillators 1 cm (a) and 2 cm (b) thick: 1, 2, 3) disperse scintillators at the respective energy ranges 15-1250, 20-1250, and 30-1250 keV; 4, 5, 6) the same for combination scintillators; the points are experimental values (keV): ◆) 15-1250; ●) 20-1250; ▼) 30-1250.

granules leads to a larger energy loss resulting from the escape of secondary electrons from the granules. However, the sensitivity of such a detector is less than that of a detector with K-430 because of poorer optical characteristics.

For a combination detector, it is more advantageous to use the FS-4 phosphor because granule size is of no importance in this case. The numerical value of the coefficient A for combination scintillators was obtained experimentally from the ratio of "practical yields" (ratio of scintillation detector current to absorbed energy) for a type FS-4 ZnS(Ag) compensator and a scintillating plastic.

Table 1 gives values for the factor A and for the technical light yield for combination scintillators 1 and 2 cm thick, with the light yields being given relative to the light yield from an optimal disperse scintillator of the same thickness.

For these scintillators, Fig. 2 shows the dependence of the calculated values of the variation in sensitivity on the ratio of the base weight to compensator weight, P_{base}/P_{comp} (the energy dependence of G_{comp} and G_{base} and the energy exchange between base and compensator were taken into account in the calculations). It is clear that the calculated and experimental values for the variation in sensitivity for disperse and combination scintillators are in good agreement.

Finally, it must be pointed out that for both combination and disperse scintillators in which ZnS(Ag) is used as a compensator and a polystyrene scintillating plastic is used as a base, the variation in sensitivity at energies above 30 keV is practically identical. At energies below 30 keV, the sensitivity variation for combination scintillators is considerably less than that for disperse scintillators: 75% less in the range 14-125 keV for 1 and 2 cm thicknesses, and 55 and 65% less for thicknesses of 1 and 2 cm, respectively, in the range 20-1250 keV.

LITERATURE CITED

1. E. Belcher and J. Geilinger, Brit. J. Radiology, 30, 103 (1957).
2. M. I. Arseev and N. E. Sulimova, Pribory i Tekh. Éksperim, No. 4, 59 (1963).
3. R. Kempe, Kernenergie, 10, 553 (1963).
4. M. I. Arsaev, V. A. Krasnikov, and V. G. Margulis, At. Énerg., 27, 336 (1969).
5. M. I. Arsaev, in: Nuclear Instrument-Making [in Russian], No. 8, Atomizdat, Moscow (1968).
6. M. I. Arsaev, V. A. Krasnikov, and V. G. Margulis, Monocrystals, Scintillators, and Organic Phosphors [in Russian], No. 5, Pt. 2, Khar'kov (1970), p. 112.

POSSIBILITIES OF OIL-WELL LOGGING WITH A Ge(Li) γ-DETECTOR AND Po – Be NEUTRON SOURCE

L. I. Gorov, A. M. Demidov, and V. A. Ivanov

UDC 550.835:553.9

This paper describes the possibilities for performing neutron logging of exploratory oil-wells with a Ge(Li) γ-detector and a Po–Be neutron source.

The studies were made with a model of an oil-well that resembled the actual conditions. The stratum model used is shown schematically in Fig. 1. The tank 9 in which it was set up was 800 × 800 × 700 mm in size. The steel casing 4 had an internal diameter of 150 mm and a wall thickness of 10 mm; the cement ring 7, which surrounded the casing, was ~35 mm thick.

The tank was filled in turn with fresh water, transformer oil, and dry sand 8 (porosity, 40%) saturated with fresh water or oil.

Inside the steel pipe there was a Ge(Li) γ-detector 1 with a 2.5 cm^3 sensitive volume and a Po–Be source with an activity of $2\text{-}3 \cdot 10^7$ n/sec. The detector was shielded against the neutron and γ-radiation from the Po–Be source by a lead block 2, which was 150 mm long and 60 mm in diameter, and by a 4 mm layer of Li^6F or by a shield of boron carbide (B_4C) 3 and lead 2. The separation between detector and source was ~200 mm. To account for the effect of moderator (oil or water) in a well, a paraffin cylinder 6, with a shape which corresponded to the eccentric location of a logging instrument in a well, was emplaced in the model well. The first experiments were carried out with the detector and source in a steel pipe 125 mm in diameter with a wall 10 mm thick (simulation of the wall of logging device). Subsequently, the additional pipe was removed, and studies were made of the use of aluminum or zirconium alloys for the casing of the logging device.

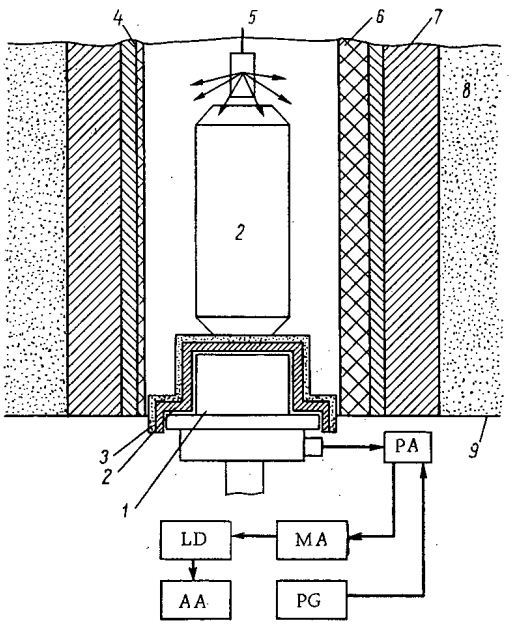

Fig. 1. Diagram of experimental arrangement: PA) preamplifier; MA) main amplifier; LD) linear discriminator; PHA) pulse height analyzer; PG) pulse generator.

The electronics consisted of a preamplifier, main amplifier with discriminator, and a 110 channel pulse height analyzer, and provided a resolution of 9-18 keV in the energy region E_γ = 1.8-8 MeV during the experiments. Determination of γ-line energies was made with a precision pulse generator having an error less than ± 5-7 keV.

The determination of oil- and water-bearing strata and of rock porosity and the establishment of the oil–water boundary is associated with the elemental analysis of the main components of the stratum. In the case of sandstone, the elements are silicon, oxygen, carbon, and hydrogen (in limestone, there is calcium in place of silicon) [1-3].

Such elements as silicon, calcium, and hydrogen are easily determined through the γ-radiation from radiative capture of thermal neutrons [1]. Characteristic lines are

Translated from Atomnaya Énergiya, Vol. 30, No. 1, pp. 66-69, January, 1971. Original letter submitted June 18, 1969.

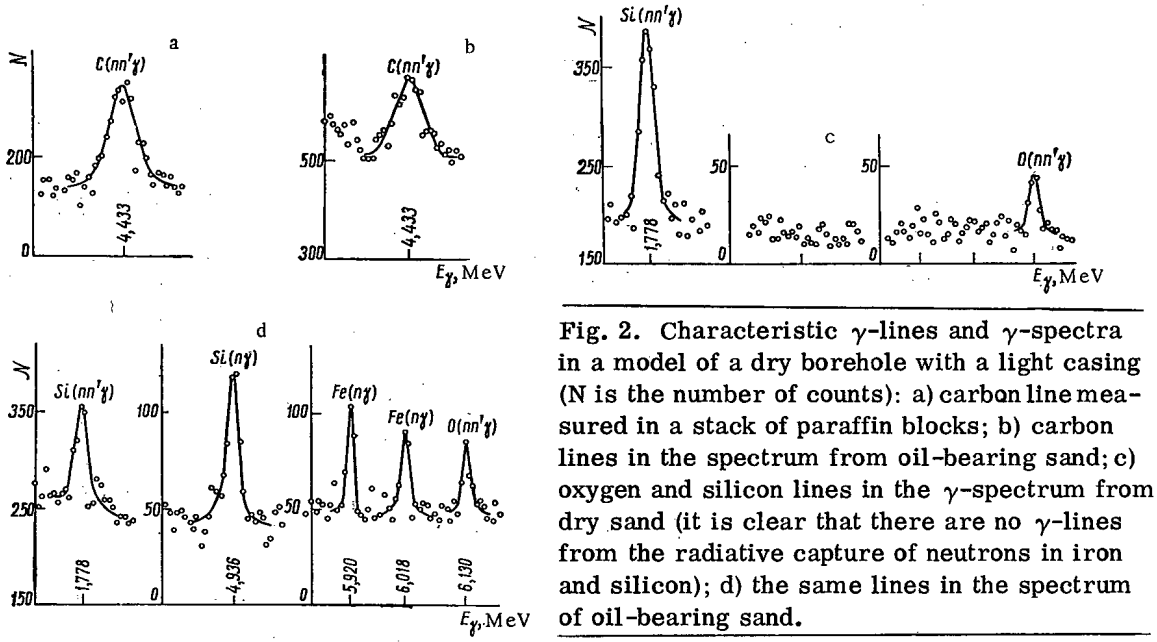

Fig. 2. Characteristic γ-lines and γ-spectra in a model of a dry borehole with a light casing (N is the number of counts): a) carbon line measured in a stack of paraffin blocks; b) carbon lines in the spectrum from oil-bearing sand; c) oxygen and silicon lines in the γ-spectrum from dry sand (it is clear that there are no γ-lines from the radiative capture of neutrons in iron and silicon); d) the same lines in the spectrum of oil-bearing sand.

the 4.936 MeV line of Si^{29}, the 6.420 MeV line of Ca^{41}, and the 2.223 MeV line of D^2. At the same time, oxygen and carbon have very small thermal neutron capture cross sections and are practically undetected. However, in both oxygen (O^{16}) and carbon (C^{12}), the first excited states are very high, which creates a favorable opportunity for their detection by means of the γ-radiation from inelastic scattering of fast neutrons. Here the characteristic lines are the 6.131 MeV line of O^{16} and the 4.443 MeV line of C^{12}.

A feature of the γ-radiation accompanying fast neutron scattering is the broadening of the γ-lines when the lifetime of the state is less than the slowing-down time of the recoil nucleus. The observed broadening of γ-lines depends on the angle between the direction of the incident neutron beam and the direction of observation; it also depends on the neutron energy ($\sim\sqrt{E_n}$) and the mass of the recoil nucleus ($\sim 1/m$). The lifetime of the 4.433 MeV line in C^{12} is $4.6 \cdot 10^{-14}$ sec, which is less than the slowing down time of the recoil nucleus. If the angle of observation is close to 90°, the broadening is minimal and should be 50-60 keV for neutrons from the Po–Be source. The experimentally determined width of the 4.43 MeV line was 50 keV (for the case of a pure graphite pile).

The great width of the 4.43 MeV line from C^{12} sharply reduces the sensitivity of the neutron method for the determination of carbon content in rock because the inherent resolution of a germanium detector at this energy is 10-12 keV. However, the Doppler broadening of the C^{12} γ-line is four to five times less than the halfwidth of the peak obtained in a spectrometer with a NaI(Tl) crystal. The Doppler broadening of the 6.131 MeV line from O^{16} ($nn'\gamma$), and also of the 1.78 MeV line from Si^{28} ($nn'\gamma$), is considerably less.

Preliminary experiments with a Ge(Li) γ-detector and Po–Be source were performed under less rigorous conditions than those described above: the oil-well was dry, there was no cement ring, and the wall thickness of the steel casing was 5 mm. In the resultant spectra, one could clearly distinguish the characteristic lines from the radiation capture of thermal neutrons in H^1, Si^{28}, and Fe^{56}, and from inelastic scattering of fast neutrons by Si^{28}, O^{16}, and C^{12}. Some of the results are shown in Fig. 2.* Also shown are the γ-lines from C^{12}, which were obtained when the source and detector were surrounded by paraffin.

A feature of the γ-spectra obtained in a dry oil-well without a cement ring is the complete absence of γ-lines from the radiative capture of thermal neutrons in sand. With oil- or water-saturated strata, the lines from radiative capture appear (lines from inelastic neutron scattering are present in both cases). Consequently, in a dry oil-well without a cement ring, the hydrogen concentration in rock can be determined from the ratio of the intensities of the 4.936 MeV line from Si^{29} ($n\gamma$) and the 1.78 MeV line from Si^{28} ($nn'\gamma$).

* Always present in the spectra are peaks resulting from the emission of two annihilation quanta in addition to the 1.78 MeV line from Si^{28} ($nn'\gamma$) and the 2.223 MeV line from H(n, γ)D for which the total absorption peaks are given.

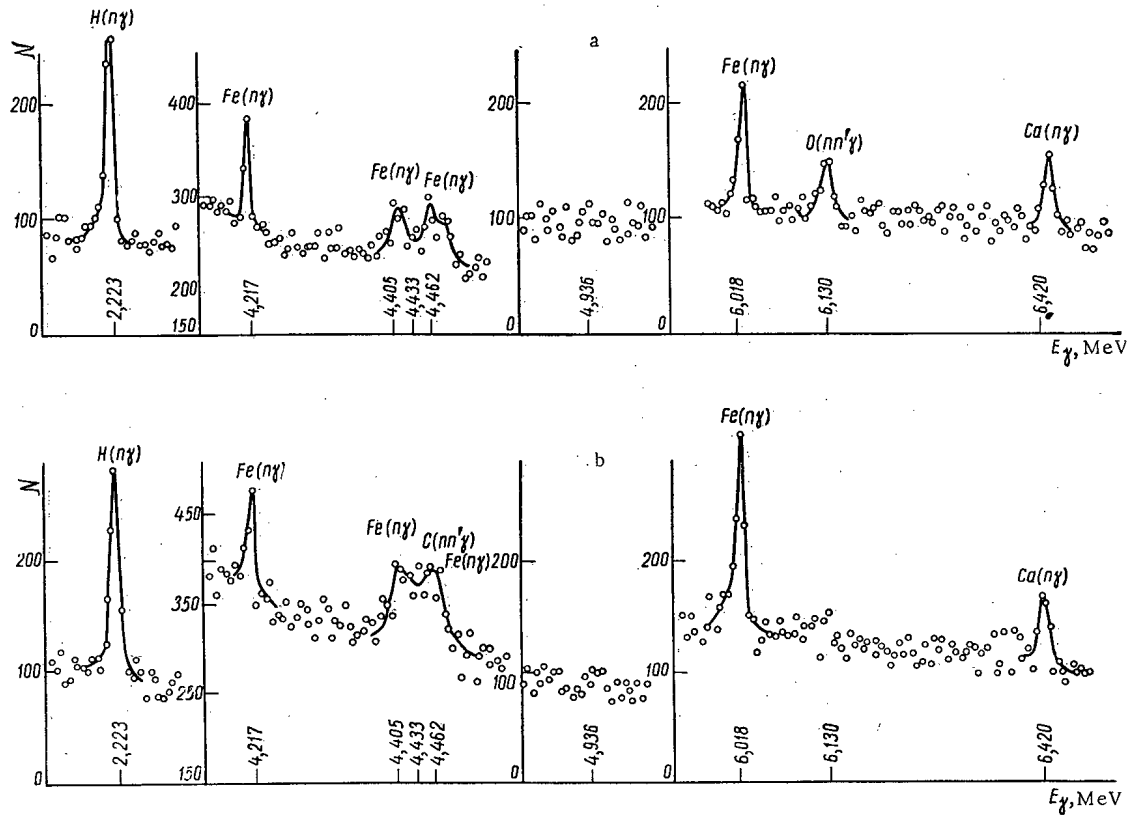

Fig. 3. Characteristic γ-lines of hydrogen, carbon, oxygen, calcium, and iron in γ-spectra obtained in a model of an actual borehole with the tank filled with (a) fresh water and (b) oil (it is obvious that the characteristic 4.936 MeV γ-line of silicon is absent).

The type of moderator (oil or water), and particularly, the oil–water boundary, are determined by the presence in the spectrum of the characteristic γ-lines of carbon (the contribution of the 4.405 MeV and 4.462 MeV lines from $Fe^{56}(n\gamma)$ to the $C^{12}(nn'\gamma)$ peak in Fig. 2b is ~20%).

In the experiments with a model of an actual oil-well, it is necessary to note that the same characteristic γ-lines were present but conditions for making an analysis of elemental content were not as good.

A comparison is given in Figs. 3 and 4 of portions of γ-spectra obtained from dry sand, sand saturated with fresh water and oil, and for the case where the tank was filled with water and oil without sand. The presence of hydrogen nuclei in the cement ring (65% CaO, 15% H_2O, and 20% SiO_2) and in the oil-well leads to a situation where γ-lines from the radiative capture of thermal neutron in hydrogen, silicon, and iron are present even in spectra obtained from dry sand. However, the intensity of these lines in the case of sand saturated with water or oil is considerably greater than in the case of dry sand (a factor of two for the hydrogen line at 2.223 MeV), which makes it possible to arrive at some conclusion with respect to the hydrogen concentration in surrounding rock.

Of undoubted interest is the peak resulting from the inelastic scattering of fast neutrons by oxygen. This peak is clearly distinguished in all cases except for the experiment with the tank filled with oil without sand present. The intensity of the peak at 6.131 MeV from O^{16} varies as a function of rock composition in proportion to the oxygen content and also because of the variation in the fast neutron flux distribution in the stratum. In the experiments, particular consideration was given to the peak at 4.43 MeV, which is the most reliable indicator of the presence of oil. In Figs. 3 and 4, the peaks at 4.217, 4.405, and 4.462 MeV belong to iron, and the peak at 4.420 MeV is from Ca^{41}. A broad line belonging to C^{12} is observed against the background of the lines enumerated above in Figs. 3b and 4c. The contribution of the peaks resulting from the radiative capture of thermal neutrons in iron can be taken into account sufficiently accurately by means of the intensity of the iron line at 4.217 MeV. The ratio of the intensities of the γ-lines with energies

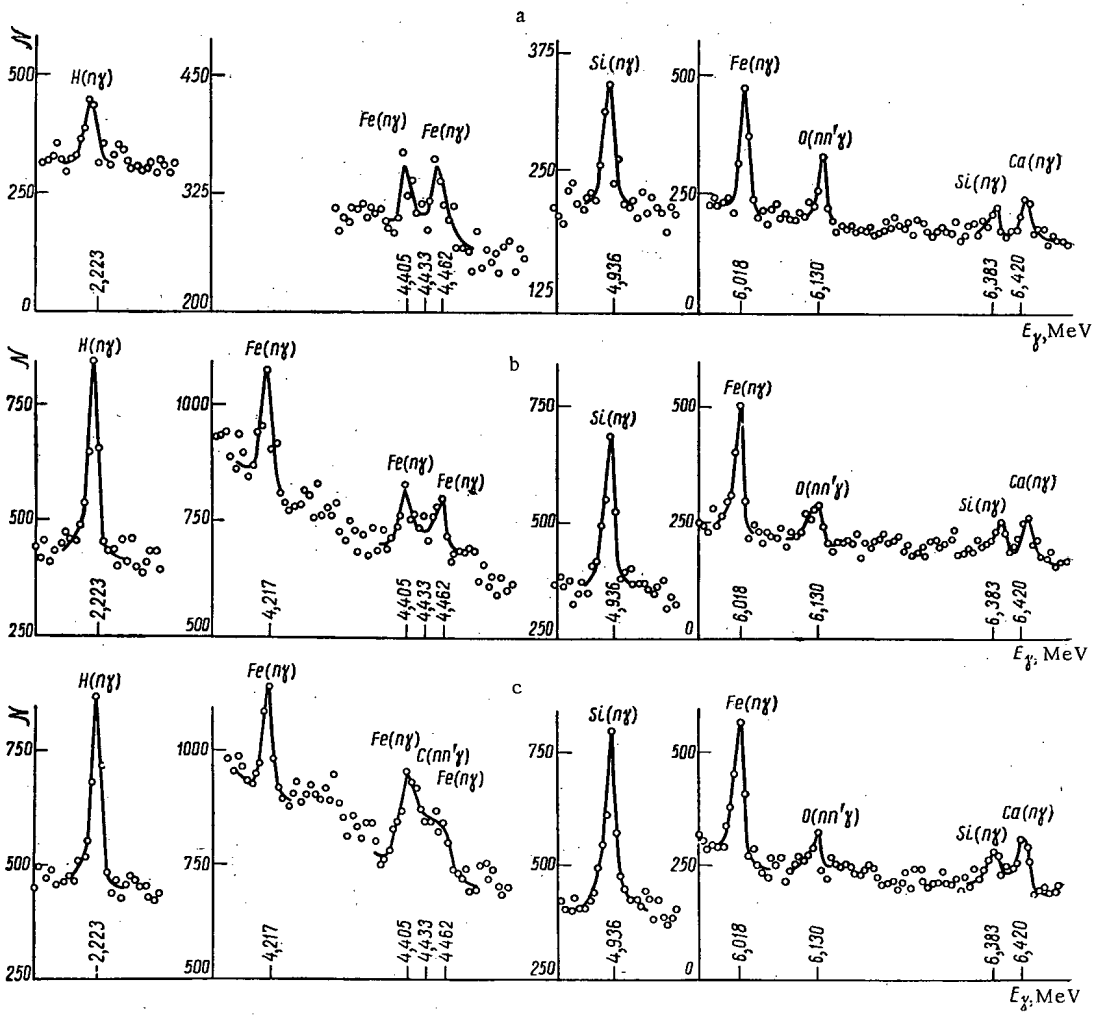

Fig. 4. Characteristic γ-lines from hydrogen, carbon, oxygen, silicon, calcium, and iron in γ-spectra obtained in a model of an actual borehole with the tank filled with (a) dry sand, (b) sand and water, (c) sand and oil.

of ~4.4 MeV to the intensity of a characteristic Fe^{57} γ-line, the 4.217 MeV line, for example, can be taken as a quantity which characterizes oil content in rock. When the tank was filled with water, this quantity was 3.35 ± 0.54; when it was filled with oil, the value was 4.65 ± 0.65.

In working with sizable samples, the ratio of peak height to base is considerably poorer because of the large background of scattered γ-rays. The γ-rays from the radiative capture of thermal neutrons in Fe^{56} causes the greatest difficulty. In this regard, the use of a pulsed neutron generator is of interest because it appears possible to achieve a time separation in the detection of γ-rays from the radiative capture of thermal neutrons and those from inelastic scattering of fast neutrons.

In conclusion, we wish to thank Yu. S. Shimelevich and N. V. Popov for fruitful consultations during the preparation and performance of the experiments.

LITERATURE CITED

1. A. M. Demidov, L. I. Govor, and V. A. Ivanov, Program and Abstracts of Papers at the XIX Annual Conference on Nuclear Spectroscopy and Nuclear Structure [in Russian], Part I, Nauka, Erevan (1969).
2. Problems in Nuclear Geophysics [in Russian], Nedra, Moscow (1964).
3. Portable Neutron Generators in Nuclear Geophysics [in Russian], Gosatomizdat, Moscow (1962).

DEPTH VARIATION OF ABSORBED DOSE IN MATERIALS IRRADIATED BY FAST ELECTRONS

L. V. Chepel'

UDC 621.039.83

The efficient utilization of the radiation from electron accelerators in continuous irradiation processes requires that the depth of penetration of the electrons be nearly equal to the thickness of the irradiated material. However, in view of the characteristics of the interaction of fast electrons with matter, the distribution of absorbed dose through the material will vary by nearly 100% (Fig. 1) [1]. Therefore it is common practice to move the material to be irradiated through the electron beam [2], frequently several times [3]. This permits an efficient utilization of the electron energy and at the same time improves the uniformity of the irradiation of the material with depth. An example is the irradiation of thin material (thickness appreciably less than the electron range) wound on a spool rotating with a constant linear speed, or material "snaked" through a series of rollers. In this case it is necessary to satisfy the above relation between the electron range and the total thickness of the material being irradiated.

Figure 1 shows the depth distribution of absorbed dose in material irradiated by electrons as a function of the electron range R. Then for a thickness h of the irradiated material the electron energy will be completely utilized if the material passes through the beam n times in such a way that each time there will be a new discrete value of the absorbed dose given by the curve of Fig. 1. In this case n is given by $n = R_m/h$, and the depth variation of the irradiation of the material should decrease with increasing n.

An attempt was made in [4] to estimate the variation of the absorbed radiation dose when the electron source was a pulsed accelerator. It was assumed that the distribution of absorbed electron energy was uniform over a thickness of material equal to $2R_m/3$.

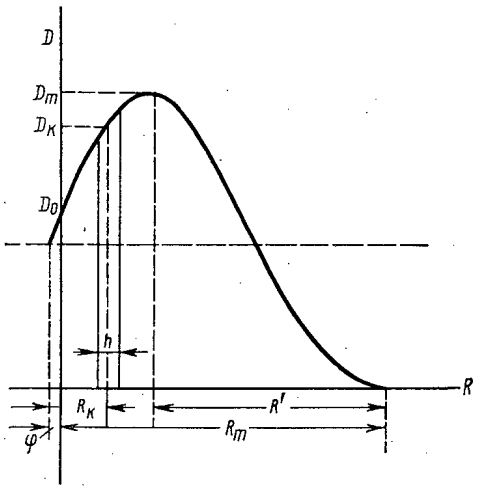

Fig. 1

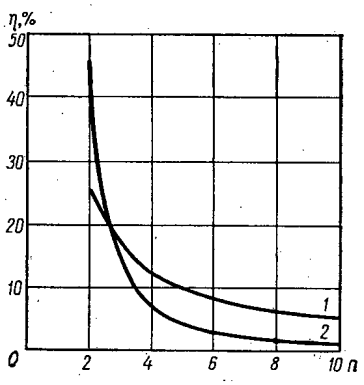

Fig. 2

Fig. 1. Depth distribution of absorbed dose in material irradiated by electrons as a function of electron range.

Fig. 2. Variations of absorbed radiation dose (η) as a function of n.

Translated from Atomnaya Énergiya, Vol. 30, No. 1, pp. 70-72, January, 1971. Original letter submitted January 13, 1970.

TABLE 1. Formulas for Estimating Variation (η) of Absorbed Dose in Irradiated Material of Uniform Thickness

Type of winding	General term of summation	Variation of absorbed dose in irradiated material	
		general form	special case
Spool	$D_k \simeq 0.5D_m\left[1+\sin\left(\frac{4.5}{R_m}hk+0.2\right)\right]$	$\eta=\frac{\sum_{k=0}^{k=n-1} D_k-\sum_{k=1}^{k=n-1} D_k}{\sum_{k=0}^{k=n-1} D_k+\sum_{k=1}^{k=n-1} D_k}$	$\eta \simeq \frac{1.2\,\mathrm{tg}\frac{2.25}{n}}{2n\,\mathrm{tg}\frac{2.25}{n}+1}$
"Snake" (n even)	$D_{2k} \simeq 0.5D_m\left[1+\sin\left(\frac{4.5}{R_m}h2k+0.2\right)\right]$	$\eta=\frac{2\left(\sum_{k=0}^{k=\frac{n}{2}-1} D_{2k}-\sum_{k=1}^{k=\frac{n}{2}} D_{2k-1}\right)-D_0}{2\left(\sum_{k=0}^{k=\frac{n}{2}-1} D_{2k}+\sum_{k=1}^{k=\frac{n}{2}} D_{2k-1}\right)-D_0}$	$\eta \simeq \frac{\mathrm{tg}^2\frac{2.25}{n}}{2n\,\mathrm{tg}\frac{2.25}{n}+1}$
"Snake" (n odd)	$D_{2k-1} \simeq 0{,}5D_m \times \times\left\{1+\sin\left[\frac{4.5}{R_m}h(2k-1)+0.2\right]\right\}$	$\eta=\frac{2\left(\sum_{k=0}^{k=\frac{n}{2}-\frac{1}{2}} D_{2k}-\sum_{k=1}^{k=\frac{n}{2}-\frac{1}{2}} D_{2k-1}\right)-D_0}{2\left(\sum_{k=0}^{k=\frac{n}{2}-\frac{1}{2}} D_{2k}+\sum_{k=1}^{k=\frac{n}{2}-\frac{1}{2}} D_{2k-1}\right)-D_0}$	

Let us consider a more accurate solution of this problem when the depth variation of absorbed dose in the material can be described analytically. For matter with a density close to unity and electron energies from a few tenths of an eV to a few MeV the curve of Fig. 1 can be quite accurately approximated by a segment of a sinusoid with a period $T = 2R'$ and a phase $\varphi = \sin^{-1}(2D_0/D_m - 1)$,

$$D=0.5D_m\left[1+\sin\left(\frac{2\pi}{T}R+\varphi\right)\right]=0.5D_m\left\{1+\sin\left[\frac{\pi}{R'}R+\arcsin\left(2\frac{D_0}{D_m}-1\right)\right]\right\}. \quad (1)$$

Equation (1) takes account of the change in shape of the absorption curve at low electron energies (less than 1 MeV, where the ratio D_0/D_m increases due to the absorption of an appreciable part of the beam energy in the diaphragm of the beam exit window. The same will be true if absorbing filters are introduced into the beam to flatten the dose from D_0 to D_m.

In a special case of the curve of Fig. 1 the coefficients appearing in Eq. (1) have the values $D_0 \simeq 0.6\,D_m$, and $T = 2R' \simeq 1.4\,R_m$, and the distribution of absorbed dose has the form*

$$D \simeq 0.5D_m\left[1+\sin\left(\frac{4.5R}{R_m}+0.2\right)\right]. \quad (2)$$

Neglecting the gap between layers, in the general case when $h < R_m$, the dose D_Σ absorbed in the material in its multiple passage through the beam is given by

$$D_\Sigma=\sum_{k=1}^{k=n} D_k \simeq 0.5D_m \sum_{k=1}^{k=n}\left[1+\sin\left(\frac{4.5R_k}{R_m}+0.2\right)\right], \quad (3)$$

where

$$R_k=kh-\frac{h}{2}. \quad (4)$$

Hence after summing by using the well-known formula [6] we obtain

$$D_\Sigma \simeq 0.5D_m n\left(1+\frac{0.5}{n\sin\frac{2.25}{n}}\right). \quad (5)$$

When $h \ll R_m$

* This expression has nearly the same coefficients as a similar expression obtained in [5].

$$D'_{\Sigma} = \overline{D}n \simeq \frac{1}{h} \int_0^{R_m} D\, dR, \tag{6}$$

where D is the average value of the absorbed dose over the segment R_m. After integrating and using Eq. (2) we have

$$D'_{\Sigma} \simeq 0.61 D_m n. \tag{7}$$

It is easy to show that in the limit $n \to \infty$ Eq. (5) goes over into (7) and the difference between D_{Σ} and D_{Σ}' is no more than 1% for $n > 6$.

According to (4) the dose calculated from Eq. (5) is the "average" (close to the arithmetic mean) of the doses at opposite surfaces of the irradiated material, and for small values of n the depth variation of the absorbed dose can become appreciable.

Table 1 gives formulas for estimating the depth variations of the absorbed dose in irradiated material, derived from Eq. (2) for a special case. Figure 2 shows the variation of the absorbed dose as a function of n, obtained for a single material of uniform thickness irradiated when wound on a spool (curve 1), and when "snaked" through rollers (curve 2). It can be seen that the second method of moving the material through the beam is to be preferred for $n > 3$. In general the calculational method discussed can be used within the limits of validity of Eq. (1) to describe the actual depth variation of absorbed dose in irradiated material to the accuracy given.

LITERATURE CITED

1. I. A. Charlesby, Atomic Radiation and Polymers, Pergamon, New York (1960).
2. D. Trageser, Nucl. Instrum. and Methods, 11, 248 (1961).
3. D. M. Margolin et al., Pribory i Tekh. Éksperim., 3, 186 (1967).
4. L. V. Chepel', A. Kh. Breger, and V. L. Karpov, in: Electron Accelerators [in Russian], Atomizdat, Moscow (1966), p. 399.
5. K. I. Nikulin and G. A. Obraztsov, Atomnaya Énergiya, 23, 50 (1967).
6. I. S. Gradshtein and I. M. Ryzhik, Tables of Integrals, Sums, Series, and Products [in Russian], Fizmatgiz, Moscow (1960), p. 43.

XXVIII SESSION OF THE SCIENTIFIC COUNCIL OF THE JOINT INSTITUTE FOR NUCLEAR RESEARCH

V. A. Biryukov

The XXVIII session of the Scientific Council of the Joint Institute for Nuclear Research (JINR) was held in Dubna in June, 1970. The session was opened by the director of the institute, Academician N. N. Bogolyubov, who reported on the fulfillment of the decisions of the scientific council.

The first session of the scientific council was devoted to the 100th anniversary of the birth of V. I. Lenin. Professor D. I. Blokhintsev gave a report entitled "Lenin and physics." He discussed the difficulties and contradictions in the development of physics near the beginning of the twentieth century and the large role played by Lenin, not only in defending science from various idealistic interpretations, but in explaining the fundamental aspects of natural science. Lenin's work "Materialism and Empiriocriticism," in which he gave a profound analysis of the methodological problems of natural science of that day and indicated the paths to their solutions, was of particular importance for physics. In examining this work, Bogolyubov discussed Lenin's opinions on the problem of the relative and absolute, the inexhaustibility of the electron, regularity, space, time, the microscopic world, and the unity of the universe.

Vice-directors of the institute Academician Kh. Kristov and Professor N. Sodnom discussed scientific-organizational problems. They reported on the work of the council section on high-energy physics and low-energy physics and the decisions adopted by them. The council approved new compositions for the specialized committees of the institute.

The results of studies which have been ordered by the scientific council were reported at the session. E. D. Vorob'ev discussed a study of the possible production of monochromatic particle beams on the U-200 accelerator. V. P. Dmitrievskii discussed the development of a proton cyclotron with an energy adjustable up to 40 MeV on the basis of the magnet of the U-120 accelerator. Nguyen Ding Te and I. M. Gramenitskii discussed the possibilities and programs of physical research on the 2 m bubble chambers – the propane bubble chamber at the Serphkhov accelerator and the liquid hydrogen one currently being tested in Dubna. Yu. K. Akimov reported, on behalf of the Council on Radio Electronics, a study of the possible standardization of the electronic apparatus in the JINR and in the institutes of the participating countries.

The JINR laboratories were represented at the session by reports on the scientific research completed. G. V. Efimov discussed a study of nonlocal quantum theory of a one-component scalar field. The axioms of nonlocal theory have been formulated. A class of relativistically invariant generalized functions has been introduced which may play the role of cutoff functions in perturbation theory for the S-matrix. For interaction Lagrangians of the polynomial type, the S-matrix is finite and satisfies the requirements for unitarity and macroscopic causality in each order of the perturbation theory. The electromagnetic and weak interactions of leptons have been treated by perturbation theory. It has been suggested that the neutrino is a "carrier" of nonlocality; this essentially reduces to the appearance of a form factor in the propagator for a free neutrino. The fields of charged leptons (the electron and the μ-meson) are assumed point fields, so the gradient invariance of the theory is ensured. Renormalization of the theory leads to an additional, purely neutrino–neutrino interaction.

V. G. Solov'ev discussed the development of the self-consistent-field method in nuclear theory. The method as formulated by Bogolyubov has been used in these studies. A system of basic equations has been obtained for a semimicroscopic description of nuclear vibrations. It has been shown that the equations of

Translated from Atomnaya Énergiya, Vol. 30, No. 1, pp. 73-75, January, 1971.

the self-consistent field method yield equations for the effective fields in the theory of finite Fermi systems, secular equations for models with pairing and multipole forces, and equations for the theory of pairing vibrations.

Laboratories in Alma-Ata, Budapest, Dubna, Krakow, Sofia, Tashkent, and Ulan-Bator have carried out a joint study of the interaction of π^--mesons at energies of 45 and 60 GeV with nucleons and nuclei, using nuclear emulsions irradiated at the Serpukhov accelerator; K. D. Tolstov discussed this study. The number of particles created in collisions with nucleons and the asymmetry in the CM system have been studied as a function of the energy; the dependence of this asymmetry on the number of particles created has also been studied. It has been shown that there is a significant increase in the cross section for coherent particle generation at nuclei as the energy increases. There is particular interest in the study of coherent generation of particles and complete nuclear decay, in which the questions of the physics of high-energy particles are intertwined with the physics of the atomic nucleus.

I. A. Savin discussed an experimental study of the regeneration of K^0-mesons on the accelerator of the Institute for High-Energy Physics. He discussed the physical program and the state of the experiments, in which one of the fundamental theorems of elementary-particle physics – the Pomeranchuk theorem – may be checked; estimates have also been obtained for the size of neutral K-mesons. The research is being carried out by modern procedures with magnetostrictive chambers and counters operating in combination with the BÉSM-3m computer. The entire apparatus consists of 18 high-efficiency chambers giving the X- and Y-coordinates of the tracks within 0.3 mm, and about 50 counters reading the events and triggering the spark chambers. The computer receives the information from the chambers and counters, refines it, and stores it on magnetic tape. The operation of the spark chambers and the counters is also monitored by means of a special program. The information recorded is later treated in Dubna on BÉSM-6 and SDS-1604 A computers.

L. L. Nemenov discussed a study of the reaction

$$\pi^- p \to n e^+ e^-, \qquad (1)$$

which has been carried out on the synchrocyclotron at a meson energy of 275 MeV. These experiments have permitted a study of the inverse photoproduction of the π-meson, $\pi^- p \to n\gamma^*$ (a time-like photon); in principle, an analysis of reaction (1) can reveal data about the electromagnetic structure of the π-meson and the nucleon in the time-like region. In all, 63.4 ± 11.7 events corresponding to reaction (1) have been detected. On the basis of these statistics, the cross section for the reaction is $\Delta\sigma_{exp} = (6.4 \pm 1.5) \cdot 10^{-34}$ cm^2. Current theoretical calculations yield $\Delta\sigma_{theor} = (8.2 \pm 1.6) \cdot 10^{-34}$ cm^2 under the assumption that $r_\pi = r_p = 0$. Calculations of the theoretical cross sections for various combinations of r_π and r_p yield, along with the experimental data, the 95%-probability estimates $r_\pi, r_p \leq 0.7$ F.

V. G. Zinov discussed a study of the spectra of charged particles emitted during the capture of μ^--mesons by nuclei. In experiments on the synchrocyclotron, the charged particles emitted during the absorption of μ^--mesons by the nuclei ^{28}Si, ^{32}S, ^{40}Ca, and ^{64}Cu have been identified by mass. The energy spectra and probabilities for proton and deuteron emission at energies above 15 MeV have been measured. The energy spectra have been obtained up to $\simeq$ 60 MeV. As the nuclear charge decreases, the relative number of deuterons in the total number of charged particles increases from 34.1 ± 2.6% for ^{28}Si to 17.2 ± 3.6% for ^{64}Cu at secondary particle energies above 18 MeV. The proton emission probability reaches a maximum of $(13.04 \pm 1.05) \cdot 10^{-3}$ near calcium for proton energies above 15 MeV. The experimental results indicate a cluster nature for the absorption of μ-mesons predominantly in the surface layer of the nucleus.

Yu. Ts. Oganesyan reported the results of fusion and a study of the spontaneously fissionable isotope of the element 105. When ^{243}Am was irradiated by ^{22}Ne ions accelerated on the cyclotron, an emitter of spontaneous fission fragments was detected with a decay halflife of 1.8 ± 0.5 sec; the yield corresponds to a formation cross section of $(5.0 \pm 1.5) \cdot 10^{-34}$ cm^2 for the spontaneous fission branch. The integral angular dependences of the products of the ^{243}Am + ^{22}Ne reaction were measured, as was the dependence of the cross section for the formation of the new isotope on the energy of the bombarding ions. It follows from these data and from an analysis of control experiments that the atomic number of the isotope undergoing spontaneous fission with $\tau_{1/2} \simeq 2$ sec is 105. Oganesyan also discussed a study of the spontaneous fission of the isotopes ^{256,257}103. It has been shown that the decay halflife with respect to spontaneous fission for these nuclei is above 10^5 sec. The properties of the isotope ^{258}103 have been evaluated from the experimental data.

I. Zvara reported experiments carried out for a chemical identification of element 105. The experiments were carried out by the gas-adsorption separation of the chlorides of the elements formed simultaneously in the nuclear reactions. This method yields evidence for the formation of a new element by means of its purification from the background sources of different chemical natures, i.e., by a purely chemical nature. The recoil atoms ejected from the ^{243}Am target during its bombardment by ^{22}Ne ions were retarded in a hot-nitrogen flux, and then a stream of nitrogen with chlorinating agents was added to the flux. The arrangement of a highly turbulent flow resulted in the deposition of the nonvolatile chlorides on the tube walls. Then the flux passed through a region of high temperature gradients (from 300 to 50°C) in which the chlorides of the nuclear-reaction products deposited in an order depending on their volatility in the various zones. Mica detectors were used to detect the spontaneous fission. It was shown in several series of experiments that the spontaneous fission activity in the elements is that of an element whose chloride is less volatile than niobium chloride but no less volatile than hafnium chloride. These properties agree with those predicted for ekatantalum – element 105. Eighteen decays have been detected.

In a report to the scientific council, V. I. Moroz reported the completion of a new program for geometric reconstruction (GEOM-7) for the propane and hydrogen bubble chambers for events with from three to six objects. The program takes into account the ionization loss, which changes as a function of the particle mass, and the nonuniformity of all three components of the magnetic field. The parameters of the particles leaving tracks are determined by the least-squares method with an account of the multiple-scattering matrix and the experimental errors. The electron parameters are also calculated with an account of the radiation-fluctuation matrix. The current version of the program is designed for the operation of semiautomatic measuring instruments connected directly to a BÉSM-4 computer; the spatial coordinates are reconstructed and the calculated results are stored on magnetic tape during the measurements. The parameters are determined from the spatial coordinates on a BÉSM-6 computer, for which the program is written with dynamic memory distribution in FORTRAN. The program permits the simultaneous treatment of up to five different experiments.

G. I. Zabiyakin discussed the development of calculation apparatus in the JINR. The design of automatic experimental apparatus is an urgent problem in the development of modern physical research. The basis for the development of automatic apparatus in physical centers is the electronic digital computer. Over the last few years, the JINR has significantly strengthened its computational base. The computers currently in use at the institute are a BÉSM-6, five BÉSM-4's, a Minsk-2, a Minsk-22, and an SDS-1604 A. The experimental features placed additional requirements on the computers, so the JINR has been involved in computer development. Among the apparatus designed is a multimachine input–output system based on the BÉSM-6, including remote stations with small machines of the TPA type. The possibilities of the BÉSM-4 machines are being expanded: special channels are being developed to receive experimental information, and the machines are being given additional memory units. The new methodological possibilities allow experimenters to use small computers for their experiments. These small and comparatively inexpensive machines permit large-scale mechanization, in a literal sense, of the acquiring of experimental information. However, the problem posed is even broader – to create an optimum system of computers in the JINR with a broad network of information-exchange lines, specialization, and multipurpose operation of the individual computers. In other words, the intention is to create a large computer system for the physical center with large, medium, and small computers.

The JINR has reconstructed a fast pulsed reactor and has started up the new IBR-30 reactor, as was reported by V. T. Rudenko. The basic reason for the reconstruction of the IBR-1 with an injector was to increase the average power and to expand the experimental capabilities of the apparatus while retaining the high-quality neutron pulses. The IBR-30 with linear electron accelerators as injector is a multipurpose instrument which can be used in various operating modes. It combines several types of reactors: a single-pulse Godiva reactor, an IBR-1 fast pulsed reactor, a low-frequency reactor, a pulsed booster, and a pulsed super booster. Rudenko reported the construction of a new reactor and its characteristics.

F. L. Shapiro discussed studies which have been carried out in the JINR with ultracold neutrons and some aspects of the future of this field.

Following the recommendations of judges, the scientific council awarded JINR prizes for the best work carried out in the JINR during 1969. The first prize for scientific research was awarded to a collective of authors who wrote "Measurement of the slope parameter for the differential cross section for elastic pp-scattering in the energy range 12-70 GeV;" the second prize was awarded to the authors of "Theory for

intranuclear cascades at high and ultrahigh energies" and "Production of light isotopes with a large neutron excess in nuclear reactions with heavy ions." The first prize for scientific methodology was awarded to the collective of authors of "The IBR-30 research reactor;" the second prize was awarded to the authors of "A new method for detecting particles (a proportional chamber)," "Methods for producing high-activity rare earth preparations for nuclear spectroscopy," and "System of mathematical operation of the BÉSM-6 with a translator from FORTRAN."

PHILADELPHIA MAY 1970 INTERNATIONAL MESON SPECTROSCOPY CONFERENCE

A. A. Kuznetsov

An international conference on meson spectroscopy was held in Philadelphia (USA) in May, 1970. The number in attendance at the conference was about 250, mostly American physicists.

The conference adopted the system of review reports containing an ample amount of experimental information on the formation of meson resonances (in different types of interactions) and their properties.

There was great interest shown in the work done at the JINR High Energies Laboratory in the study of neutral boson resonances decaying to π^0-mesons and γ-photons (Z. Struhalski), as well as work on the study of mesons with strange particles taking part in the decay processes (A. A. Kuznetsov).

Among the other reports of major interest were those dealing with research based on the large CERN boson spectrometer, dealing with the problem of the A_2-meson, as well as a program of work on searching for mesons of mass equal to (or greater than) the mass of two nucleons. A report by M. Martin (CERN) contained fresh data on the properties of the A_2-meson. A wealth of statistical material was adduced to demonstrate that the A_2-meson forming in the reactions $\pi^- + p \rightarrow K^\circ + K^-$ and $\pi^- + p \rightarrow p + \pi^+ + \pi^- + \pi^-$ disintegrates to form two mesons: the A_2^{π}-meson (of lighter mass) with the mass (1265 ± 6) MeV and the A_2^{H}-meson (of heavier mass) with the mass (1331 ± 6) MeV. Observation of two resonances close in mass in the region of the A-meson, and having the same decay channel ($A_2 \rightarrow K^\circ + K^-$), indicated that the A_2^{L}- and A_2^{H}-mesons have the quantum numbers $J^P = 2^+$. This experiment was completed with the aid of the CERN boson spectrometer with the momentum of the π^--mesons at 7.0 GeV/c in the $0.2 \leq |t| \leq 0.3$ $(GeV/c)^2$ range of the four-dimensional transferred momentum, and with mass resolution ±8 MeV.

Fresh data obtained on the decay of the A_2-meson through various channels by means of bubble chambers were communicated by A. Barbaro-Galtieri (Berkeley). Approximation of the peak in the mass range of this meson was carried out without taking splitting into account. The data reported are listed in Table 1.

TABLE 1. New Data on Decay of A_2-Mesons

Decay channel of A_2-meson	Mass, MeV	Width, MeV	Percentage ratio
$A_2 \rightarrow \rho\pi$	1302±4	83±15	71±14
$A_2 \rightarrow \eta\pi$	1314±8	113±25	18±4
$A_2 \rightarrow K\bar{K}$	1306±8	100±25	11±2

A report by B. Barysz (Caltech) discussed experimental data on resonances with mass equal to (or greater than) the mass of two nucleons, and found as a result of pp-interactions. Analysis of the energy dependence of the cross sections of several I = 1 reactions indicates the existence of the following boson resonances: a) mass 1930

TABLE 2. Comparison of Data on Decays of Heavy Meson Resonances by Channels $\pi\pi$ and $\rho\pi\pi$

Data obtained with CERN boson spectrometer			Data obtained with bubble chambers		
mass, MeV	width, MeV	$\pi\pi/\rho\pi\pi$ percentage ratio	mass, MeV	width, MeV	$\pi\pi/\rho\pi\pi$ percentage ratio
1929±14	35	92	1975±12	52	Small
2195±15	13	94	2157±20	68±22	50
2660±20	85±30	—	2660±10	50	30

Translated from Atomnaya Énergiya, Vol. 30, No. 1, pp. 75-76, January, 1971.

TABLE 3. Comparison of Experimental and Theoretical $e^+ + e^-$ Interaction Cross Sections

Reaction	Experimental data	Theoretical data (quantum electrodynamics)
$e^+ + e \rightarrow \begin{cases} e^+e^- \\ \mu^+\mu^- \\ \gamma\gamma \end{cases}$	$(3,35 \pm 0,25) \cdot 10^{-32}$ $(1,6 \pm 1,5) \cdot 10^{-33}$ $(1,81 \pm 0,6) \cdot 10^{-33}$	$3,5 \cdot 10^{-32}$ $2,0 \cdot 10^{-33}$ —

MeV, width ≈35 MeV; b) mass 2200 MeV, width ≤13 MeV, and c) mass 2380 MeV, width ≤30 MeV.

Resonances in the $2250 \leq M \leq 2500$ MeV range of effective masses were discussed in a report by G. Smith (Michigan). It was found that a resonance of mass (2382 ± 24) MeV and width 26 MeV (CERN data) is observed in the reactions $\widetilde{PP} \rightarrow$ and $\widetilde{PN} \rightarrow KK^+(m\pi)$ at antiproton momenta from 1.5 to 2.0 GeV/c, and a resonance of mass (2360 ± 25 MeV) and width < 60 MeV (Brookhaven data) is observed in the reactions $\widetilde{NN} \rightarrow K^* + K + \pi + \pi$ and $\widetilde{NN} \rightarrow K^*\widetilde{K}\pi\pi$. The close values for mass and width of the peaks reported are indications of the possible existence of several competing decay channels for the same resonance.

A report by D. Miller (Indiana State University) contained new data on decays of heavy meson resonances through the channels $\pi\pi$ and $\rho\pi\pi$. These data were obtained by processing bubble-chamber plates. Inelastic π^--p- and π^+p-interactions (momentum 10 GeV/c) in the $0.1 < |t| < 0.3$ $(GeV/c)^2$ range of values of the four-dimensional transferred momentum were studied. The experimental data were compared with similar data obtained on the CERN boson spectrometer. The results of that comparison appear in Table 2.

The energy dependence of the differential cross sections in the reactions

$$K^+ + p \rightarrow K^* + \Delta^{++};$$
$$K^- + n \rightarrow K^* + \Delta;$$
$$K^- + p \rightarrow K^+ + n;$$
$$K^+ + p \rightarrow K^* + p$$

over the energy range from 3 to 10 GeV was analyzed in a report by G. Kaye (University of Michigan). Experimental data were compared with results of calculations based on different theoretical models.

A report submitted by an Italian group communicated some tentative results on a verification of the applicability of quantum electrodynamics, with the reactions $e^+e^- \rightarrow e^+e^-$, $e^+e^- \rightarrow \mu^+\mu^-$, and $e^+e^- \rightarrow \gamma\gamma$ cited as illustrative examples (see Table 3).

An interesting report was given by D. Kline (Wisconsin) on reactions characterized by Feynmann diagrams with baryon exchange in which mesons are formed. It was reported that there is no production of the ρ-meson in reactions of the above type, while the ω-meson is produced with a fairly large cross section.

The state of affairs at which the Omega Project (CERN large spark spectrometer) has arrived was discussed at the conference (Beusch), and reports were made on the program of experiments on the CERN boson spectrometer at Serpukhov (Waitsch), on the Brookhaven [National] Laboratory large magnetic spark spectrometer (S. Lindenbaum), on the large spark spectrometer at Stanford Laboratory, and on the development of new spark chamber procedures (D. Fisher). It was reported at the conference that the Omega Project will be completed by the spring of 1972. The planned magnetic field intensity is 18 kG. Optical spark chambers will be used in this project.

Hybrid facilities, incorporating various combinations of spark chambers, track-delineating spark chambers, proportional chambers, and even bubble chambers, are now being assembled in many laboratories in the USA. For example, D. Fisher (Brookhaven) reported on a hybrid project combining a proportional chamber and spark chamber. This facility offers the advantages of the excellent time resolution inherent in proportional chambers and the option of selecting out events and expensive counting capabilities of spark chambers. Tests on a prototype have shown that this type of hybrid chamber offers a resolution of 75-85 nsec at different voltages across the "delay interval" (900 to 600 V). The chamber recovery time is 50 to 100 μsec. A description of the large Brookhaven Laboratory spark chamber was contained in a report by S. Lindenbaum.

II HELSINKI INTERNATIONAL CONFERENCE ON REACTOR NUCLEAR DATA

S. I. Sukhoruchkin

A second international nuclear data conference was held in Helsinki in June, 1970. Since the time of the first Paris (1966) conference, a large amount of experimental material on neutron cross sections and other topics of interest in reactor design has been accumulated and systematized in dozens of large laboratories and at nuclear data centers, so that there was naturally great interest in the work of this conference (in which 163 scientists participated).

Each session usually began with an introductory review report illuminating the present state of the topic, followed by original papers and, at the end of the session, a review paper was read accompanied by an evaluation of the extent to which nuclear data needs had been satisfied, i.e., a comparison was made of the accuracy required and achieved in the data discussed, and ranges of greatest discrepancy in the data were singled out, with proposals and recommendations tendered. Basic results and conclusions from the reports heard were discussed once again at the concluding session of the conference.

At the first session, devoted to general topics in the utilization of nuclear data, review papers were presented, including "Status of nuclear data needs" by G. Schmidt (IAEA), "Effect of inaccuracies in nuclear data on reactor calculations and performance" by B. Hutchins (General Electric Corp., USA), "Importance of nuclear data for astrophysics" by D. Clayton (Rice University, USA), and "Data needs for controlled thermonuclear fusion devices" by Yu. F. Chernilin (I. V. Kurchatov Institute of Atomic Energy, USSR) (an interesting report by D. Crocker from Harwell was also given on a topic similar to that of the report mentioned last).

B. Hutchin's report was a particularly timely one, since it relates existing uncertainties in nuclear data to the economics of large fast breeders. This paper also discussed uncertainties existing several years ago, and the anticipated spread in future data. It was reported that the α parameter (ratio of capture cross section to cross section for Pu^{239} fission) shifted, in terms of the influence of inaccuracies in nuclear data on economic costs (losses), from first place in 1968 to third place in 1970 (now trailing behind the cross section for capture in U^{238} and the parameter $\bar{\nu}$, the number of secondary neutrons). But the final accuracies required for fast breeder design calculation data, 3% for α, 0.5% for $\bar{\nu}$ numbers, and 2% for capture cross section in U^{238}, can probably be attained by 1975. There is no doubt that these high accuracies can be attained only through simultaneous utilization of differential data obtained with very high resolution, and data on special integrated experiments. In that sense, the completion of the "first generation" of measurements and estimates of α to within ~10% (up to energies < 10 keV) in 1970, which has made it possible to make a jump from 50% uncertainty, is the first necessary step on the path to satisfying the most rigid, but economically fully justified, requirements in reactor design work. The first session closed with a report by E. Lynn (Harwell) on progress in understanding the process of neutron interaction with complex nuclei.

Highly accurate measurements were discussed at the second session, where a review report by A. Deruyter (Gel, Belgium) began a highly detailed analysis of the state of affairs in the study of standard cross sections, to which normalization of data is usually referred. At the present time, normalization of data to the fission cross section of U^{235}, which had been popular in much earlier work, is now encountering grave doubts. Structure detected in the fission cross section of U^{235} renders the normalization results dependent upon the energy resolution of the measurements taken. Deruyter suggested using the cross sections of the reaction $B^{10}(n, \alpha)Li^7$ and the cross section for scattering on hydrogen as the primary standards, and the fission cross section of U^{233} and the cross sections of the reactions $Li^6(n, \alpha)$, $He^3(n, p)$, $Au^{197}(n, \alpha)$, etc., as

Translated from Atomnaya Énergiya, Vol. 30, No. 1, pp. 76-78, January, 1971.

the working standards. Seven original reports given at this session were devoted to concrete aspects of measurements of the standard cross sections alluded to above.

Nuclear data for fissionable nuclides (A > 220) were discussed at two sessions (for the resonance range of energies and the region of fast neutrons). Two sessions were devoted to cross sections of nonfissionable nuclides. Review reports were presented at these sessions by James (Harwell), P. Ribon (Saclay), G. V. Muradyan (IAÉ, USSR), J. Storey (Harwell), B. Penitz and V. Davy (Argonne National Laboratory, USA), S. Sergeac (West Germany), A. I. Abramov (Power Physics Institute [FÉI], USSR), and V. Benzi (Bologna, Italy). Some of the original reports presented were also of a review character. For example, reports on cross sections of fissionable nuclides devoted to results obtained with spectrometers operated at electron accelerator facilities at Gel and Scalay each consisted of seven and four reports. The results of measurements done on the cross sections of plutonium and curium isotopes, with underground nuclear explosions utilized as a research tool, were described in two reports from Los Alamos. Two other problems were given attention in reports by IAEA experts at two conferences held at Studsvik (Sweden) immediately prior to this conference, specifically on the status of data on parameters $\bar{\nu}$ and α (review papers at the conference with conclusions and recommendations deriving from the earlier Studsvik conference were made by representatives of the respective conferences, J. Colvin from Harwell and S. I. Sukhoruchkin from ITÉF [Institute of Theoretical and Experimental Physics, USSR]). The conference on $\bar{\nu}$ values confirmed a continuing discrepancy in the value of $\bar{\nu}$ of the standard californium source, as well as some contradictions in data on the energy dependence of $\bar{\nu}$ for both U^{235} and Pu^{239}. A review of the present state of α measurements will be published subsequently.

A large number of reports on measurements and estimates of the cross section for capture in U^{238} were presented at the conference. As mentioned earlier, uncertainties in the capture cross section and in the $\bar{\nu}$ number are the weakest points in fast reactor design data at the present time. A very interesting discussion was stimulated by review reports of C. Campbell (Winfrith Heath, Britain) and H. Kusters (Karlsruhe, West Germany), as well as by a paper submitted by J. Barret (Cadarache, France), in which the relative role of differential and integral data in fast reactor design calculations was discussed. The British viewpoint was that differential data can be measured with slightly lower accuracy than required for calculations, but that normalization and fitting of these data would be possible on the basis of integrated data. That is the way the paramount problem in reactor design, designing and constructing an economically feasible fast reactor prototype, is being solved in Britain and France. H. Kusters, and also B. Hutchins (USA), remarked in this connection that the role of differential data must not be disparaged in any case, since only differential data are capable of providing information for safety calculations and predictions on long-term behavior of a breeder reactor. Hence, only some reasonable balance struck between the two types of data could satisfy reactor calculation needs. R. Taschek (Los Alamos, USA) correctly noted, in his remarks at the concluding session, that reactor designers must devote increasing attention to a sound economic justification of needs in differential measurements, and must pose the problems to be resolved in this area to experimental physicists.

The last session of the conference was devoted to problems and methods in evaluation of nuclear data. A review report was presented by S. Perlstein (Brookhaven, USA) in the name of four world data acquisition centers. The report centered on questions resolved at the conference of four nuclear data centers in Moscow (information on which may be found in Atomnaya Énergiya, 28, No. 5, p. 450 (1970)). A report by G. Alter (Atomics International Corp., USA) presented a detailed description of a system of graphical presentation and comparison of data on neutron cross sections (SCORE) which enables the person evaluating the data to include cross sections directly in the design calculation process, and to keep track of progressing stages in the calculations, e.g., the process of fitting fission cross sections to multilevel formulas, and so forth. In addition to these two reports, there were 15 other communications on different topics concerning data evaluation, including two Soviet papers (from FÉI) on estimates of the U^{238} capture cross section and calculations of the density of excited levels of nuclei.

The IAEA-sponsored Helsinki conference demonstrated the very extensive expansion of experimental data in the area of measurements of neutron cross sections, progress achieved in methods for treating the data in reactor calculations, and the fruitfulness of broad international collaboration in this crucial area of science.

The proceedings of the conference (126 papers included) will be published by IAEA in the immediate future.

V YUGOSLAV SYMPOSIUM AND SUMMER SCHOOL ON THE PHYSICS OF IONIZED GASES

N. V. Fedorenko

The fifth Yugoslav symposium and summer school on the physics of ionized gases was held at Herceg Novy from July 6 to July 16, 1970. The scientific agenda of the symposium and school covered low-temperature plasmas, atomic collisions in a gas, and atomic collisions in solids. These three trends are represented at Yugoslav physics institutes, and the topics covered in the symposium and school are traditional on that account. Original papers by Yugoslav physicists predominated. The lecturers at the school were mostly foreign invited guests, whose scientific interests lie along the same lines as those developing in Yugoslavia. The morning sessions were devoted to lectures forming a part of the school, and the afternoon or evening sessions were symposium sessions punctuated by brief fifteen-minute reports. The program of the school and symposium was not overloaded. This made it possible for the Yugoslav scientists to utilize the free time of the lecturers for unofficial talks on scientific topics of mutual interest.

Over 150 scientists attended the symposium and school, about a third of them foreigners. The Soviet delegation consisted of ten. About a third of the lectures given in the course of the school were delivered by Soviet lecturers. All of the reports by Soviet scientists were heard with great interest.

Low-Temperature Plasma. Most of the work on plasma physics covering work done in Yugoslavia and included in the symposium agenda dealt with propagation of waves through plasma (B. Anicin, Boris Kidric Institute), behavior of plasma in crossed fields (D. Tosic, B. Kidric Institute), and high-pressure arc discharges (Institute of Physcis at the University of Belgrade). Investigations of plasma turbulence in the positive column of a discharge were undertaken at the Jozef Stefan Institute (S. Poberaj); spectroscopic investigations of plasma are underway at several places, specificially at the Ruder Boskovic Institute (Z. Sternberg). The lecture program of the school was formulated pretty much in line with these interests. G. Dravin (Fontenay-aux-Roses, France) gave a series of lectures on spectroscopic plasma diagnostics, thermal equilibrium citeria, and collisional processes in plasma. A lecture by R. Wienecke (West Germany) was devoted to physical phenomena in an arc discharge in a strong magnetic field, and a lecture by D. Miller (West Germany) dealt with ultraviolet emission from arc discharges.

Soviet scientists serving this division of the school gave lectures on corpuscular plasma diagnostics (V. V. Afrosimov), plasma research by microwave techniques (M. M. Larionov and V. A. Ipatov), and applications of the Doppler effect at the cyclotron frequency in plasma diagnostics (B. I. Ivanov).

Atomic Collisions in Gas. Experimental research on the physics of atomic collisions is being actively pursued by B. Cobic at the Boris Kidric Institute. Work on the theory of atomic collisions is also being pursued there (R. Janev et al.). Experimental research on collisions between electrons and atoms were conducted by M. Kurepa at the Institute of Physics of the University of Belgrade. A sensitive procedure for recording individual photons is also being developed with success at that institute (V. Urosevic). The work done by all these research groups in Yugoslavia, and also to a partial extent during stays of Yugoslav physicists in the USA and Britain, were presented at the symposium.

The school's program on the physics of atomic collisions was covered by lectures given by Soviet and Yugoslav scientists. These lectures provided a fairly complete picture of the present status of the physics of atomic collisions. Lectures by I. P. Zapesochnyi dealt with excitation and ionization in electron-atom collisions. A lecture by V. V. Afrosimov dealt with utilization of a coincidence procedure in the detailed investigation of electron capture and loss processes in atomic collisions. A lecture by V. A. Belyaev dealt with determinations of cross sections at low energies, using a combined-beam procedure.

Translated from Atomnaya Énergiya, Vol. 30, No. 1, pp. 78-79, January, 1971.

A lecture by R. N. Il'in was devoted to the production of highly excited hydrogen atoms and their ionization in an electric field. A lecture by N. V. Fedorenko reviewed data reported on electron capture and losses by ions and hydrogen atoms over a broad range of energies. Lectures by G. F. Drukarev and M. I. Chibisov dealt with the theory of atomic collisions.

Atomic Collisions in Solids. This area of work in Yugoslavia was begun by B. Perovic and her colleagues, and is now being carried out at the Boris Kidric Institute and at the University of Belgrade. This is also a small group working at the Jozef Stefan Institute (B. Navincek). The work by Yugoslav physicists in this area has long been acknowledged. In contrast to the other divisions of the school, most of the reports on research on collisions in solids were made by foreign scientists. Several papers were devoted to studies of the penetration of fast foreign ions through semiconducting crystals. This work has a practical side to it: the production of custom-ordered prespecified semiconductor structures. Other papers dealt with research on interactions of ions and electrons in alkali halide compounds, and work with thin metallic films, with the object of throwing light on the mechanism underlying collisions between ions and atoms of the crystal lattice.

The school lecturers dealing with atomic collisions in solids were all foreigners. One of the lectures on radiationless processes taking place on the surface of solids was delivered by the renowned American scientist G. Hackstrom. Also of interest were lectures by G. Carter (Britain) on his investigations of penetration of ions through semiconductor materials (gallium arsenide and gallium phosphide).

A list of expanded annotations of all the original papers was published and circulated before the start of the symposium. The extent of each annotation ranged from one to four pages. Many of the annotations also included graphs and diagrams. The complete texts of these papers will probably be published by the end of the year [1970] in an appendix to the new Yugoslav physics publication Fizika. Lectures given at the school are to be published as a separate brochure, also by the end of 1970.

XV INTERNATIONAL SUMMER SCHOOL ON THE STRUCTURE OF THE NUCLEUS

V. G. Solov'ev

The XV international summer school on the structure of the nucleus was held in August, 1970 at Herceg Novy (Yugoslavia). About 100 physicists from 13 different countries of Europe and North America were in attendance.

The central focus in the work of the school was the presentation of the Hartree–Fock–Bogolyubov method and its applications to various problems in the theory of the atomic nucleus. Lectures by F. Herbut and M. Vudjičić (Belgrade) described the method of the self-consistent field developed by N. N. Bogolyubov in 1959, and extended its mathematical development. Lectures by V. G. Solov'ev (JINR, Dubna) gave a presentation of treatment of small harmonic oscillations proposed by N. N. Bogolyubov within the framework of the self-consistent field method. The application of this method by R. V. Dzholos and V. G. Solov'ev to nuclear oscillations was presented. It was shown that equations for the effective fields in the theory of finite Fermi systems developed by A. B. Migdal, and secular equations of the model with paired and multipole forces, can be derived from the equations of the self-consistent field method. Topics in the Hartree–Fock–Bogolyubov theory were also reflected in lectures given by D. Brink (Britain). Seminar participants were also provided with descriptions, based on the Hartree–Fock–Bogolyubov method, of neutron–proton correlations (H. Wolter, West Germany), and anharmonicity of nuclear oscillations (J. Mayer, West Germany). The Hartree–Fock–Bogolyubov method was applied to the treatment of nuclear rotational motion within the framework of the forced rotation model (P. Ring, West Germany).

Lectures given by Professors O. Brink (Oxford, Britain), K. Bloch (Saclay, France), D. Sprang (Hamilton, Canada), W. Greiner (Frankfurt, West Germany), and M. Jean (Orsain, France) were highly interesting. The lectures by D. Brink, devoted to collective motion in nuclei, presented the method of the coordinate generator, and demonstrated the relationship between this method and the method of approximate second quantization and the Tamm–Dankov method. Applications to light nuclides were presented. Lectures by K. Bloch discussed the asymptotic method of determining single-particle levels in a deformed potential well at large deformations. Lectures by W. Greiner gave accounts of the region of superheavy elements, nuclear quasimolecules, and fission of nuclei shaped as oblate ellipsoids. Stress was laid on the importance of heavy-ion accelerators in the study of the structure of the nucleus. D. Sprang gave a review of work studying the behavior of nucleon–nucleon forces outside the energy surface. Interactions between pions and nuclei were the subject of a lecture by M. Jean.

Prominent in the school agenda were the seminars at which those in attendance at the school told of the work they were engaged in. There was exceptional interest shown in reports by F. Hamilton (USA) on electromagnetic transitions in deformed nuclei, L. Papineau (France) on analog states in deformed nuclei, L. A. Malov (JINR, Dubna) on collective states of nuclei in the region of the actinides, J. Wilczycki (JINR, Dubna) on neutron-rich isotopes of the light elements, M. Stefanone (Italy) on nonstatistical effects in the capture of resonance neutrons, and so forth.

The school was well organized. The proceedings of the school will be made available in a separate edition.

Schools of this type are extremely important from the standpoint of improving the skills and experience of young scientists, and even of fairly experienced theoretical physicists and experimental physicists. The schools provide consistent presentations of the achievements of modern physics. In addition, each participant gains the opportunity to discuss the problems which disturb him with highly trained scientists.

Translated from Atomnaya Énergiya, Vol. 30, No. 1, p. 79, January, 1971.

ENVIRONMENTAL PROBLEMS IN THE VICINITY OF NUCLEAR ELECTRIC POWER STATIONS

A. D. Turkin

The problem of safe operation of nuclear electric power generating stations has been coming to the forefront with the steadily increasing role played at atomic energy in satisfying the world's needs for power. Concern is being expressed in many countries around the world on the degree of hazard in possible increases in radioactivity in the biosphere, and the long-term effects on the environment of the heat released by nuclear power plants to the hydrosphere.

The aims of a symposium on environmental problems in the vicinity of nuclear power plants that was organized by IAEA and held in New York in August, 1970 were to analyze experience in the construction and operation of nuclear power stations, and also the measures taken to minimize whatever harmful effect nuclear power stations might have on the environment.

A quantitative estimate of radiation protection of the population can be made only on the basis of numerical values of the risk probability for any case of radiation exposure. However, in the opinions voiced by E. Pochin (Britain) and C. Morgan (USA), the methods used at the present time to make such estimates fail to provide realistic estimates of the risk. The reason for this failure is that information is still lacking on the frequency of harmful effects caused in humans at low exposure doses. Available quantitative data on the frequency of occurrence of definite modes of radiation injuries, principally malignant tumors, were obtained at dosages of several hundred rads. Conversion of these data to low exposure doses may lead to actual risk values which are far too high. In order to evaluate the probable risk of radioactive contamination of the environment, we have to determine the extent of the release of contaminants, the isotope composition of the contaminants released, and also the probability of discharges of radioactivity from potential sources, the amount and age distribution of people who might become subjected to radiation exposure under different meteorological conditions. The degree of effectiveness of protective measures taken must also be taken into account, and estimates must be made of possible genetic effects. Neglect of the above factors in estimates of radiation hazards from wastes could lead to serious errors. The homogeneity of the criteria for estimating radiation hazard due to radioactive wastes can be based on ICRP recommendations, stating that the exposure dose for individual persons in a population must not be greater than 0.5 rem / year, and the exposure dose for the population taken as a whole must not be greater than 5 rem over a 30 year period, or 0.17 rem/year. Special attention is reserved here for secondary standards governing the critical tolerance levels of releases of radioactive isotopes to the surroundings.

In the Soviet Union, the critical tolerance levels for releases of radioactive isotopes of inert gases have been set for nuclear power generating stations at 3500 Ci/day, or 0.1 Ci/day in the case of I^{131}. The positions taken in the USA on controls over radioactive discharges envisage regulations applying to each nuclear facility separately, depending on the siting and the prevailing meteorological conditions. The critical tolerance levels for radioactive isotopes of inert gases at 13 nuclear power plants in the USA range from 10 to 85,000 Ci/day, of $3 \cdot 10^4$ to 0.4 Ci/day in terms of I^{131}. Many years of operating experience with nuclear power plants in the USSR, USA, Britain, Japan, and other countries has demonstrated that real discharges vented to the atmosphere amount to several percentage points of the critical tolerance levels.

One of the major problems in achieving radiation safety at large nuclear power stations is theoretical analysis of the limiting possible damage accompanying discharge of large amounts of radioactive substances to the surroundings. The difficult task in the prognosis of scales of limiting possible damage is, in the view of P. Candes (France), estimating the fraction of fragments accumulated in fuel and discharge to the external environment. This amount can be assigned the value 30% in the case of the critical possible damage at a sodium-cooled reactor.

Translated from Atomnaya Énergiya, Vol. 30, No. 1, pp. 79-80, January, 1971.

Considerable attention was given at the symposium to problems connected with the temperature effects brought about by nuclear power stations and fossil-fuel power stations on the ecological systems of reservoirs into which heated water is dumped. J. Donald (USA) and P. Corvoisier (Switzerland) discussed thermal standards relating to this point, but without making any quantitative recommendations. Their failure to advance quantitative recommendations stems from the fact that the heat accumulation effect is absent in living organisms, so that the concept of absorbed thermal dose loses its validity.

The volume of radiation control and monitoring of the environment must be clearly defined when nuclear power stations are in the design stage. In the view of H. Dunster (Britain), dosimetry of the external environment must be completed in the first two years of operation of the nuclear power station in line with a developed program, which can then be curtailed and simplified, as the data accumulate, down to the point where some of its parts are phased out.

Many of the reporters at the symposium pointed out that the future belongs to nuclear power not only in the light of economic considerations but also in relation to minimized contamination of the environment as compared to fossil-fuel electric power stations. At the same time, the siting of nuclear power plants to be constructed, from the standpoint of providing radiation protection to the population of the area, remains an unresolved problem.

The cost feasibility of siting of nuclear power plants near large cities or directly in the confines of a city brings to the fore the problem of ensuring radiation safety for the surrounding population. Moreover, the American specialists L. Roddis, J. Ramey, and H. Slater drew attention to certain difficulties in the building of nuclear power stations due to the still persisting negative opinions entertained by the USA public toward nuclear power stations. Saiki pointed out that not more than 50% of the people in Japan living in the vicinity of nuclear power stations have put themselves on record for the further use of nuclear power stations.

Nevertheless, the problem of siting nuclear power stations in large cities is being solved in Japan. Engineering designs for a municipal nuclear power plant are being completed in 1-2 years. Construction of a 1000 MW(e) reactor power plant is underway in Britain at a site several miles out from a city populated by over 100,000 people.

The siting of large nuclear power stations in thickly populated regions requires fabrication and availability of reliable equipment free of radiation hazard to the population of the area, and cleanup of radioactive wastes. F. Wachsmann reported on engineering plans for siting an underground nuclear power plant in West Germany in a thickly populated area, and another nuclear power plant project for underwater siting. This siting of a nuclear power station will greatly localize release of radioactive materials in the event of accidents.

The lack of any commonly agreed upon methodology for forecasting human exposure dosage, or international recommendations on the level of contamination manageable in thickly populated areas is holding back municipal siting of nuclear power plants to some extent. It was also reported at the symposium that the hazard presented by the presence of a nuclear power plant to the population of the surrounding area is no greater than the hazard presented by conventional fossil-fuel-burning electric power generating stations.

An estimate made by F. Sowby (Britain) indicates that the radiation risk at a nuclear power plant is several thousands of times below the natural risk (presented by possible transportation accidents, death due to illness, etc.).

CONTINUOUS γ-FACILITIES FOR LIQUID-PHASE AND VAPOR-PHASE RADIATION PROCESSES

V. A. Gol'din, A. Kh. Breger,
É. L. Mendel'son, G. I. Lukishov,
E. B. Mamin, and V. P. Smirnov

A pilot γ-irradiation facility, the RKhUND-20000 continuous irradiator designed for radiation-chemical processes under conditions approximating full-scale production conditions to the maximum, with liquid-phase and vapor-phase reagents flowing through the reaction vessel housed with the irradiator (Co^{60}) unit, has been developed and put into operation at the L. Ya. Karpov Physicochemical Institute. The physical and engineering parameters of the facility are entered in Table 1. The design of the facility (Fig. 1) includes a squirrel-cage type irradiator-reservoir, a guide tube, a three-compartment mobile cylinder, compartmented seals, and a trolley hoist.

The irradiator-reservoir consists of 20 isolated smoothly bending channels 4, in the bottom of which are placed 80 standard Co^{60} preparations 6. The irradiator is housed in the steel casing 5 of the facility, and the free space inside that casing is stuffed with iron shot (ρ = 4.6 kg/cm^3); the fully assembled facility is installed in a concrete-lined pit sunk in the room floor. The guide tube features a calibrated inner hole 9.

The three-compartment mobile cylinder consists of a cavity accommodating the reaction vessel 8, the top (3) and bottom (10) lead shielding plug providing the necessary radiation protection for the servicing personnel. Communication channels 1 linking the process portion of the facility (not shown in Fig. 1) to the

TABLE 1. Physical and Engineering Data on the RKhUND-20000 and Gammatok Irradiator Facilities

Parameters	RKhUND-20000	Gammatok
Irradiator		
Class of facility	PN-1	PN-1
Size, mm	⌀ 400 × 1450	⌀ 900 × 2000
Weight, kg	500	1800
Activity, gram-equivalent Ra	20 000	56 000
Number of channels	20	16
Number of sources in channel	4	5
Cooling system	Air	Water
Working volume, liters	9	35
Geometric dimensions of basic reaction vessel, mm	⌀ 130 × 300	⌀ 260 × 650
Co^{60} preparations		
Geometric dimensions, mm	⌀ 11 × 81	⌀ 11 × 81
Activity, gram-equivalent Ra	250	700
Dose rate		
Dose rate at center of reaction vessel, r/sec	220	260
Dose rate in channels for irradiation of lumped systems, r/sec	—	380
Dose rate in channels for irradiation of lumped systems, r/sec	—	220
Specific rate of consumption of biological shielding (iron shot), kg/gram-equivalent Ra	0,033	0,036

Translated from Atomnaya Énergiya, Vol. 30, No. 1, pp. 81-83, January, 1971.

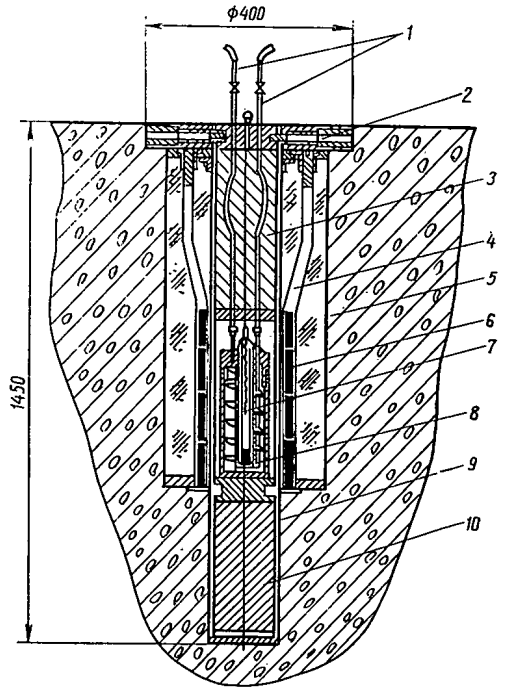

Fig. 1. RKhUND-20000 facility (vertical cross section).

reaction vessel pass through the top shielding plug 3. The facility is equipped with a thermocouple 7.

The compartmented electromagnetic seals 2 over an annular slit between the mobile cylinder and the guide tube, and which protects personnal from the scattered γ-radiation along the annular slit while performing the function of a device interlocking the mobile cylinder in the working and idling positions of the facility.

An experimental checkout of the biological shielding revealed that the dose rate at any point on the surface of the radiation-chemical process facility accessible to personnel was not above 0.6 μR/sec, in agreement with design calculations. The proposed design solution made it possible to provide the necessary biological shielding with a relatively small amount of shielding material (the facility uses 150 kg of lead shot and 500 kg of iron shot).

The facility is provided with an autonomously operating interlock and alarm system. The electrical circuitry incorporates, as sensors, USIT devices (annunciating alarm for the radiation situation and interlocking movement), limit switch contacts (interlock and alarm annunciation in response to the position of the mobile cylinder), and a current relay (interlock of the electric power drive for the mechanism displacing the facility). The controls are operated from a central control panel. The process monitoring and control instrumentation was developed to match the various radiation-chemical processes for which the facility was designed.

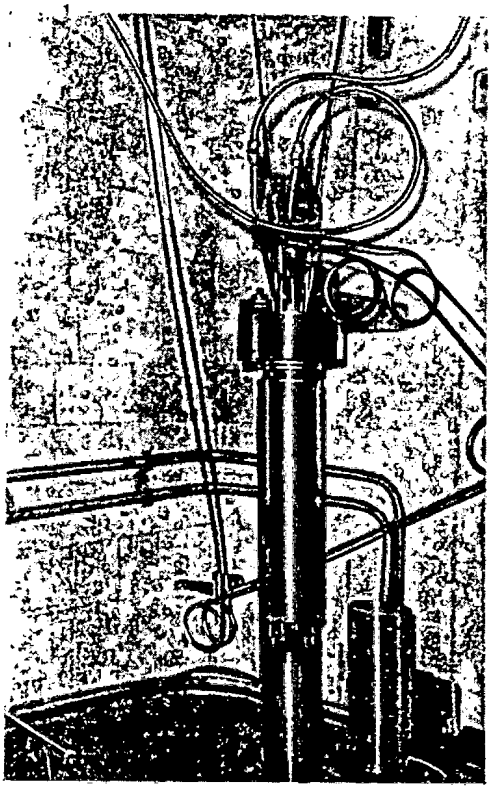

Fig. 2

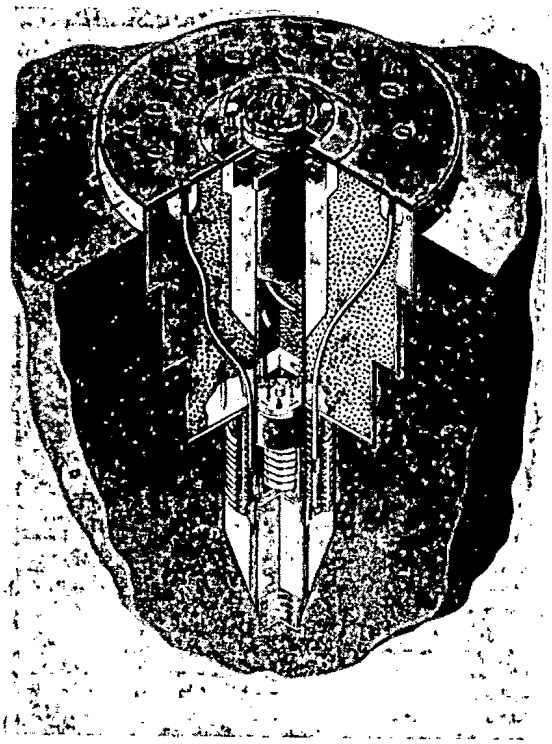

Fig. 3

Fig. 2. General view of RKhUND-20000 facility in operation.

Fig. 3. General view of Gammatok pilot radiation-chemical process facility.

The facility is charged with Co^{60} preparations by a "dry" method, directly from a KTB-12 multicharge transport container placed above the channels into a fixed charging device.

Several dosimetric systems were studied in line with the proposed utilization of the process facility under full-scale factory conditions, and a system was chosen (+9% aqueous glucose solution) which would make it possible to determine absorbed doses directly in the reaction vessels under both static conditions and circulation conditions. The design dose rates were confirmed by experiment, and found to be within the range of accuracy stipulated for the procedure (± 7%).

In combination with specially designed process equipment, the RKhUND-20000 facility has been used in the production of polymaleamides, in batch production of 1 kg polymer per hour (Fig. 2).

A variant of the RKhUND-20000 process pilot facility known as the Gammatok (see Table 1) is now being developed. In this variant (Fig. 3), the basic inner reaction vessel is accompanied by an additional (outer) vessel which makes it possible to up the γ-radiation efficiency to 30%. The presence of seven additional isolated channels makes it possible to carry out irradiation of agitated objects and lumped objects parallel with the basic production process, for research purposes.

The proposed cost of the Gammatok facility, minus the cost of the γ-radiation sources, will not be greater than 10,000 rubles. Tentative cost estimates of expenses in pilot plant production of polymaleamides using the Gammatok process facility show that the facility will take not longer than 2.5 years to pay for itself, and that the radiation component of the net production costs will not be greater than 70 kopeks/kg in the production of 60 tons of this material per year.

The use of facilities of this type for various high-efficiency radiation-chemical processes in full-scale production appears highly promising at this stage.

ISOTOPE γ-FACILITY FOR MICROBIOLOGICAL RADIATION CHEMICAL RESEARCH (MRKh-γ-25M)

D. A. Kaushanskii

The MRKh-γ-25M γ-irradiation facility (Fig. 1) designed for microbiological and radiation-chemical research, and developed at the Special Design Agency of the N. D. Zelinskii Institute of Organic Chemistry of the USSR Academy of Sciences, can be installed in an ordinary laboratory room built for biological or chemical work; the arrangement is compact and of relatively small dimensions. The facility leads itself well to research under static, through-flow, and circulatory-static conditions, over a broad range of temperatures (from −40 to +550°C) and pressures (from 10^{-5} mm Hg to 100 atm), using modern analyzing instruments. The facility can also be used in radiation microbiology and immunology (sterilization of vaccines isolated from microbial cells; production of vaccines by radiation inactivation of living organisms; sterilization of sera; sterilization of complexes of microbial antigens and chemical vaccines), in medicine (sterilization of absorbent and suturing materials, medicinal preparations, transplants, etc.), in agriculture

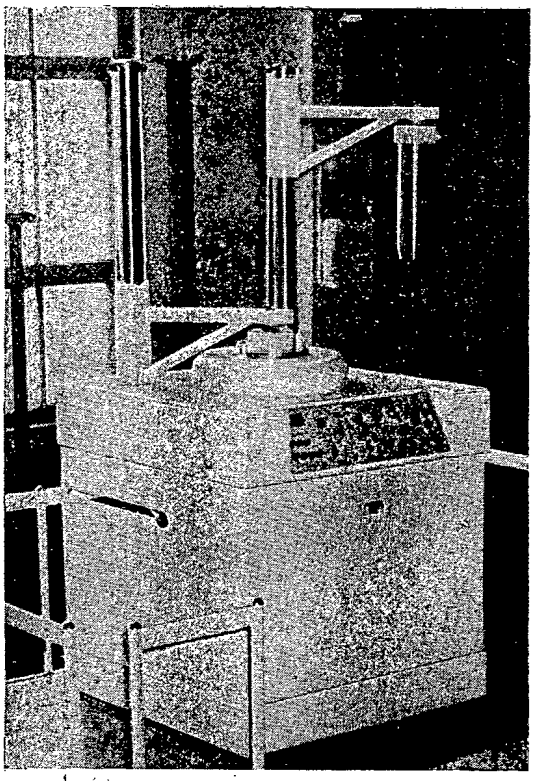

Fig. 1

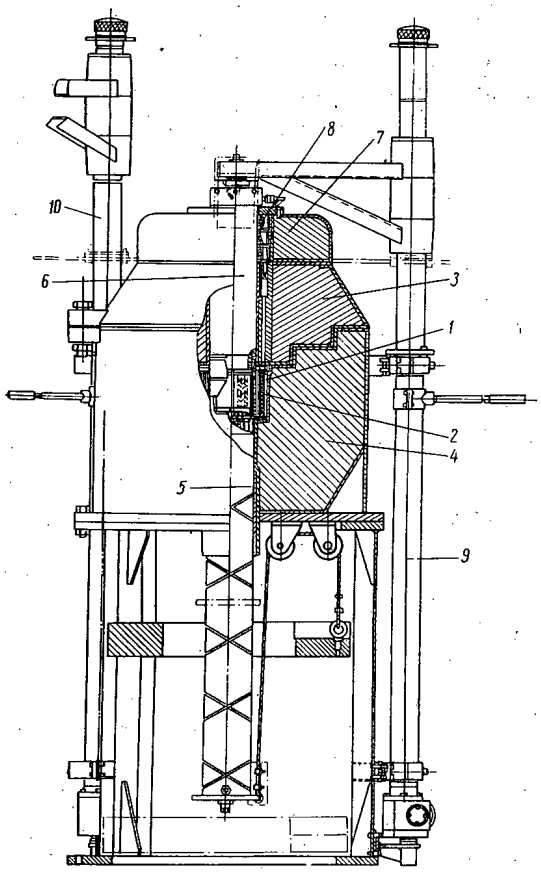

Fig. 2

Fig. 1. MRKh-γ-25M isotope γ-radiation facility for radiation research.

Fig. 2. Side view of MRKh-γ-25M irradiator facility (cutaway section).

Translated from Atomnaya Énergiya, Vol. 30, No. 1, pp. 83-85, January, 1971.

TABLE 1. Dependence of Dose Rate on Irradiator Activity

Total irradiator activity, Ci	Number of radiation sources	Activity of single radiation source, Ci	γ-Equivalent, gram-equivalents Ra	Dose rate at center of working chamber, 10^6 R/h
2300	18	~128	200	0.25
4600	36	~128	200	0.5
8080	18	~450	700	0.7-0.9
10750	24	~450	700	1.0-1.2
16200	36	~450	700	2.0

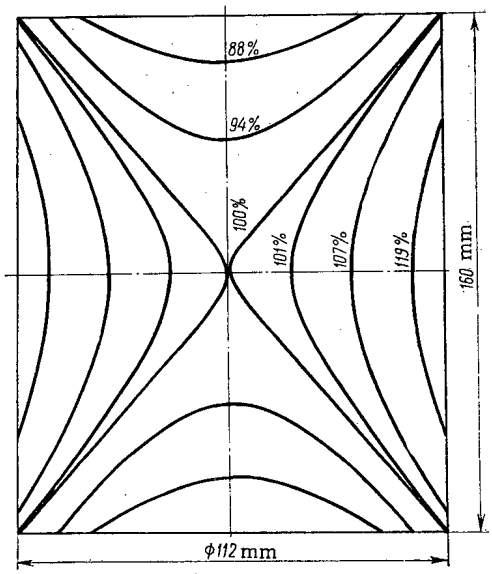

Fig. 3. Dose field in air of the working chamber of the MRKh-γ-25M facility.

(radiation selection, biochemistry, etc.), in solid state physics (study of radiation effects on semiconductors and dielectrics, research on the nature of radiation damage and radiation-induced flaws, etc.), and in electronics (effect of radiation stability of different components in electronic equipment, and so forth).

The MRKh-γ-25M irradiation facility* is provided with a set of three plugs and a working chamber; the plugs have channels for feeding in or removing irradiation products, which are designed to take pressures up to 10 atm in one plug and up to 100 atm in the other plug; channels in the third plug are thermostated. In addition, each plug has two channels to accommodate electrical cables and thermocouples. A variable dose rate is achieved through the use of a set of lead filters, and by displacing the working chamber through different distances from the irradiator.

The irradiator in this facility can be charged with Co^{60} radiation sources of total activity ranging from 2300 to 16,200 Ci depending on the need (see tabular data). The basic data on the MRKh-γ-25M γ-radiation facilities are:

Radiation sources	Co^{60}
Irradiator activity needed to produce maximum dose rate	16,200 Ci
Maximum dose rate (in air) at center of working chamber	$2 \cdot 10^6$ R/h
Volume of working chamber	1.2 liter
Dose field nonuniformity:	
in radial direction	+10%
in axial direction	−25%
Temperature at which working chamber is thermostated	18-20°C
Number of plugs with working chamber	3
Number of communications in each plug with chamber:	
for liquid (gas)	2
for electricity	1
for thermocouple	1
Time required to lift (lower) working chamber	30 sec

* This facility is a redesigned, modernized variant of the familiar MRKh-γ-100 γ-radiation facility widely used in radiation research in the USSR, and in other countries as well, and which was awarded the 1968 Grand Gold Metal at the X Jubilee Trade Fair in Brno (Czechoslovakia) and Gold Metal of the Exposition of Achievements of the [USSR] National Economy.

Timer relay operating period	From 5 to 20 min
Dose rate on surface of facility	To 2.8 mR/h
Dimensions, with hoist-lift mechanism, but minus platform	125 × 135 × 320 cm
Weight	~5.5 m
Frequency of three-phase current	50 Hz
Voltage	220/380 V
Power intake	0.3 kVA

The cylindrical irradiator takes up the bulk of the space (Fig. 2) occupied by this facility. The cartridge 1 of the irradiator consists of 36 tubular cells situated on a circle and rigidly intercoupled. The cartridge is free to rotate while it is being charged with fresh radiation sources 2; but the cartridge remains in fixed position while the facility is in operation. Each tubular cell in the cartridge accommodates two Co^{60} sources 11 mm in diameter and 81.5 mm high. The irradiator unit is placed at the center of a container shell consisting of a top cover 3 and body 4.

The container shell performs the role of biological shielding; the dose rate on the surface of the container shell is not greater than 2.8 mR/h. A rod with a thermostated inner volume 5 and transporting the working chamber with plug 6 runs down the container axis through a guide tube. The working chamber stands 160 mm high and extends 112 mm in diameter. A single-piece collar 7 with a structure shielding the annular slits from γ-radiation (an antiradiation seal) 8 is mounted on the top of the container. The working chamber (rod plus plug) is displaced by the hoist and rotating mechanism 9. A second hoist and rotating mechanism 10 functions as a mirror-image counterpart to the mechanism 9, and is located on the left-hand side of the facility. This second hoist and rotating mechanism, with plug and chamber, makes it possible to stretch the time over which the irradiator radiations can be efficiently utilized.

Back-up limit switches are provided in order to precisely fix the position of the working chamber relative to the irradiator, and to impart greater reliability and greater ease to the work of the operator, and automatically switch the working chamber off to a stop to within ±1 mm of the required position. Control is facilitated by the introduction of a programmed clockwork mechanism (timer relay) into the control system; this relay automates the power drive switching functions after a specified time has elapsed with the experiment in progress, and the working chamber is automatically stopped in the "object outside of exposure zone" position by the limit switches.

The irradiator is recharged with fresh radiation sources every five years, in order to maintain the initial dose rate. The service life of the radiation sources in the first loading is 15 years.

Design and experimental investigations revealed that the dose rate distribution in working chambers of 1.2 liter volume are characterized, for the MRKh line of irradiators, by the data shown in Fig. 3.

An experimental prototype of the MRKh-γ-25M facility has been in operation since August, 1969. Batch production of the facility was started in 1970.

THE KRK-2 RADIOISOTOPE POTASSIUM CONCENTRATION GAGE

I. I. Kreindlin, S. V. Mamikonyan,
L. V. Matveev, and O. G. Mikhailov

The KRK-2 radioisotope potassium concentration gage (see Fig. 1) has been developed at the All-Union Radiation Engineering Scientific Research Institute (VNIIRT). This instrument is destined to measure and record the percentage content of potassium chloride in commercial products of potassium combines, and is also intended for use as a sensor in an automatic process control system.

Determinations of the potassium chloride concentration are based on measurements of the natural γ-emission of the isotope K^{40}. The radiation flux is proportional to the content of the potassium chloride in the product. The radiation is recorded with the aid of a high-efficiency scintillation detector [NaI(Tl) crystal 70 × 70 mm, and FÉU-56 photomultiplier tube], and an electronic system consisting of two pulsed scalers, high-current clock driver, and modules for processing measurement results (memory storage, write-out on digital printer, digital-to-analog converter).

The instrument is equipped with a system for monitoring errors which makes it possible to check errors in the entire measuring system automatically, and to maintain high accuracy in the measurements. Checking of malfunctions is based on recording the flux of γ-photons from a control radiation source (Ra^{226} isotope).

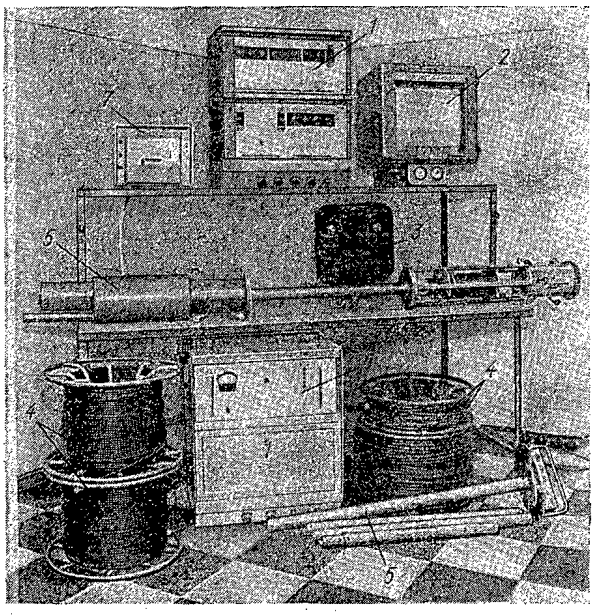

Fig. 1. Complete set of equipment for KRK-2 radioisotope potassium concentration gage: 1) electronic measuring module; 2) electronic automatic EPP-09 potentiometric recorder; 3) hopper fill level indicator; 4) connecting cables; 5) detector; 6) power supplies; 7) BZ-15 digital data printout module.

Measurements are performed in three cycles in the "control on" mode: radiation emitted by the product and by the control source is recorded simultaneously in the first cycle. Pulses from the gage output over a certain time interval set by the clock driver are sent to the measuring scaler module.

After the first cycle has been completed, a small quantity of pulses N_1^1 will have been recorded in the measuring scaler module, with $N_1^1 = K_p^1 + K_c^1$, where K_p^1 is the number of pulses from the product recorded, and K_c^1 is the number of pulses from the control source recorded, in the first cycle.

In the second cycle, complementary pulses are supplied to the measuring scaler module and control source module simultaneously from a stable-frequency generator, until the entire counting capacity of the measuring scaler module is filled up and it is reset in its initial state, while the control source module will have N_2^2 pulses, $N_2^2 = E - (K_p^1 + K_c^1)$, where E is the counting capacity of the control source module.

In the third cycle, only γ-photons from the product are recorded, and pulses from the gage arrive at the measuring scaler module and control source simultaneously.

Translated from Atomnaya Énergiya, Vol. 30, No. 1, pp. 85-86, January, 1971.

When the measurement time in the measuring scaler module is completed, pulses will have been recorded totalling K_p^3, and this can be treated as the result of the measurement, while the number of pulses in the control source module becomes $E-(K_p^1 + K_c^1) + K_p^3 = E-K_c^1 + (K_p^3-K_p^1)$. The value of the difference $K_p^3-K_p^1$ is close to zero, and the average of $E-K_c^1$ is very close to a certain fixed quantity when the parameters of the measuring system remain unaltered. When the value of $E-K_c^1 + (K_p^3-K_p^1)$ remains within acceptable limits, the "working" signal is automatically generated, otherwise the "malfunction" signal is generated.

The instrument design features a detector device, a fill level indicator, an electronic measuring module, the ÉPP-09M3 automatic recording potentiometer, the BZ-15 digital data printout module, a power supply package, and connecting cables.

The KRK-2 potassium concentration gage makes it possible to measure KCl concentration in potash ore, and its beneficiation products, to within ±1% KCl content, with reproducibility of the readings to within ±0.3% KCl content. The range of measurements was taken over ±5% from the specified average KCl concentration. The stability of the gage readings is not inferior to 0.4% KCl when the instrument has been in continuous service for 24 h. Results of the measurements are recorded on digital display tubes of the electronic module and on paper tape run through the BZ-15 digital data printout, and also on strip chart processed by the ÉPP-09M3 automatic recorder.

The analog signal arrives at the automatic control system in the form of direct current from 0 to 5 mA in amplitude, proportional to the measured KCl concentration over a range of ±5% KCl from the specified average taken over the digital output. Changes of 0.1% in instrument readings correspond to a 50 μA change in output current. The measurement time without the control is not longer than 10 min, and not longer than 20 min with the control on indicating proper functioning of the system.

The instrument can be operated either manually or under automatic control, and the periodicity of the measurements can be set from 15 to 60 min in the automatic case. The range of working temperatures are +10°C to +35°C for the modules, from −20°C to +40°C for the measuring gage. The instrument is supplied from an ac power line 220 V $^{+10\%}_{-15\%}$, and the power intake is not greater than 600 VA. The modules are of conventional design and format, and the detector device is dustproof and splashproof. The length of the connecting cables extending between the detector and the instrument modules ranges to 250 meters.

Prototypes of the instrument have undergone state inspection tests and are now in service at the First Soligor Potassium Combine.

BRIEF COMMUNICATIONS

The second unit of the Belyi Yar I. V. Kurchatov nuclear power station has generated three billion kWh electric power as of November 9, 1970, and the power station as a whole has generated a total of 6.2 billion kWh as of that date.

* * *

In late October, by invitation of our editorial panel, the editor-in-chief of the Polish periodical Nukleonika, Professor S. Szczeniewski, and the editorial secretary W. Zelazny, visited Moscow. Their visit was a natural continuation of the friendly liaisons established between our two editorial offices. During their visit, talks were held, culminating in the signing of a joint communique calling for further strengthening of ties between the periodicals Nukleonika and Atomnaya Énergiya, with the object of improving the flow of information on the status of nuclear science and nuclear engineering in Poland and in the USSR. Our Polish colleagues took the opportunity to acquaint themselves with the hospitality of Moscow, and visited the Power Physics Institute [FÉI] at Obninsk.

* * *

The XX session of the UNO Science Committee on Atomic Radiation Effects was held in Geneva in September, 1970. Documents prepared by the UNO secretariat, and including the latest data on the genetic sequelae of exposures to ionizing radiations, radiation-induced cancers and malignancies, effect of radiation on the immunological reaction of the organism, exposure doses to the population from professional and medical irradiation, and from radioactive contamination of the environment, were discussed at the session in line with Resolution No. 2496 of the XXIV session of the UNO General Assembly, which approved the preceding report of the Committee and recommended that the Committee continue its activities.

The time for presentation of the next report to the General Assembly was set, and the report is to include data and evaluations on the above topics. The Committee decided to turn to the UNO member-nations, to specialized institutions, and to IAEA, with requests to make available information on radioactive pollution of the environment originating in different sources, and on exposure doses due to those sources.

* * *

In July, 1970, a seminar was held in Moscow for workers in the food processing industry in Moscow and in the Moscow district, on the topic "Experience in the applications of radioisotope instruments and techniques at food processing plants," with discussion of regularized use of radioisotope instrumentation for process monitoring and control in the food indsutry, as well as discussion of research findings in the field of radiation processing of foodstuffs.

Translated from Atomnaya Énergiya, Vol. 30, No. 1, p. 86, January, 1971.

OBITUARIES

ABRAM ISAAKOVICH ALIKHANOVA

The editorial staff of the periodical Atomnaya Énergiya expresses its deep sorrow on hearing of the death of Academician Abram Isaakovich Alikhanova, a member of the editorial panel, an outstanding Soviet physicist, Hero of Socialist Labor, recipient of State Prizes, and one of the founders of Soviet nuclear physics, who passed away on December 8, 1970, in Moscow, in the 67th year of his life. The editorial staff shares the bitterness of this loss with the relatives and close friends of the deceased.

Translated from Atomnaya Énergiya, Vol. 30, No. 1, January, 1971.

SERGEI TIKHONOVICH KONOBEEVSKII

The outstanding Soviet scientist, leading specialist in the field of the physics of metals and radiation materials science, member of the Communist Party of the Soviet Union since 1948, and Corresponding Member of the Academy of Sciences of the USSR, Sergei Tikhonovich Konobeevskii, died on November 26, 1970, in the 81st year of his life.

The scientific activities of S. T. Konobeevskii began in 1920, when he carried out the first x-ray structural research on metals subject to plastic deformation in our country. As a result of these investigations, S. T. Konobeevskii produced a theoretical interpretation of x-ray diagrams of deformed metals, including interpretations of the texture of rolled steel.

In recent years, many research projects on the study of the structure of metals and alloys, and particularly classical investigations of the decay of supersaturated solid solutions, were completed at the x-ray laboratory founded by S. T. Konobeevskii as part of the State Central Institute of Nonferrous Metals, and at the x-ray structural analysis department of Moscow State University which was under the direction of S. T. Konobeevskii and his disciples; this research culminated in the discovery of the mechanism underlying the ageing of alloys, and the development of the relevant theory.

For over 30 years, S. T. Konobeevskii continued his activities in college-level teaching. Many of his pupils have been doing fruitful teaching work in colleges, at research institutes, and in plants through the country, and many of them have gone on to become outstanding Soviet scientists.

In 1947, S. T. Konobeevskii was the head of a research project on radiation materials science. He and his school carried out fundamental research on the study of the effects of reactor irradiation on the structure and properties of nuclear fuel and structural materials, and in particular discovered, and analyzed

Translated from Atomnaya Énergiya, Vol. 30, No. 1, January, 1971.

theoretically, such phenomena of practical importance as radiation-induced homogenization of uranium –molybdenum alloys, and stress relaxation in uranium and in uranium alloys induced by neutron bombardment. Many of these research projects have been acknowledged internationally. His monograph entitled "Radiation effects on materials" has become a fundamental textbook guiding all research workers in the field of reactor materials science. S. T. Konobeevskii had taken an active part in the work of the periodical Atomnaya Énergiya, in whose pages he published many of his articles on reactor radiation effects on materials for the first time. The Soviet government made a high estimate of the scientific merits and accomplishments of S. T. Konobeevskii, as reflected in the awarding of two Orders of Lenin, the Order of the Labor Red Banner, and various medals.

A fond memory of Sergei Tikhonovich Konobeevskii will be retained forever in the hearts of all those who knew him, worked with him, and studied with him.

SEMICONDUCTOR SOLAR ENERGY CONVERTERS

Edited by **Academician V. A. Baum**
Director, Physicotechnical Institute, Ashkhabad, Turkmenian, SSR

Translated from Russian by **Albin Tybulewicz**
Editor, "Soviet Physics — Semiconductors"

This volume presents a systematic review of the current state of solar energy physics and technology. It reports on investigations of the thermoelectric properties of semiconductors, bridging of thermal elements, and methods for rapid measurement of thermal and electrical properties of semiconductors, and also discusses practical terrestrial applications for thermoelectric, thermionic, and photoelectric solar energy converters such as pumping water in arid regions (including associated equipment used to track the sun). Methods are given for solving problems involving the concentration of direct solar radiation and thermal optimization of absorbers which form part of the solar generator units. Also included are descriptions of calorimetric apparatus for testing the solar radiation concentrators of thermoelectric energy converters. This collection is an important contribution to the field of solar energy research and applications which also presents practical and theoretical guides for related scientific disciplines concerned with thermionic solar converters.

CB Special Research Report
Approx. 222 pages 1969 $27.50

PLENUM PUBLISHING CORPORATION
Plenum Press • Consultants Bureau • IFI/Plenum Data Corporation
227 WEST 17th STREET, NEW YORK, N. Y. 10011

In United Kingdom: Plenum Publishing Co. Ltd., Donington House, 30 Norfolk Street, London, W.C. 2.

RAREFIED GAS DYNAMICS

By **M. N. Kogan**
Computer Center, Academy of Sciences of the USSR, Moscow

Translated from Russian

Translation edited by **Leon Trilling**
Professor of Aeronautics and Astronautics, Massachusetts Institute of Technology

Presents an extensive study of recent uses of the Boltzmann equation in solving problems that require a kinetic description and for which gas-dynamic methods are inapplicable. Considerable attention is given to derivations from the Boltzmann equation, along with corresponding boundary conditions and establishment of areas of applicability. Also discussed are small and large Knudsen number expansions and their relation to specific cases of free molecule flows. Of particular interest to astrophysicists and aerospace engineers, this book, suitable as a graduate text, is unique in both coverage of subject matter and inclusion of up-to-date material.

Approx. 504 pages PR 1969 $25.00

PLENUM PUBLISHING CORPORATION
Plenum Press • Consultants Bureau • IFI/Plenum Data Corporation
227 WEST 17th STREET, NEW YORK, N. Y. 10011
In United Kingdom: Plenum Publishing Co. Ltd., Donington House, 30 Norfolk Street, London, W.C. 2.